THE INFLUENCE OF RAINFALL AND RIVER INCISION ON THE MOVEMENT RATE OF A SLOW-MOVING, SOFT-ROCK LANDSLIDE IN THE RANGITIKEI, NEW ZEALAND

A thesis presented in partial fulfilment of the requirements for the degree of

Master of Science

in

Physical Geography

At Massey University, Manawatu Campus

Palmerston North, New Zealand

Charlotte Naomi Holdsworth

2018

Abstract

The Rangitikei Slide, a slow-moving landslide near Taihape, New Zealand, was monitored to determine the movement patterns and identify the primary movement drivers. The sediment delivery of landslide material to the Rangitikei River was also estimated to inform the sediment yield from slow-moving landslides connected to a fluvial system. RTK-dGPS monitoring, photogrammetry, and pixel tracking of time-lapse imagery was used to categorise movement patterns, and pixel tracking at different temporal resolutions (weekly and hourly) in conjunction with environmental data identified the drivers and classified the influence on movement. The findings aimed to improve the understanding of these landslide types in New Zealand in order to propose more effective management strategies both locally and around the world. It was found that the landslide comprised several blocks exhibiting different movement rates, and that movement was influenced by a seasonal trend likely from groundwater fluctuations increasing pore pressures in the landslide mass. River erosion by the Rangitikei was identified as a key movement driver and has likely influenced movement since landslide initiation. This was supported by historic aerial imagery and photogrammetry, which showed that the landslide has preserved historic movement phases and these indicate fluvial influence. The estimation of sediment contributions found that ~19,000 t/year of sediment is entering the Rangitikei River from the toe, which is considered a conservative estimate. This contribution is substantial; the Rangitikei Slide is producing almost 3,000 times more sediment per kilometre than the non-landsliding areas of the Rangitikei Catchment. Based on these findings, several management options were proposed for the Rangitikei Slide, with recommendations included for managing slow-moving landslides around the world. It was also evident that further research is needed to better understand slow-moving landslides due to the significant hazard they represent in regard to their sediment contribution to the surrounding environment.

Acknowledgements

Table of Contents

List of Figures

List of Tables

1   Introduction: Large, slow-moving soft-rock landslides

Landslides involve the movement of slope material under the influence of gravity and can be extremely destructive; between 1971 and 1974, it was estimated an average of 600 lives were lost each year globally due to slope failures, and $1.8 billion per year of landslide damage has occurred in Italy over the last 45 years (Aleotti & Chowdhury, 1999). Rapid landslides with extensive displacements, such a debris flows, typically have the most severe losses due to commonly large runout areas (Hungr, 1995; Aleotti & Chowdhury, 1999; Massey, 2010; Mansour *et al.*, 2011). Landslides range in speed between extremely slow-moving (mm/year) to extremely rapid (m/sec) (Varnes, 1978; Mansour *et al.*, 2011; Hungr, 2014). Although slow-moving landslides (0-13 m/month) are not generally life-threatening, they are often underestimated in their ability to deform the landscape over time and warp infrastructure, with the cumulative movement leading to total disruption of facilities (Cruden and Varnes, 1996; Massey, 2010; Mansour *et al.*, 2011).

Slow-moving landslide impacts have been previously underestimated in New Zealand compared to more classically hazardous landslides, but this changed in the 1960s following more in-depth studies, allowing for better understanding of these features (Falconer, 1963; Brown 1974; Thompson, 1982). The first study by Falconer (1963) focused on an old, deep-seated landslide at Tahunanui which experienced slow movement periods following intense rainfall. A well-studied slow-moving landslide is the Utiku Slip, which was identified after proposals for road and rail alterations initiated detailed geological and site investigations. These investigations concluded the area had weak geology and landsliding. Reports on the slip have been previously completed by New Zealand Railways, the Ministry of Works and Development, the New Zealand Geological Society, and the Rangitikei Catchment Board (Thompson, 1982). However, more work is needed on slow-moving soft-rock landslides at different temporal scales to further the current understanding, as there is a lack of data on event-scale factors on landslide movement.

There is also an important relationship between landslides and fluvial systems in regard to erosion and sediment delivery. The influx of sediment into rivers can cause a number of issues: water pollution; sedimentation leading to potential river avulsion; and increased flood risk. Deep-seated landslides are instrumental in connecting hillslopes to valley floors and river systems, and can account for a significant proportion of the regional sediment yield and denudation rates for uplifting landscapes (Bilderback, 2012). This highlights the importance of deep-seated landsliding in landscape evolution, as they influence sediment generation and storage and can transmit changes in the fluvial systems to the rest of the landscape.

It was hypothesised at the start of this study that the Rangitikei Slide had several sections (landslide blocks) exhibiting different movement rates based on local knowledge from the land manager and initial site visits. It was also hypothesised that the primary movement drivers were likely groundwater fluctuations and toe erosion by the Rangitikei River, due to comparative studies of nearby landslides. However, the Rangitikei Slide had the unique feature of residing on a sharp bend of a significant North Island river, making toe erosion almost certainly an important factor in movement.

1.1   Deep-seated, slow-moving landslides

Slow-moving landslides occur world-wide (Handwerger *et al.*, 2013; Haghshenas Haghighi & Motagh, 2016), and cause significant impacts on property and infrastructure; this includes damage to lifeline infrastructure, loss of land, and a high sediment supply to rivers. Shallow landslides have commonly been attributed as the landslide type with the highest sediment contribution, but deep-seated landslides are emerging as a key feature in the fluvial-sediment relationship (Gerrard & Gardner, 2000; Korup, 2005; Bilderback, 2012). Deep-seated landslides also have a notable ability to shape the landscape through sediment delivery (Korup, 2006; Massey, 2010).

According to Thompson (1982), large-scale slope failures generally exceed 200 m x 200 m in dimension, and are typically deep-seated, although the width is often at least double the depth (Ellen *et al.*, 1995). Slow-moving landslides have different classifications due to their movement type, material, and rate of movement, generally based on the Varnes (1978) classification scheme, which has been used in previous New Zealand landslide studies (Massey, 2010; McCabe, 2013). Numerous slow-moving landslides are categorised as translational, which Hungr *et al.* (2014) suggests can be some of the largest and most damaging landslides on Earth.

The classification scheme (Figure 1) depicts that translational landslides, or rockslides, involve the movement of the entire mass from one place to another using a planar failure surface, which can be over 10 m below ground level (deep-seated) (Varnes, 1978; Massey, 2010; McCabe, 2013). This planar sliding mechanism does not self-stabilise, meaning slides are generally extremely rapid once they begin. However, in very weak rocks and with a low dip angle, these slides can be very slow-moving (Hungr, 2014). This slow-moving variety is common in New Zealand, classified as landslides with less than 13 m of movement per month (Varnes, 1978; Mansour *et al.*, 2011; Hungr, 2014). These landslides usually develop within rock or earth slopes as flows, slides, or complex phenomena (a combination), with movement occurring occasionally or continuously with seasonally variable movement rates (Cascini *et al.*, 2014).
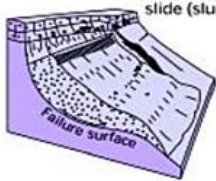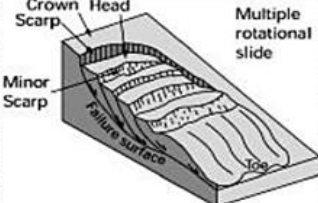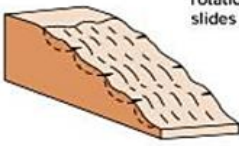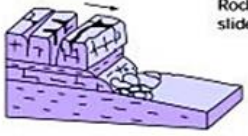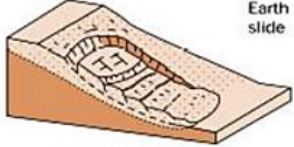
Figure 1. Slide types described in the Varnes classification scheme, with many slow-moving landslides categorised as translational rockslides (modified from Massey, 2010).

Slow-moving landslides can be separated into three movement classes; extremely slow-moving, very slow-moving, and slow-moving. Extremely slow-moving landslides move at rates of 0 - 16 mm/year, very slow-moving landslides move between 16 mm - 1.6 m/year, and slow-moving landslides move 1.6 - 160 m/year, or approximately 13 m per month (Cruden and Varnes, 1996; Mansour *et al.*, 2011). There have been cases where categorically slow-moving landslides have rapidly accelerated after long periods of slow displacement, causing significant damage and in rare cases, death (Massey, 2010; Mansour *et al.*, 2011).

Over 7,000 landslides have been mapped in New Zealand (Dellow *et al.*, 2005; Massey, 2010; Massey *et al.*, 2013), occurring in the weak Neogene-aged sedimentary rocks. These Neogene rocks are considered weak to very weak, supporting the formation of slow-moving, deep-seated, translational landslides. A study by Massey (2010) noted that the Utiku and Taihape landslides were complex translational rock slides, with an earthflow formed at the toe of the Utiku slide (Cruden and Varnes, 1996). Both landslides had similar materials and geotechnical properties, and were comprised of slide blocks moving along thin clay horizons parallel to bedding. The Utiku slide is made up of two perpendicular planes that form a wedge, with the slide surface daylighting at the Hautapu River, where the landslide terminates (Massey, 2010). The Taihape landslide is close to planar in geometry, and terminates at the Otaihape Stream, although the slide surface is several metres below the base of the stream. Both the Taihape and Utiku landslides are well-studied (Cruden and Varnes, 1996; Massey, 2010; Massey *et al.*, 2013; Massey *et al.*, 2016; Massey *et al.*, 2016a; McCabe, 2013; McColl & McCabe, 2016), and are considered representative of the 7,000 mapped, large translational landslides in New Zealand (Dellow *et al.*, 2005; Massey, 2010).

1.1.1 Stability thresholds for landslides

Slope stability can be altered if stability thresholds are crossed (Glade *et al*., 2005), which changes the state from stable to marginally stable to actively unstable (Figure *2*). The slope stability is a determining factor in landslide formation and movement. These stability thresholds are influenced by different factors, which are described below.
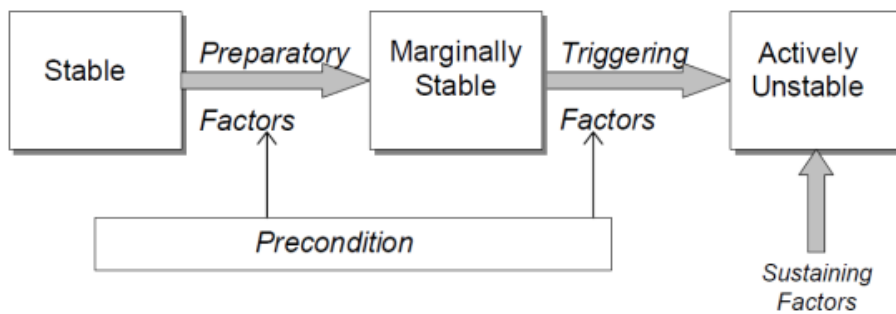
Figure 2. Diagram showing the conceptual stability timeline (Glade et al., 2005).

1.2 Landslide initiation and motion

Translational landslides generally slide along weak bedding-parallel layers or thin clay seams within the stratigraphy (Figure 3) (Mountjoy & Pettinga, 2006; Massey, 2010). In the Taihape region, these clay layers are likely of volcanic origin, deposited as ash and weathered to clay with high levels of montmorillonite (Brown, 1974). These seams destabilise slopes due to their low friction angle, with some clays exhibiting a friction angle of less than 10° (Massey, 2010). This means that the slope can utilise these clay seams as a planar failure surface along which the landslide can move if the slope angle is steep enough to initiate movement. The Taihape region has several examples where clay layers have been identified as a primary movement factor, particularly for the Utiku Slip (Brown, 1974; Massey, 2010) and the Taihape landslide (Thompson, 1982; Massey, 2010). These clay layers have also been a notable factor for the Confluence landslide, Tuhoe Slide, and Hautapu Slide (Thompson, 1982). A typical translational slide in Neogene sedimentary rock is generally deep-seated with a clay layer exploited as the failure surface (Figure 3).
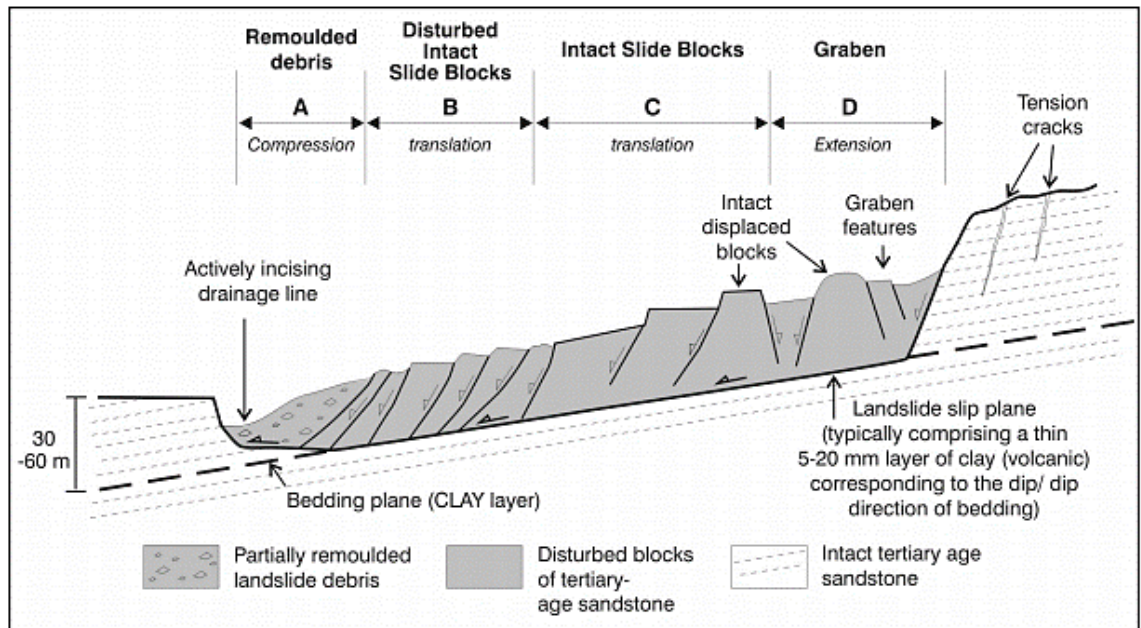
Figure 3. Schematic cross section of a translational slide in Neogene sedimentary rocks (Massey, 2010)

The upper area of large, slow-moving translational landslides is dominated by extensional features such as grabens, normal-scarps and tension cracks (Figure 3), and generally have distinct head scarps and clear toe areas (Ellen *et al*., 1995). If the toe materials are removed at a slower rate than the landslide movement, or there is no significant drainage line at the toe area, the lower area can express compressional stress through features such as buckling, thrusting, and uplifted blocks. The margins of the landslide may be obscure unless they have created noticeable offsets in the landscape (Ellen *et al*., 1995). The formation of a failure surface (shear surface) is often a result of brittle deformation, which occurs when stresses applied to a material are sufficiently large so that the weakest or most stressed bonds between particles will begin to break. This will continue as the stress increases until enough bonds are broken that the material is unable to bear the applied stress, developing a shear surface and reducing material strength further (Petley & Allison, 1997). There can be more than one failure surface in the stratigraphy of a landslide, with movement localised along one or several at one time (Cascini *et al*., 2014).

The movement patterns of slow-moving landslides, particularly deep-seated landslides, have been widely studied around the world (Radbruch-Hall, 1978; Pasuto & Soldati, 1990; Petley & Allison, 1997; Massey *et al*., 2013; Massey *et al*., 2016). This has resulted in two distinct patterns; long-term displacement and catastrophic displacement (Petley & Allison, 1997), although Massey *et al*. (2013) separated these into three patterns: irregular episodes of increased movement; slower post-failure displacement; and seasonal cyclic displacement. The irregular

movement episodes and post-failure displacement are included in the catastrophic movement pattern.

Long-term displacement occurs at low strain rates and is often referred to as 'creep'. This movement rate can vary, often seasonally due to pore pressures and increased precipitation, but is generally considered continuous. An early hypothesis for slow, intermittent movement was that entry of water into fissures in the landslide mass eventually slowed or ceased due to capacity, potentially raising the material strength as the locked-up water could add stability, until more water could enter the area (Falconer, 1963). This indicated a relationship between movement periods and the movement of water within the landslide mass; however, the proposed mechanism by Falconer (1963) lacks the evidence to support this. Another early movement hypothesis involved the grinding down of clays in the geology, specifically montmorillonite, and this ground material filling fissures in the landslide mass, which swelled when wet and 'lubricated' the rock mass (Claridge, 1960). These hypotheses both highlighted the importance of hydrology (water movement) in landslide behaviour, which is still a well-documented factor at present (Ellen *et al.*, 1995; Picarelli, 2007; Van Asch *et al.*, 2007; Massey, 2010; Massey *et al.*, 2013). However, both hypotheses are not considered to be the accepted mechanism for long-term displacements (creep). Rather, creep is influenced by seismic events or a rise in pore pressures. An example is the Point Firmin landslide in California, which experienced an increased rate of creep following a small earthquake (Petley & Allison, 1997). However, not all slow-moving landslides are affected by earthquakes, such as the Utiku landslide in New Zealand, where monitoring found that no movement episodes were attributed to earthquakes during that period, irrespective of magnitude (Massey *et al.*, 2016a). A rise in pore pressures is a typical movement factor for slow-moving landslides (described in more detail below), as this increases the shear stresses on the landslide material and reduces the shear strength.

According to Massey (2010), slow creep occurs alongside short duration accelerated creep events (Figure 4), before movement accelerates into large accelerated creep. These periods of increased displacement within a long-term trend of extremely slow to slow movement are common, and have been extensively documented (Peck, 1959; Ellen *et al.*, 1995; Petley & Allison, 1997; Massey, 2010; Massey *et al.*, 2013). In some cases, these accelerated creep phases can lead to catastrophic displacement.
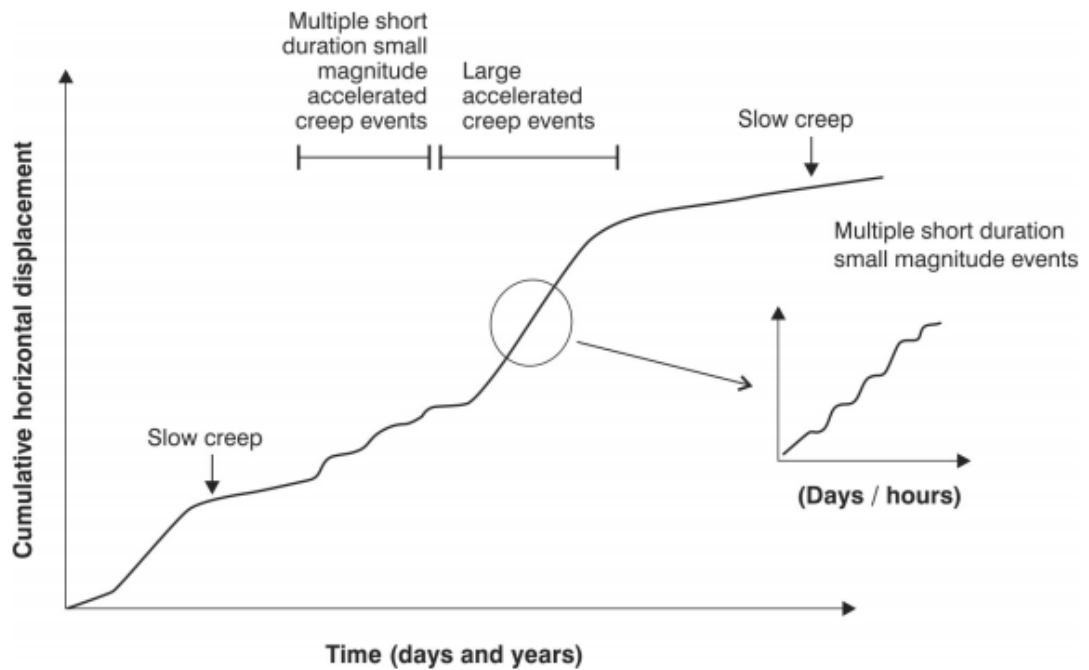
Figure 4. Schematic diagram of the typical displacement patterns of a horizontal slow-moving landslide surface over time. This was derived from studies of similar slides and their movement patterns by Massey (2010).

Catastrophic displacement refers to short-term movement at very high rates of displacement (Petley & Allison, 1997). These can occur as sudden failures after long-term, steady-state creep, or follow an increased displacement rate. While both types are similar, one shows no indication of imminent failure while the other is foreshadowed by an increase in creep displacement rates. Sudden failure does not always occur due to changes in loading or increased stresses, but can follow a steady-state condition if the stability threshold is reached (Petley & Allison, 1997). An example of this process is the Abbotsford landslide in 1979, which accelerated over months from a steady state and then catastrophically failed, damaging numerous infrastructure (Hancox *et al.*, 1980; Hancox, 2007).

Cascini *et al*. (2014) also described the characteristic movement patterns of slow-moving landslide, but separated these into three movement trends during the active movement stage, labelled as trend I, trend II, and trend III (Figure 5). Trend I shows linear movement through time, also known as a 'continuous creep' phase. This could be attributed to a range of factors, including a prolonged dry period where groundwater levels do not vary significantly, maintaining constant effective shear stresses along the slip surface. Trend II is a convex-shaped movement progression associated with a rapid increase in pore pressure from high rainfall, followed by a slow reduction in groundwater levels over time and a decrease in displacement rates. Trend III is a concave-shaped movement rate described as a non-stationary phenomenon, related to new boundary conditions such as the development of a new local slip surface connected to the

existing main slip surface (Cascini *et al*., 2014). Landslides can evolve between different movement trends through time, with movement able to increase from trend I to trend II or III depending on the movement drivers.
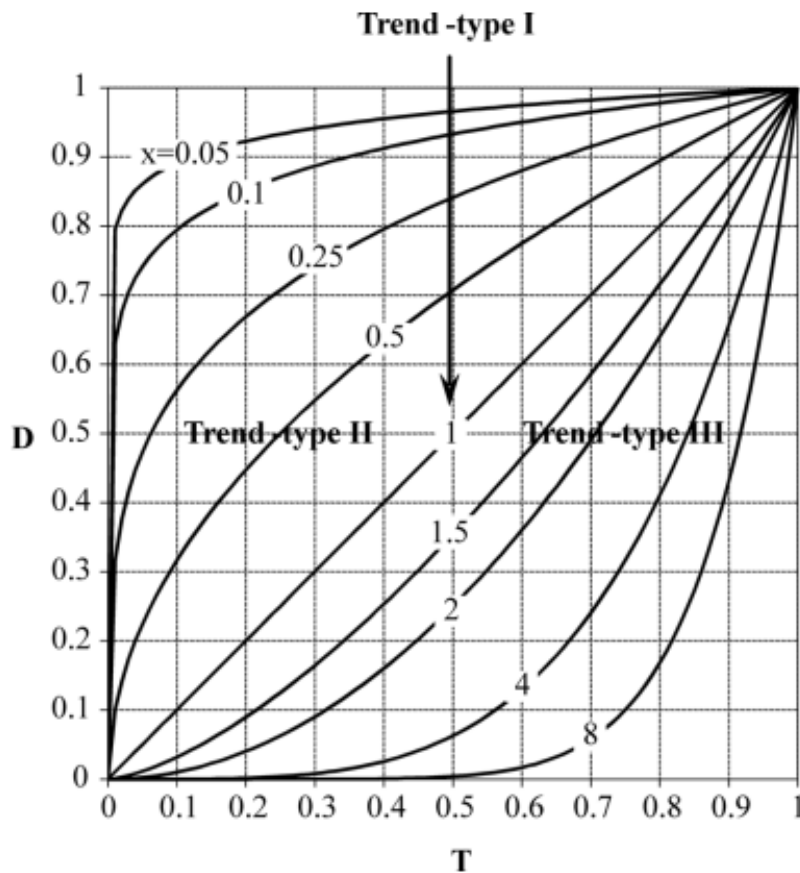
Figure 5. Movement trends of slow-moving landslides during active movement stages in a normalised cumulative displacement vs. normalised time plot (Cascini et al., 2014).

The differences between the movement descriptions by Petley & Allison (1997), Massey *et al*. (2013), and Cascini *et al*. (2014) highlight that movement patterns, while generally characterised, are specific to each landslide and can be influenced by a range of stability factors.

1.3   Stability factors of slow-moving, translational landslides

The controls on landslide initiation can be categorised into four groups; preconditioning, preparatory, triggering, and sustaining factors. Preconditioning and preparatory factors can facilitate the development of a failure surface, while triggering factors overcome the threshold into active instability (Glade *et al*., 2005), and sustaining factors encourage continued movement. These groups inform landslide initiation by identifying the different factors that can increase the susceptibility of a landscape to landsliding.

1.3.1   Preconditioning factors

1.3.1.1   Geological controls

Geology is a fundamental control of landslide initiation as certain lithologies and geological landscapes are more susceptible to slope failure due to a series of factors including bedding angle, bedding-plane defects (bedding-plane shears), and bedding-parallel clay seams (Massey *et al.*, 2013).

1.3.1.1.1   Bedding angle

Bedding is important in slope stability as angled bedding is needed for slow-moving, translational landslides to occur. The necessary bedding angle for landsliding is a downslope dip, facilitating movement of material along the bedding of the failure surface towards the toe (Ellen *et al.*, 1995; Massey *et al.*, 2013). Translational landslides can move rapidly unless the bedding angle is sufficiently low (< 10°) to allow slow to extremely slow movement (Massey, 2010).

1.3.1.1.2   Clay seams

Many of the large, translational landslides in the lower North Island are thought to be sliding along low angle, thin clay layers with low friction angles (some < 10°) that act as planar failure surfaces (Massey, 2010; Massey *et al.*, 2016a). These thin (1-10 cm) clay layers are composed of montmorillonite-type clay of the smectite group (Brown, 1974; Massey *et al.*, 2016a), which are thought to be present in most fine-grained Neogene sedimentary rocks, and considered an important factor in slope failure. The formation of clay can decrease slope strength and cohesion, particularly when the amount of clay increases with continued weathering (Irfan, 1998; McCabe, 2013). Clays vary in strength, with illite and montmorillonite clays having lower shear strengths compared to Kaolinite or chlorite clays (Ohlmacher, 2000; McCabe, 2013). A clay layer found in the Utiku landslide had high concentrations of montmorillonite, and was thought to be a controlling parameter in the location and movement of the landslide (Brown, 1974). Eight clay seams have been found in the Utiku and Tarare Sandstone Groups, at varying stratigraphic levels (Massey, 2010). It is believed that the Utiku landslide initiated prehistorically when Hautapu River incision cut across one of these weak clay seams (McSaveney & Massey, 2017). The high strength contrast between the dominant lithology and the thin clay layers influences slope stability and can dictate the location and geometry of deep-seated landslides (Mountjoy & Pettinga, 2006). However, initiation of slope failure requires both clay material and water (Yalcin, 2007), indicating that the presence of these clay layers is not often enough to induce movement.

1.3.2   Preparatory and triggering factors

Preparatory factors can diminish slope stability by reducing the stability of the slope from stable to marginally stable (McCabe, 2013). This includes slow and progressive factors such as cyclic

fatigue, where the repeated low-rate stresses acting on a slope lessens the overall strength of the slope over time, rather than occurring after the first stress event (Murphy, 2014). It can also involve factors such as toe-cutting or anthropogenic activities, which can destabilise the slope over a shorter timescale than slower factors such as weathering.

Triggering factors are those that cause the slope to move from stable or marginally stable to actively unstable (Glade *et al.*, 2005). These factors can be discrete events such as a storm or an earthquake, or a change in long-term processes such as groundwater or river incision. There is typically only one trigger per landslide failure or reactivation, and these triggers are stimuli that cause an almost immediate response in the slope (Massey, 2010). This occurs because the shear stress is greater than the shear strength (resistance), overcoming the stability threshold and resulting in failure. Some factors can be a preparatory or triggering factor depending on the stability of the slope.

1.3.2.1   Hydrological processes

Permeability is the ability of a soil or rock to transmit fluid, and this influences fluctuation in the water table through water infiltration. During higher rainfall periods, the permeability of the land determines the sensitivity of the groundwater level, as a highly permeable soil will transmit water faster than less permeable soil, affecting the groundwater fluctuation. Permeability is influenced by the average size of pores and the distribution of particle sizes within the material (Wang & Sassa, 2003).

Changes in groundwater can destabilise slopes and increase the likelihood of future failure. These changes can include greater saturation, higher groundwater levels, and subsequently increased pore pressures. Pore pressures increase as the rising groundwater level increases the head pressure within each pore, which reduces the effective stresses and the critical soil strength. Pore pressure increases at a faster rate than it drops, highlighting the impact of consecutive storm events on groundwater, as the pore pressures are unlikely to decrease between events (Picarelli, 2007; Massey, 2010). This is complicated by contrasting permeability within the slide mass and direct channels for surface water into the landslide from deformation. This often presents erratic and complex behaviour in large, slow-moving landslides in response to water input (Van Asch *et al.*, 2007; Massey, 2010). A slope with naturally high groundwater conditions may provide an ideal environment for translational landslide formation (McCabe, 2013), or a climatic change, such as increasingly wetter winters and higher rainfall frequency, which alters the groundwater regime and raises the pore pressures within the landslide mass. This reduces stability, as the pores are under increasing pressure as water levels rise and heightens the susceptibility of the material to movement (Schulz *et al.*, 2009).

Hydrological processes include both short-term processes (rainfall-induced groundwater rise) and long-term processes (river incision). Individual rainfall events are considered less effective at causing significant movement of deep-seated, soft-rock landslides (unlike in shallow landslides) compared to seasonal changes or long-term rainfall patterns (Massey, 2010). Long-term rainfall patterns (including higher rainfall frequency in winter) are more influential due to fluctuations in groundwater, facilitating significant movement and surface deformation by altering the effective normal stresses. This is due to a reduction in shear strength as pore pressure increases, reducing particle friction through buoyancy (Massey, 2010). A key factor is the antecedent conditions (pre-existing conditions), which determines the influence of any changes in groundwater, as a high groundwater level would cause increased water pressures within the pores due to a higher head pressure. Antecedent conditions are important in determining the ability of rainfall events to trigger deep-seated landslide movement. Nafarzadegan *et al*. (2013) found that the crucial soil moisture that triggered movement seemed to occur after more than 10 days of antecedent rainfall. This shows that long-term rainfall patterns and seasonal patterns can be as important as rainfall amount in deep-seated landslides (Ellen *et al*., 1995), and extended periods of rainfall is an effective trigger for movement. Initial soil porosity has also been found to influence hydrological processes, and can determine the response of a landslide to increasing pore pressures due to the permeability and pore sizes in the material (Iverson, *et al*., 2000). Massey (2010) found that pore pressures at Utiku respond to long periods of wet weather (high antecedent groundwater conditions) rather than high magnitude, short-duration rainfall events, which is likely to be similar for the nearby landslides.

Increased river incision due to long-term climatic cycles can destabilise slopes through increasing the slope angle past the natural stability angles, toe removal, and exposing failure planes. Relative sea-level lowering from long-term climatic forcing directly impacts the base level of stream networks and accelerates river incision in the headwaters (Mountjoy and Pettinga, 2006). Bilderback *et al*. (2014) found that the Waipaoa River catchment (East Coast, New Zealand) appeared to have experienced river incision following the Last Glacial Maximum (ended approximately 18 ka), causing widespread hillslope adjustment including the initiation and reactivation of deep-seated landslides. There appeared to be a lag of 4000 – 5000 years between initial river incision and major hillslope disturbance, according to tephra cover bed ages (Bilderback *et al*. 2014).

1.3.2.2   Geomorphological controls
Slope angle is a key geomorphological control on landslide initiation, as it determines slope stability. Every hillslope has a natural stability angle determined by material strength and

cohesion. Weaker rock will have a shallower stability angle than stronger rock. If this angle is steepened, stability is reduced and movement will likely follow. This is strongly influenced by tectonic deformation, which weakens rock strength through folding and faulting. This can steepen slope angles and reduce the natural slope stability angle.

River incision can be an important factor in slope stability and landslide development through the continual removal of sediment from the toe area, which undermines the slope and reduces stability for a future triggering event. This toe erosion leads to slope steepening or increased slope height (McColl, 2014). River incision can also lead to exposure of the failure surface, known as 'daylighting', which allows the landslide to move unimpeded by any debris at the toe and can result in increased landslide movement or catastrophic failure.

1.3.2.3 Anthropogenic activities

These activities can include excavation for farm tracks, roads, railways, the building of dams and increased runoff from concreted areas, which can all diminish slope stability by increased loading or by exposing the failure surfaces, 'daylighting' the slope. Construction or excavation works can increase slope height or steepness, and depending how primed the slope is for movement from local preconditioning and preparatory factors, earthworks on the slope can trigger failure (McColl, 2014). The Bird Landslide is an example of this, where the farm on the landslide underwent excavation of farm tracks and modifications to drainage (McCabe, 2013). These actions have been attributed to unloading of the toe area (removing material that was supporting the slope) and increasing slope instability. The Utiku landslide is also an example of anthropogenic activities impacting movement rates, where increased movement through the 1960s and 70's corresponds with intensive engineering on both the road and railway that dissects the landslide (McSaveney & Massey, 2017). This engineering appears to have loaded the head of the landslide and unloaded the toe, resulting in destabilisation and subsequent movement. It is now understood that the Utiku landslide is highly sensitive to environmental changes, including engineering works, following extensive studies (Ker, 1970; Stout, 1977; Massey, 2010; Massey *et al.*, 2013; Massey *et al.*, 2016; Massey *et al.*, 2016a; McSaveney & Massey, 2017)

1.3.2.4 Transient applied stresses

Earthquakes cause transient applied stresses, and large magnitude earthquakes can be a catalyst for deep-seated landslide initiation (Keefer, 1984; 2002; Mountjoy and Pettinga, 2006). Transient applied stresses are dynamic stresses from a temporary event which fluctuate the loading (Manga, *et al.*, 2012). Generally, large magnitude earthquakes induce rock mass dilation, weakening existing tectonic defects and reducing the shear strength (Mountjoy and Pettinga,

2006). Over time, the shear stresses can increase until the mobilised shear strength of the slope is overcome and the threshold for movement is crossed. Landslide movement then follows. Strong ground motion can prepare the rock for future failure by enhancing existing weaknesses in the rock mass, or can trigger movement (Mountjoy and Pettinga, 2006). Slow-moving landslides (m/yr) can experience accelerated movement following an earthquake or an evolution into a rapid landslide (m/s) (Lacroix *et al.*, 2015).

Transient stresses from earthquakes may alter hydrological properties in the slope by stimulating increased fluidity (Manga, *et al.*, 2012). Combined with rock mass dilation, water is thought capable of infiltrating down to critical lithological horizons (such as clay seams) in the rock mass by utilising new or enlarged defects, elevating pore pressures and reducing slope stability (Mountjoy and Pettinga, 2006), although there is no data to support this hypothesis. Full failure may occur years to decades later following the initial transient stresses. Earthquakes are also a form of cyclic fatigue, where the repeated low rate stresses acting on a slope lessens the overall strength of the slope over time rather than triggering failure after the first stress event (Murphy, 2014). Weakening of slope strength can occur numerous times before the reduction in inherent strength is sufficient to result in failure, therefore preparing the slope for future failure. Examples of large, deep-seated landslides that appear to have experienced cyclic fatigue include the Waipoapoa and Ponui landslides, which both exhibited tension cracks near their head scarps following the 1931 Hawke's Bay Earthquake (M_w = 7.8) but eventually failed in 1976 after a significant rainfall event (374 mm rain in 24 hours) (Mountjoy & Pettinga, 2006). It is inferred that the 1931 earthquake reduced the slope stability, priming them for failure following a significant disturbance event.

Contrary to this, Massey *et al.* (2016a) found that earthquakes did not appear to account for any episodes of movement in the Utiku landslide during their study period, regardless of the size of the earthquake. From 2008 to 2016, no increased movement in the landslide had a strong relationship with any earthquakes, even a magnitude 6.2 earthquake that occurred in 2014. For some landslides with low-angle basal slide surfaces, earthquake-induced displacements may not be a significant driver of long-term movement (Massey *et al.*, 2016a). This seems to indicate that while earthquakes can have a large impact on deep-seated and slow-moving landslides around the world, they have a lesser impact in soft-rock terrain than hydrological processes such as groundwater and pore-water pressures (Picarelli, 2007; Van Asch *et al.*, 2007; Massey, 2010; McCabe, 2013).

1.3.2.5 Sustaining factors

Once initiation has occurred, some factors can sustain movement over time through continued removal of slope stability. Sustaining factors include river incision, which facilitates toe-cutting and can constantly undermine slope stability by steepening the slope angle, encouraging movement. Hydrological processes can also be a sustaining factor, as consistently high groundwater levels can saturate the land mass (lowering the shear strength) and encourage continuous movement.

1.4 Impacts on people and infrastructure

Large, slow-moving translational landslides can be highly destructive, particularly due to the generally deep-seated nature of the failure surface. This can create a significant landslide deposit following a catastrophic failure. Sudden catastrophic failure can follow long periods of very slow movement. The Hautapu Slide in the central North Island is an example of this. Following heavy rain in 1951, the slide blocked the Hautapu River for 48 hours (Thompson, 1982). The same slide also moved 30 m, supposedly overnight, in 1981 following heavy rain. These large landslides can exhibit slow movement for many decades before slope stability alters, increasing movement rates or facilitating catastrophic failure.

The large, slow-moving landslides of the Taihape region exhibit a diversity of risk and financial profiles due to the diverse anthropogenic settings which inhabit these moving slopes. The magnitude of these impacts depends on population density and the type of infrastructure in the area, although landslide impacts on a single farm can still significantly cost the farmer, local council and insurance companies. The impacts may show seasonal trends, exhibiting higher movement rates every winter (McColl & McCabe, 2016). While daily groundwater changes from rainfall are less effective on Neogene soft-rock landslides in general, seasonal changes can produce a noticeable response in landslide movement (Massey, 2010). This is likely due to water availability in the winter compared to the summer, facilitating overall movement and surface deformation such as rolls and ripples, as seen on the Bird Landslide (McCabe, 2013).

The case studies from the Taihape region all show a range of impacts on people and infrastructure. The Rangitikei Slide and the Bird Landslide are located on farm properties, and the only people directly affected are the property owners. Therefore, the impact on people and infrastructure is limited to the families and the farm infrastructure such as fences, sheds, and farm tracks (McColl & McCabe, 2016). This is in direct contrast to the Taihape Landslide, which has affected approximately 200 households and a primary school (Massey, 2010). The impacts from the Taihape Landslide have been extensive for both people and infrastructure, with the primary school relocated off the landslide and significant damage occurring to many properties.

Alternatively, the Utiku Landslide has a minimal impact on people living near the landslide but a significant impact on infrastructure, particularly State Highway 1 and the North Island Main Trunk Railway (Brown, 1974). State Highway 1 lies directly above the retrogressing head scarp and the North Island Main Trunk Railway Line runs across the width (Massey, 2010).

Overall, the impacts from slow-moving translational landslides can be extensive and extremely costly, often resulting in loss of land, alteration to drainage networks, and damage to farming infrastructure, roads, fences, and grazing land (McColl & McCabe, 2016).

1.5   Sediment delivery from large, slow-moving landslides

Significant sediment delivery into river systems is an important impact of landslides due to river pollution and downstream aggradation (Korup *et al.*, 2004). Sediment connectivity refers to the transfer of sediment between elements of a system (Fryirs *et al.*, 2007), and facilitates sediment movement between components and along the channel network (Cavalli *et al.*, 2013). This includes transfer between sediment sources and depositional zones (Harvey, 2001; Cavalli *et al.*, 2013), such as a between hillslopes and the river channel. There is a consistent relationship between channel and hillslopes where sediment delivery from slopes influences sediment availability and flow hydraulics, and channel erosion impacts the stability of hillslopes (Harvey, 2002; Golly *et al.*, 2017). This relationship can be temporarily disrupted or limited, resulting in a disconnected or poorly-connected system. Connected systems show consistent sediment movement between both internal and external sources and downstream stores along the river profile (Hooke, 2003). Poorly connected systems show limited sediment transfer between sources and sinks, often involving sediment deposition in long-term storage areas such as alluvial floodplains (Hooke, 2003).

This is important for landslides, particularly where runout can enter the fluvial system. A system is termed well-connected when a large proportion of slope material is effectively transferred to the channel. A system is disconnected when slope material does not reach the channel and the two catchment features are considered buffered (Kuo & Brierley, 2013). Disconnection between slope and channel limits the delivery of sediment into the system, also limiting the propagation of disturbance effects downstream. Connectivity can change through time, where an event can connect or disconnect a system. An example of this is a slow-moving landslide on the Erlenbach Stream in Switzerland, which experienced accelerated movement when a flood eroded the alluvial step at the toe, but renewed the step through accumulated landslide debris, which re-stabilised the slope and reduced movement (Golly *et al.*, 2017). This shows that areas can become disconnected following flood events, but can reconnect over time through a negative feedback cycle that produces greater slope stability. This debuttressing and re-buttressing

process as a result of channel erosion and subsequent alluviation by the landslide are important controls on slope stability.

Landslides, particularly shallow landslides, have been considered the primary method of sediment transfer from slopes; however, deep-seated landslides may play a more significant role than previously acknowledged. While high magnitude rainstorms are a common instigator of shallow landslides and can increase catchment connectivity (Korup *et al*., 2004; Fuller & Marden, 2011), they can also influence increased movement in large, slow-moving landslides. High rainfall events are common in winter months (Harvey, 2001), although this depends on the factors influencing movement for each landslide type. Large, slow-moving landslides can be influenced by seasonal changes, but movement can also be triggered by discrete events such as floods. This is important to acknowledge in river management, as certain periods or following significant events will likely increase the sediment supply, which has implications for settlements downstream. These implications could include increased aggradation, and therefore increased flood risk.

Connectivity also has an influence on sensitivity, which is the susceptibility of landforms to change (Thomas & Allison, 1993; Brunsden, 2001), where this change may be a result of natural or anthropogenic events. A well-connected system is considered sensitive to disturbance due to the connection between landscape components and the ready transference of impacts along the sediment cascade (Harvey, 2001; Fuller & Marden, 2011). Alternatively, a disconnected system is considered more robust, as impacts are not as easily transferred. Therefore, landslides that are disconnected are less likely to impact the fluvial system than those that are connected. The connection between the landsliding material and the fluvial system is influenced by catchment geometry (accommodation space), strength properties of the material, and the rate of movement. This means that catchment conditions can have a strong influence on landslide connectivity.

Catchment conditions refer to the inherent properties of a catchment, including the geological and geomorphological characteristics, which have a direct influence on connectivity (Crozier *et al*., 2016). Catchment geometry can increase connectivity by reducing accommodation space for failed material at the base of steep-sided slopes, facilitating rapid evacuation into the river system (Kuo & Brierley, 2013). Slopes composed of lithologies that have a high stability angle may reduce sediment supply as they are less susceptible to landsliding. This can inhibit connectivity due to the limited sediment, restricting the transfer into the fluvial system.

Alternatively, weak lithologies can increase sediment supply due to innate instability, increasing the potential transfer of material between slope and channel as more is readily available.

Large, slow-moving landslides, particularly deep-seated landslides, have the potential to supply substantial quantities of sediment into nearby fluvial systems, especially where a river is cutting the landslide toe and facilitating movement (Gerrard & Gardner, 2000; Korup, 2005; Mountjoy and Pettinga, 2006; Bilderback, 2012). These landslides can produce both a small consistent supply and a large sudden sediment influx from a failure. Korup *et al.* (2004) discusses how catastrophic slope failure significantly alters sediment transport rates in river systems. The events had lasting impacts on nearby rivers, leaving large deposits of legacy sediment and altering river behaviour. The impacts include river avulsion, downstream aggradation, and retrogressive erosion of the headwater channel. These effects are not limited to the immediate area near the landslide site, but can extend many kilometres downstream from the failure site. Examples where catastrophic failure had lasting impacts include the Falling Mountain landslide, whose impacts have affected the area since the event took place in 1929 (Korup *et al.*, 2004), and the Mt. Adams landslide in 1999, which shifted a previously erosional environment into one of deposition, creating alluvial flats where there were once bedrock gorges.

Alternatively, sediment contributions from a smaller consistent supply (smaller than a mass failure) can have similar long-term impacts on nearby rivers. The Waipaoa catchment in the eastern North Island, New Zealand, highlights how continual erosion of gully systems can have long-term effects on the system due to storage (Gomez, *et al.*, 2003). It was found that while only 6% of the catchment was affected by gully erosion, 28.7 Mt of sediment was generated in 38 years (1950 – 1988) of which 48% was stored along 8 km of the lower Te Weraroa Stream. This sediment storage will likely take many decades to be depleted.

1.6   Management of large, slow-moving landslides

The processes that initiate translational landslides are generally attributed to stream incision at the toe, but some landslides are a result of unidentified factors (McColl & McCabe, 2016). Therefore, management of large, soft-rock translational landslides requires intimate knowledge of the processes involved in landslide initiation and motion to effectively mitigate the impacts. Management of these large landslides also needs to include scientists, the community, and the local council. Difficulty occurs when the community oppose the proposed mitigation options for a range of reasons, described aptly in Fleming *et al.* (1979):

- o   The general dislike of regulation or interference
- o   Considering landslides uncooperative to mitigation

○ Believing the landslide lacks the severity or economic loss to justify mitigation efforts

This opposition can severely reduce the effectiveness of management strategies. Therefore, clear demonstration of the economic and social benefits is key to achieve support for the mitigation options (Fleming *et al.,* 1979).

Potential management strategies can be categorised into three groups; re-active management, changes in land-use, and active management (McColl & McCabe, 2016). Re-active management involves reacting to any impacts while still retaining land functionality. Land-use changes require converting or retiring land to best reduce the impacts and potential hazards. Active management is when active measures are taken to reduce landslide movement and decrease future impacts (McColl & McCabe, 2016). The use of these strategies is dependent on cost, with active management generally very costly in the short term while re-active management can become very costly in the long term.

The Taihape case studies have experienced several different management options. For example, the Rangitikei Slide has had surface water drainage changed to reduce movement rates. This is a form of active management and has occurred on the Taihape and Utiku Landslides, where subsurface drainage was installed to remove excess water from the landslide (McColl & McCabe, 2016). The Rangitikei Slide has also experienced re-active management with the repairing of fences and farm tracks, as has the Bird Landslide. However, in 2012 some buildings and stockyards on the Bird Landslide were abandoned due to flooding (Fig. 10), and certain paddocks were retired from grazing (McCabe, 2013). This is an example of land-use change when re-active management was no longer feasible.

While these management strategies were well-meaning, some are arguably less effective with slow-moving landslides due to the generally consistent movement rates which can deform and overwhelm rigid structures. Examples include the Ca' Lita landslide in Italy, which was jeopardising numerous houses and a main road for the upper watershed area (Corsini *et al*., 2006). 'Structural mitigation' was undertaken to try to prevent damage to these structures through excavating toe advancements, surface drainage networks, and retaining walls to protect the integrity of the drainage networks. However, Corsini *et al*. (2006) were aware that semi-rigid structures such as the retaining walls would likely suffer damage as the land moved, and that the purpose was to protect the drainage networks (including drainage wells) for as long as possible rather than acting as an actual retention system. This is an example where mitigation efforts accounted for the destructive nature of slow-moving, deep-seated landslides. Sound

understanding and expert advice is critical if effective strategies are to be attempted on these large, complex landslides.

1.7   Research gap

A research gap is present around large, slow-moving landslides, with limited data on high temporal resolution movement drivers - particularly event-based movement data and the role of river incision on movement rates.

While previous literature has found strong seasonal patterns in the movement rates of these features and identified periods of accelerated movements within this larger trend (Massey *et al*., 2013), there is a lack of studies focused on movement at a daily timescale controlled by individual events. There have been recent studies using high-temporal resolution data to capture slow-moving landslides movement patterns (Utiku – Massey *et al*. 2016; Erlenbach Landslide – Golly *et al*., 2017). However, there is still limited data on the influence of individual events (i.e. flood events) on movements rates, which requires further investigation.

1.8   Objectives

There were a series of aims in this research:

- Assess the movement patterns (rate, bearing, and location) of a large, slow-moving landslide in the central North Island, New Zealand (Rangitikei Slide).
- Determine movement drivers; this could be river incision, groundwater fluctuations or seismic activity (according to studies of nearby slow-moving landslides).
- Estimate the sediment delivery from the Rangitikei Slide during the study period, to inform the level of sediment yield that can occur from slow-moving landslides connected to a fluvial system.
- Propose any appropriate management strategies for the Rangitikei Slide informed by better understanding of movement patterns and drivers, with reference to wider landslide management.

These aims will be achieved using surface monitoring techniques to identify movement patterns and compare these against measured environmental factors to determine primary movement drivers. Photogrammetry and pixel tracking will indicate geomorphic change, including sediment delivery to the Rangitikei River. This case study can be utilised to inform management of similar landslides around New Zealand (slow-moving landslides in weak Neogene-aged geology), of which there are over 7,000 mapped in New Zealand (Dellow *et al*., 2005; Massey, 2010; Massey *et al*., 2013).

2   Site description

The Rangitikei Slide is located south of Taihape in the central North Island, New Zealand, within a larger mass movement complex; the Poroa Complex (Figure 6). The North Island is influenced by a plate boundary involving the Pacific Plate subducting beneath the Australian Plate out to sea on the east coast. This tectonic activity has formed a diverse topography, including a volcanic zone in the central North Island, and areas of hill country which have been dissected by large rivers and the river terrace sequences preserved by continued uplift. Landslide susceptibility in these hill country areas, including around the study site, is high as a result of deformed geology (from tectonic influence) and thin clay seams throughout the sedimentary sequence (deposited as ash from volcanic eruptions and weathered to clay) which reduces the stability of slopes. Taihape experiences a temperate maritime climate, with warm summers and cool winters, and a mean annual rainfall of ~960 mm spread consistently across the year (Massey, 2010; McCabe, 2013; Massey et al., 2016a). The Rangitikei River runs below the landslide toe and is considered a significant feature in the landscape as it cuts across the southern edge of the Poroa Complex (Figure 6).
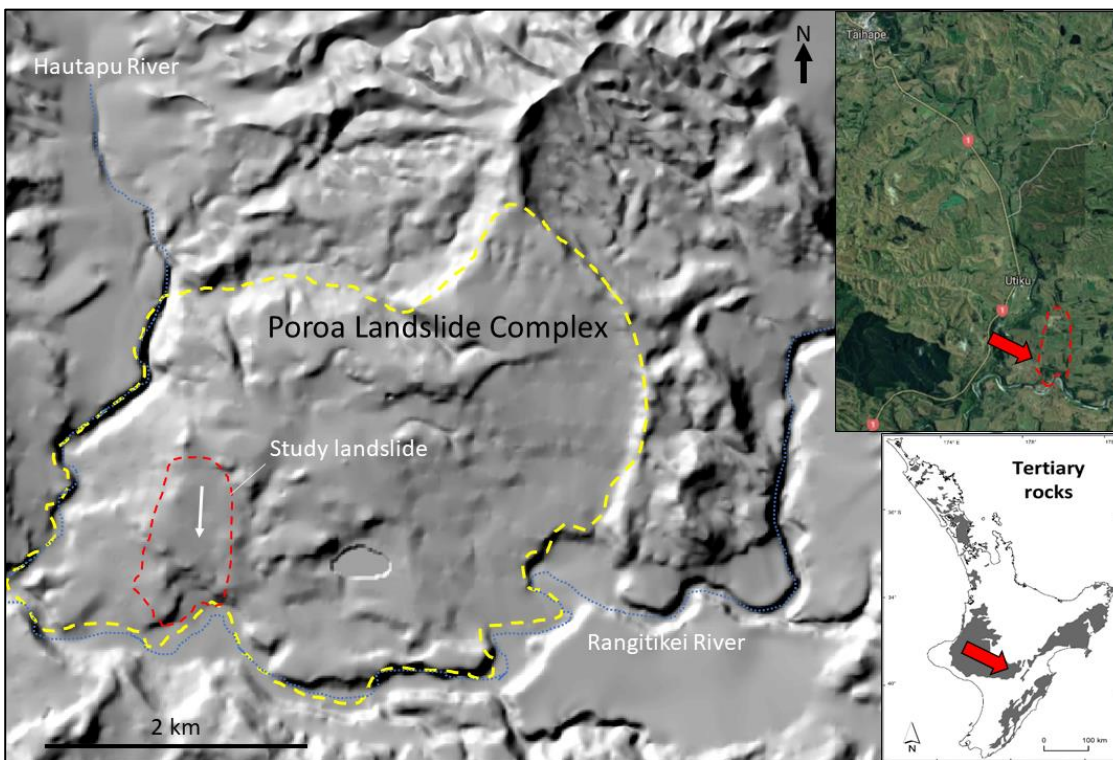
Figure 6. Study site area showing a hill shade of the Poroa Slide Complex, the location in relation to the North Island, and location in relation to Taihape.

This research is focused on a large (~50 ha), slow-moving translational rockslide (Cruden and Varnes, 1996) in Neogene-age sedimentary rocks in the central North Island, New Zealand. This

landslide was previously identified by Thompson (1982) and named the Rangitikei Slide. The purpose of this chapter is to provide a regional context for the study site.

2.1 Geological setting

New Zealand is an active tectonic setting, with a subduction zone (Figure 7) to the east of the North Island in the Hikurangi Trough between the Pacific and Australian Plates (Lee et al., 2011). Most of New Zealand was submerged around 23 Ma (start of the Neogene period) following an extensional tectonic phase (Bassett, 2014), and formed a series of young marine rocks across much of the country. Most of the geology within the Wanganui Basin, which contains the study site, was formed during the later stages of this period during the Pliocene and Pleistocene (5 Ma to present) (Journeaux et al., 1996). The rocks formed in a marine shelf environment within the basin, but during this period the northern margin was uplifted - due to a southern shift in the Wanganui basin depocentre - which resulted in older sediments becoming exposed on the northern edge. As a result, the sediments become progressively younger as you move southward (Journeaux et al., 1996). The study site location is within the back arc of the subduction zone, south of Mt. Ruapehu (Figure 7), which means there is a strong tectonic influence in the form of deformed basement rocks from folding and faulting in the axial ranges. The study site contains Neogene sediments (24 Ma) which formed during the extensional phase (when New Zealand was submerged) and experienced the subsequent compressional phase that uplifted New Zealand. The Wanganui basin, and other areas of the country, still experiences uplift, which has been quantified recently at approximately 1.5 to 2.0 mm/year (Pillans, 1986; Pulford & Stern, 2004). These processes have created an environment susceptible to deep-seated landslide formation due to the weakened geology (from folding and faulting) and the presence of clay seams throughout the stratigraphy (weathered volcanic ash) that can be utilised as landslide failure surfaces.
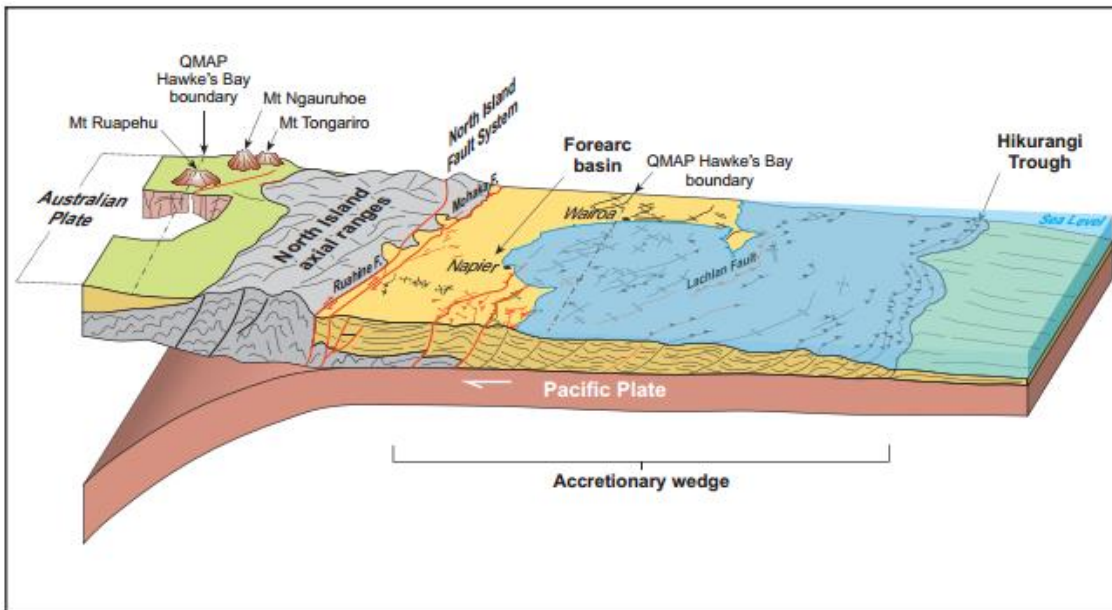
Figure 7. Schematic of the current tectonic setting for the east coast of the North Island, New Zealand. The Pacific Plate is subducting under the Australian Plate ~43 mm/yr (Lee et al., 2011). This has formed numerous faults and folds across New Zealand, and encouraged uplift. From Lee et al. (2011).

2.1.1 Geology

The cover rocks of the Taihape region comprise Neogene (24 Ma) sedimentary rock, predominantly marine sediments that accumulated in a shelf environment (Journeaux et al. , 1996; QMap Series, Lee et al., 2011; Massey et al., 2013; Massey et al., 2016). The study site is comprised of the Paparangi Group, the Utiku Group, and the Tangahoe Mudstone, which lie within the Rangitikei Supergroup. The Neogene sedimentary rocks cover over 40% of New Zealand (Figure 8), but are particularly concentrated in the central North Island. The study site geology includes silty, fine sandstones and sandy siltstones (Massey et al., 2013), with occasional shell beds and concretionary layers' present (Massey et al., 2016a).

The Taihape region is dominated by 'soft' Neogene sedimentary rocks with clay-rich bedding thought to be present throughout. The Neogene sedimentary rocks are categorised as 'soft' due to the low intact strength or low Uniaxial Compressive Strength (q_u), which falls between weak and very weak in the New Zealand field classification guide (NZGS, 2005). This means that the rocks can be cut with a knife in some areas or crumbles under the force of a geological hammer in others (Massey, 2010). The soft and poorly consolidated nature of the rocks has been linked to the susceptibility of Neogone-age material to landsliding (Massey, 2010). There are also other factors influencing the susceptibility including incising rivers, bedding-plane defects, and bedding-parallel clay seams (Massey et al., 2013).

Figure 8. Location of Neogene sedimentary rocks around New Zealand, and the Utiku landslide highlighted in a significant area of Neogene rock (Massey et al., 2013).

Many of the large, translational landslides in the lower North Island are thought to be sliding along thin, low angle clay layers with low friction angles (some < 10°) that act as planar failure surfaces (Massey, 2010; Massey et al., 2016a). These thin (1-10 cm) clay layers are composed of

montmorillonite-type clay of the smectite group (Brown, 1974; Massey et al., 2016a), which are thought to be present in most fine-grained Tertiary sedimentary rocks, and are considered an important factor in slope failure. Clays vary in strength, with illite and montmorillonite clays having lower shear strengths compared to kaolinite or chlorite clays (Ohlmacher, 2000). A clay layer found in the Utiku landslide had high concentrations of montmorillonite, and was thought to be a controlling parameter in the location and movement of the landslide (Brown, 1974). Eight clay seams have been found in the Utiku and Tarare Sandstone Groups at varying stratigraphic levels (Massey, 2010), which are likely present in the Rangitikei Slide stratigraphy. The high strength contrast between the dominant lithology and the thin clay layers influences slope stability and can dictate the location and geometry of deep-seated landslides (Mountjoy & Pettinga, 2006). The Paparangi Group (Figure 9A) is comprised of massive mudstone and concretionary sandstone, with the silty sandstone near the base fining upwards into mudstone with large concretions present (Lee et al., 2011). The mudstone is 440 m thick in the Rangitikei River valley. The Group formed in an outer shelf to upper bathyal environment in the middle to late Pliocene.

The Utiku Group (Figure 9B), measuring 310 m thick, is composed of alternating fine-grained sandstone, concretionary sandstone, and sandy mudstone, and can have a 10-20 m thick limestone cap on top (Thompson, 1982; Journeaux et al., 1996; Lee et al., 2011). This group is understood to be of middle Pliocene age, and deposited at inner to mid-shelf marine depths. The Utiku Group can be separated into individual lithologies; the Tarare (bottom), Kawhatau, and Manui (top) formations. The Tarare formation, also known as the Tarare Sandstone, comprises siliclastic silty sandstone and sandstone layers, with some concretions and fossils present (Journeaux et al., 1996).

Figure 9. A) Photo showing the poorly bedded, gently dipping Paparangi Group mudstone along the Rangitikei River, in a cliff approximately 70 m high (Lee et al., 2011). B) An outcrop of the Utiku Group in the Rangitikei Valley. The grey section in the middle is likely sandy mudstone (Lee et al., 2011).

The Kawhatau formation is similar, consisting of siltstone and sandstone layers, and the Manui formation includes silty sandstone and sandstone layers. The Tangahoe Mudstone, previously known as the Taihape Mudstone (Thompson, 1982), is found at the bottom of the Rangitikei Supergroup and is of early Pliocene age (3.6 – 5.3 million years old). The Tangahoe Mudstone, referred to as the Taihape Sandstone by Thompson (1982), is described as a silty sandstone, with an upper sandstone and lower siltstone unit, which conflicts with the mudstone classification (Massey, 2010). The Tangahoe Mudstone, up to 500 m thick, extensively crops out in the Taihape area, and has large concretions common in the upper section. It is pale to medium grey in colour, massive to weakly bedded, and has a locally unconformable contact with the overlying Utiku Group (Lee et al., 2011). It is also the primary lithology of the Poroa Complex (Figure 10), and thus the Rangitikei Slide (Figure 11).

The overlying cover beds contain landslide deposits (Figure 12), including poorly to unconsolidated deposits ranging from coherent to broken rock (QMap Series Lee et al., 2011), fan deposits, both alluvial and colluvial, and river terraces. Thompson (1982) highlighted the dominance of landslide debris and numerous slides or slump blocks throughout the complex (Figure 13) (Thompson, 1982).
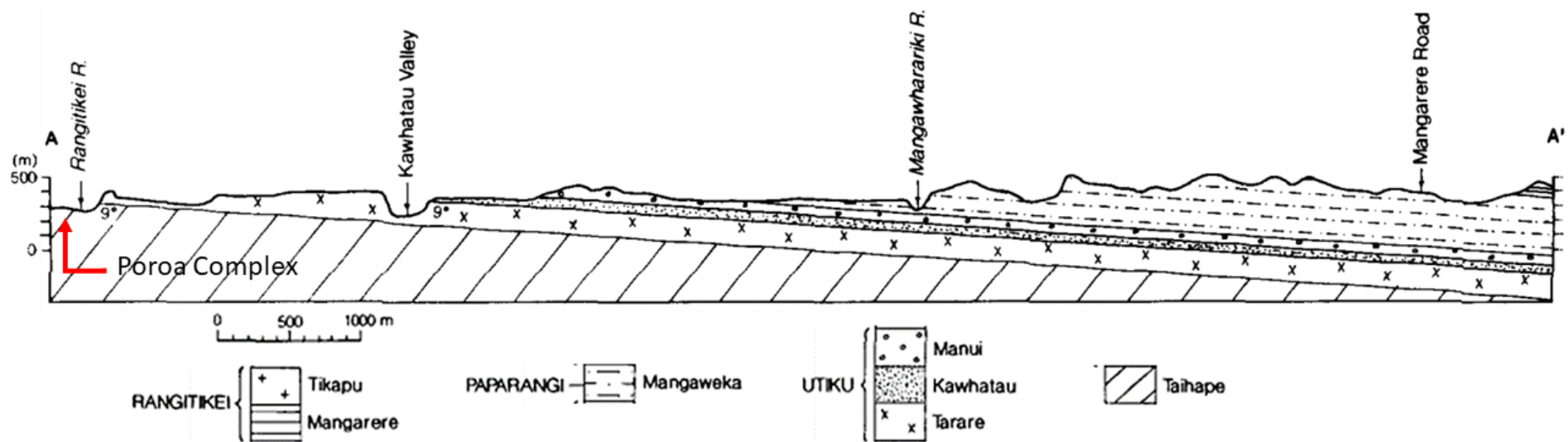
Figure 10. North-south cross-section of the Taihape-Mangaweka area, from just above the Rangitikei River, past the Mangaweka township to Manarere Road. This highlights the shallow dip, and that the Poroa complex is primarily composed of Tangahoe (Taihape) Mudstone (Journeaux, Kamp, & Naish, 1996).
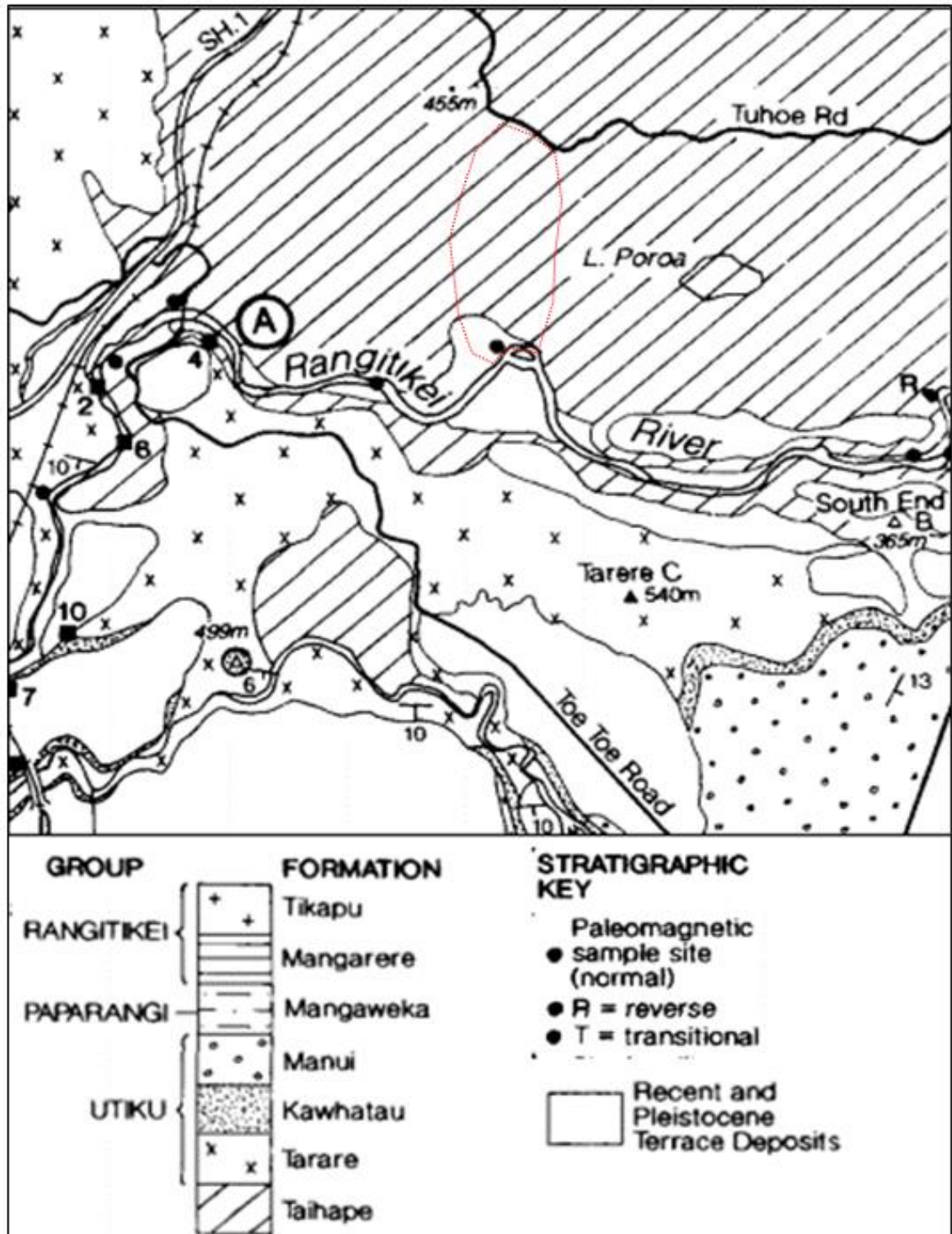
Figure 11. Geological map of the study site area (Rangitikei Slide shown in red), with a sample site taken from the earthflow area of the Rangitikei Slide by Journeaux et al. (1996). The map shows that the majority of the Rangitikei Slide comprises Taihape mudstone, with the toe area predominantly composed of recent terrace deposits.
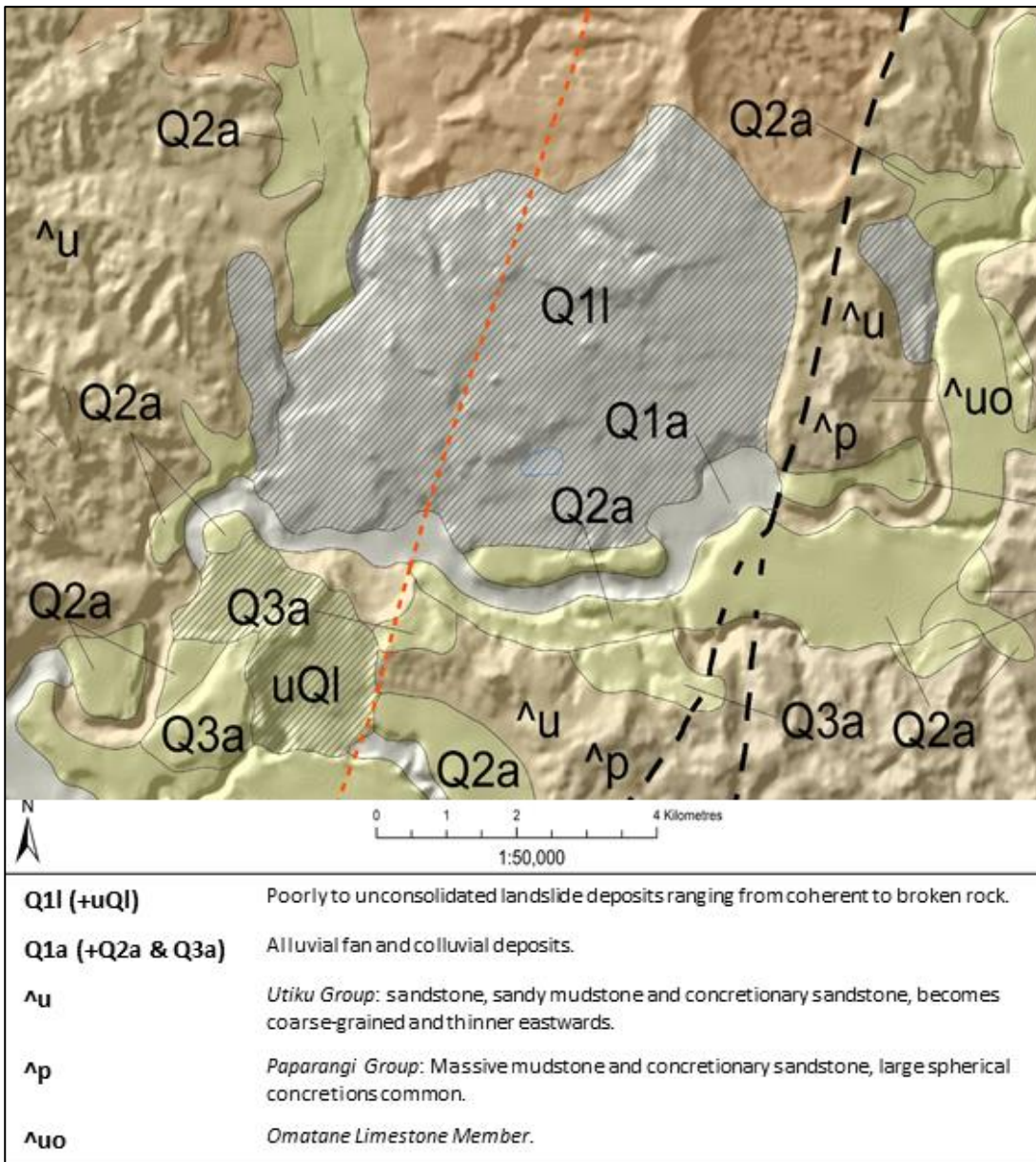
Figure 12. Geology of the Poroa Complex, taken from the Qmap of the Hawkes Bay geology (Lee et al., 2011). The map shows the locations of the Poroa complex, Utiku Slip, the study landslide, and where the Utiku anticline (red dashed line) and Omatane Fault (black dashed line) run through the complex.
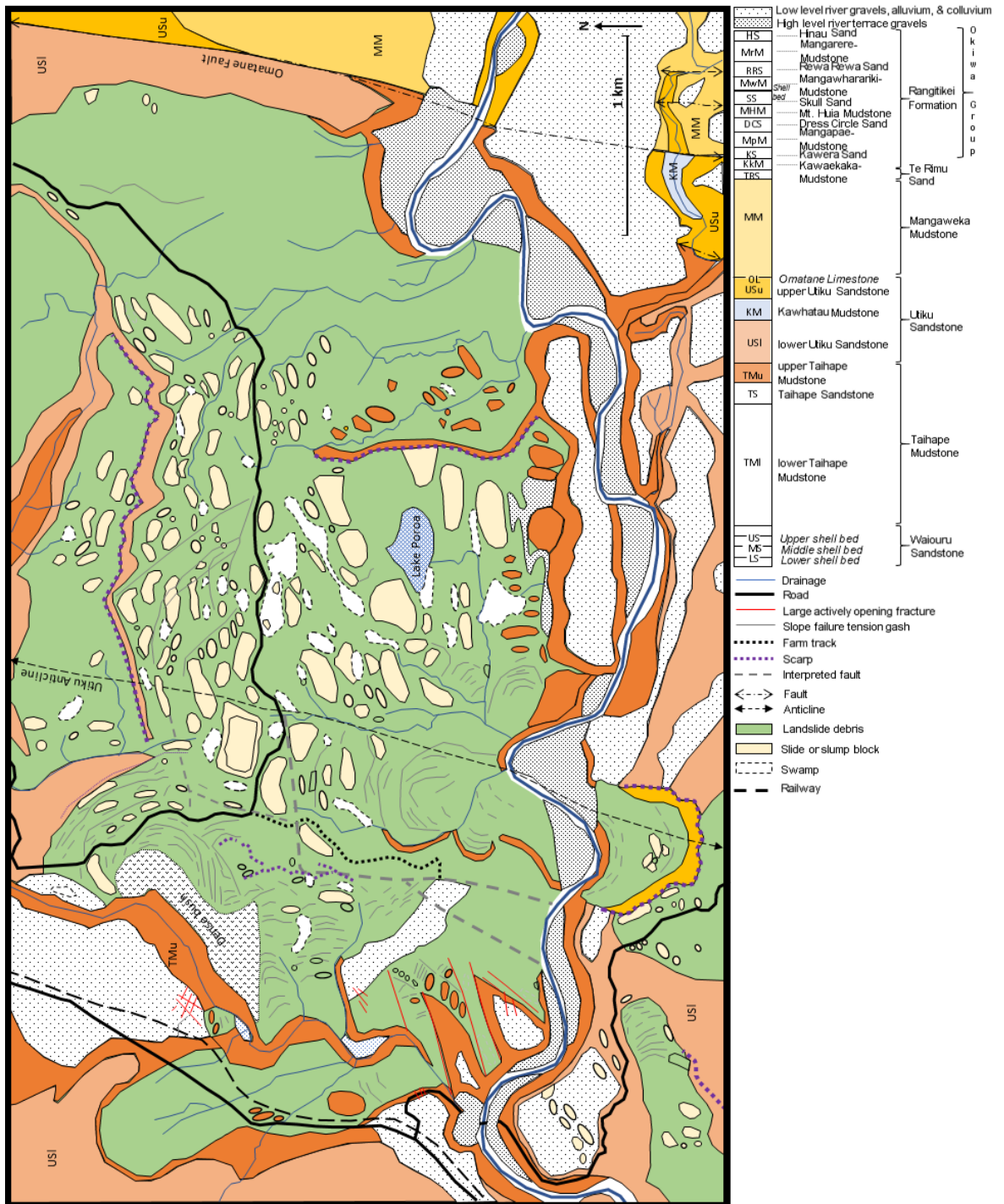
Figure 13. Geological map of the Poroa complex, redrawn from Thompson (1982).

The bedding within the Poroa complex has a dip of 3-7° and a direction locally variable between south-east and south-west (Thompson, 1982; Massey, 2010; McColl & McCabe, 2016). This local variation in dip results from folds and faults that distort the landscape, due to continuous east-west compression from the plate margin along the east coast of New Zealand (Massey, 2010). This compression formed an anticline through the Poroa Complex, trending NNE-SSW, with the western side dipping to the southwest and the eastern side dipping to the southwest (Figure 12 and Figure 13) (Thompson, 1982; Massey, 2010; Lee et al., 2011).

29

2.2 Geomorphology

The Taihape area is categorised as dissected hill country due to the steep terrain which has been cut by numerous high order rivers such as the Rangitikei. River incision is significant in the area, with several levels and ages of river terraces visible around the landscape (Figure 14) (Massey, 2010; Massey et al., 2016a). These terraces range from low, recent alluvial terraces (Ohakean and younger) to older high terraces, which have been approximately dated up to 20,000 years B.P. The terrace across the Rangitikei river from the study site is a Rewan terrace, with an Ohakean terrace above it and more Ohakean terraces further upstream (Figure 14).

The Poroa complex is particularly impacted by river incision, as the Rangitikei and Hautapu Rivers dissect the western and southern edges (Figure 14), cutting the toes of the many sections and undermining slope stability. It has been theorised that post-glacial river incision initiated many of the landslides around New Zealand (Bilderback, et al., 2014), with the age of some failures near the study site dated around 17,000 BP (Thompson, 1982). There is a noticeable pattern between landsliding areas and incising rivers (Thompson, 1982; Massey, 2010), where many landslides occur on the slopes of rivers. This can be linked to incision, where downcutting destabilises slopes and initiates mass movement formations. This relationship is similar to gully formations, with river incision causes destabilisation and initiates gullying. These gullies are also prevalent around the North Island and there is a concentration on the east coast, where a combination of river incision and deforestation has enabled gully formation and the sedimentation of waterways. It has been established that both gullies and mass movements are pervasive components of post-glacial landscapes (Gage & Black, 1979; Gomez & Livingston, 2012). Post-glacial landscapes experienced significant incision following associated climate changes, and this oversteepened valley sides which initiated slumps and earthflows (Gomez & Livingston, 2012). For example, Cerovski-Darriau et al. (2014) found that the Waipaoa River, a river that contains several significant gully systems, rapidly incised up to 120 m as a result of post-glacial warming, creating perched hillslopes unadjusted to the new channel elevation. This promoted gullying and mass movement formation. In the Taihape region, the slopes are steep with many river banks oversteepened to form cliff faces, which contrasts against the many river terraces (Figure 15), and slopes are often marred with shallow landslide scars following high rainfall events, indicating the erodibility of the landscape.
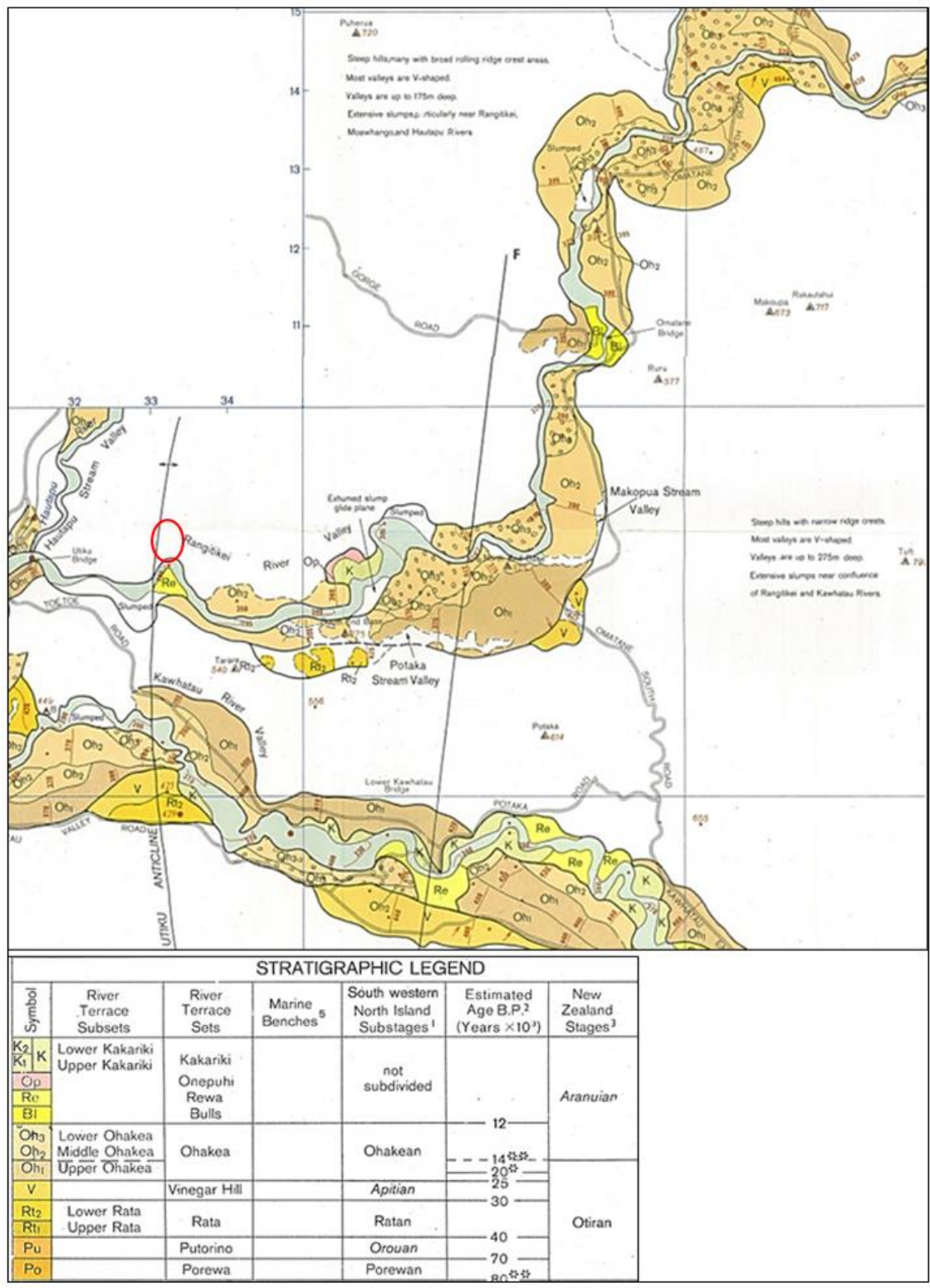
Figure 14. Map of the river terraces in the Rangitikei Basin, with the river bend below the study site depicted with a red arrow (Milne, 1973)
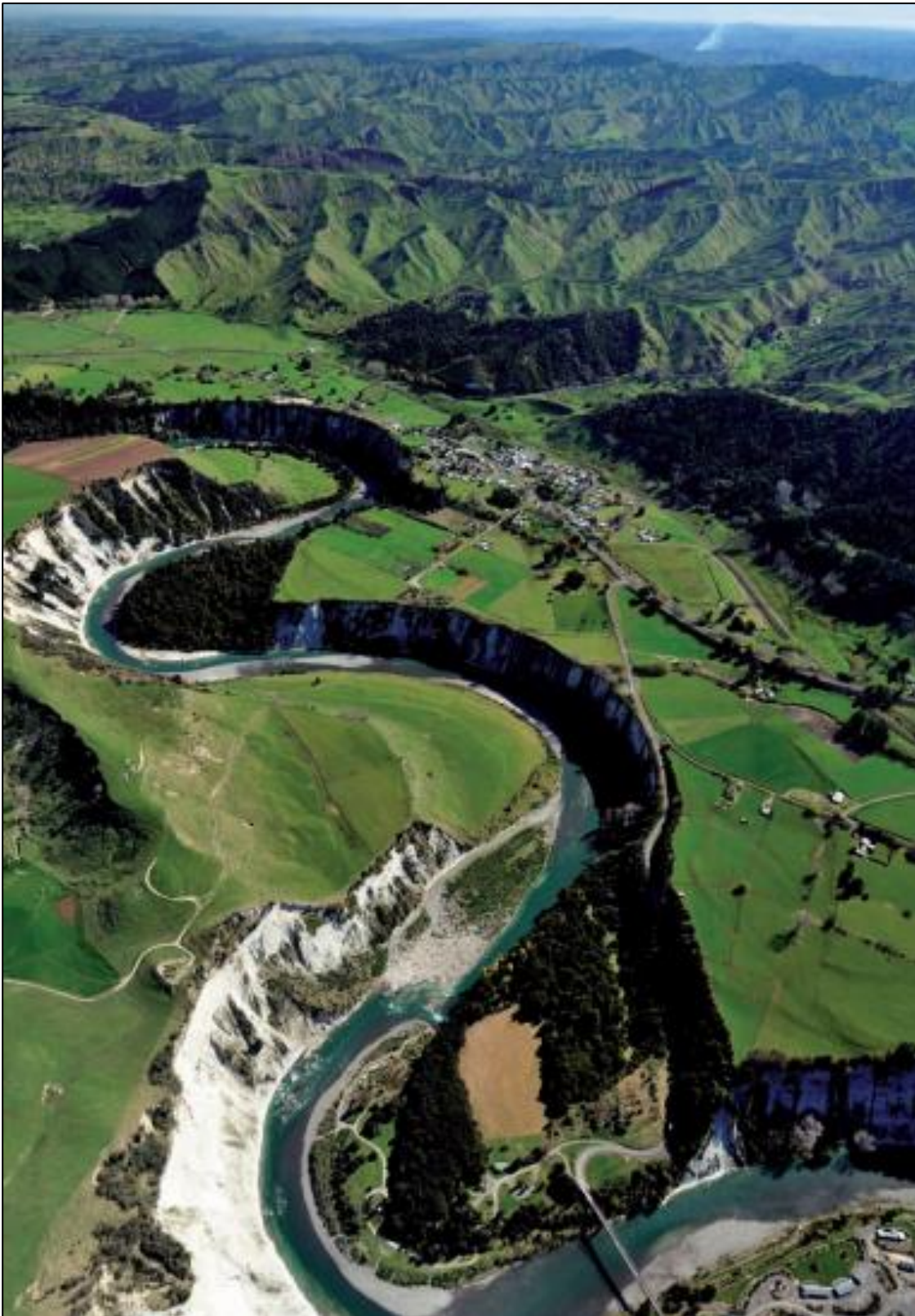
Figure 15. Photo of the Rangitikei River beside the Mangaweka township, showing significant incision creating river terraces. This area is less than 10 km downstream from the Poroa Complex and represents the typical valley terrain of the area (Lee et al., 2011).

2.3 Climate

The Taihape area experiences a temperate maritime climate, with warm summers (December - February) and cool winters (June - August), and average daily temperatures of 22°C and 11°C respectively (Massey, 2010; McCabe, 2013). According to the Taihape rain gauge, the mean annual rainfall in the area is ~960 mm, varying little between winter (mean monthly rainfall 70 mm) and summer (mean monthly rainfall 81 mm), with no distinctive east-west rainfall gradient (National Institute of Water and Atmospheric Research; Figure 16); Massey, 2010; McCabe, 2013; Massey et al., 2016a).
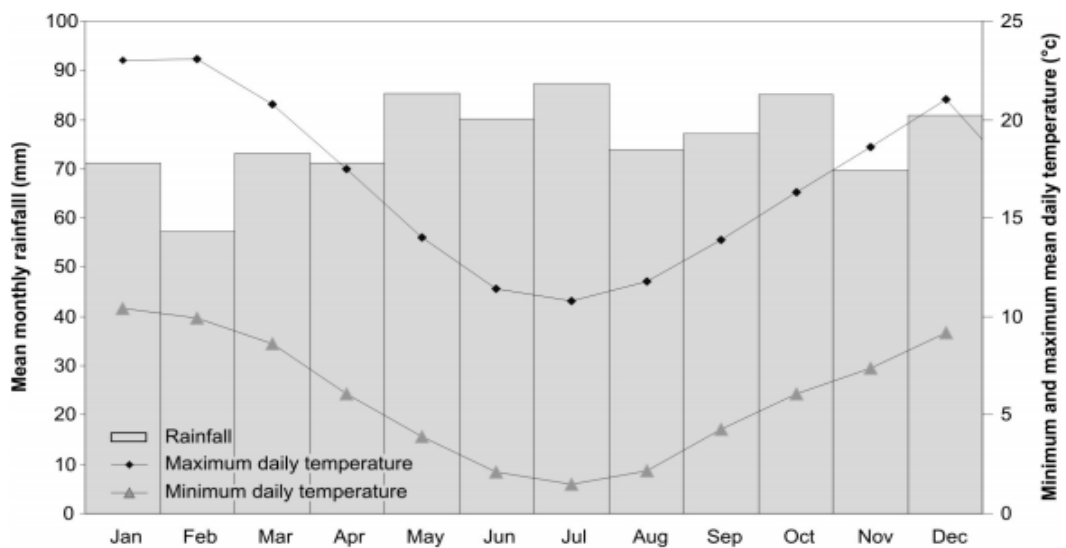
Figure 16. Taihape rainfall and temperature trend from 1951 to 2009 (from NIWA in Massey, 2010). The graph shows the mean monthly rainfall and the max. and min. daily temperature within this period.

2.4 Poroa complex

The Rangitikei Landslide lies within the Rangitikei catchment, and is an active section of the Poroa mass movement complex. The Poroa complex covers an area of 1,100 ha (10 km^2) and is bounded to the west by the Hautapu River and to the south by the Rangitikei River (Figure 17), highlighting the likely influence of incision in translational landslide movement (Massey, 2010; McColl & McCabe, 2016). The Poroa complex, also known as the Poroa Slide complex (Thompson, 1982; Massey, 2010), comprises approximately 20 landslides (Thompson, 1982; Massey, 2010), with many of these believed to be moving along the same clay layer as the Utiku Slip, which is on the opposite side of the Hautapu River (Figure 18). The Utiku clay layers have been cut by the Hautapu River, allowing them to 'daylight' (Massey, 2010). While the Utiku Slip, unusually, moves along strike, the Poroa landslides appear to be generally moving down-dip. The dip-direction, and therefore movement direction at the Poroa complex varies from NW to SE due to the presence of an anticline through the centre of the complex (Massey, 2010).
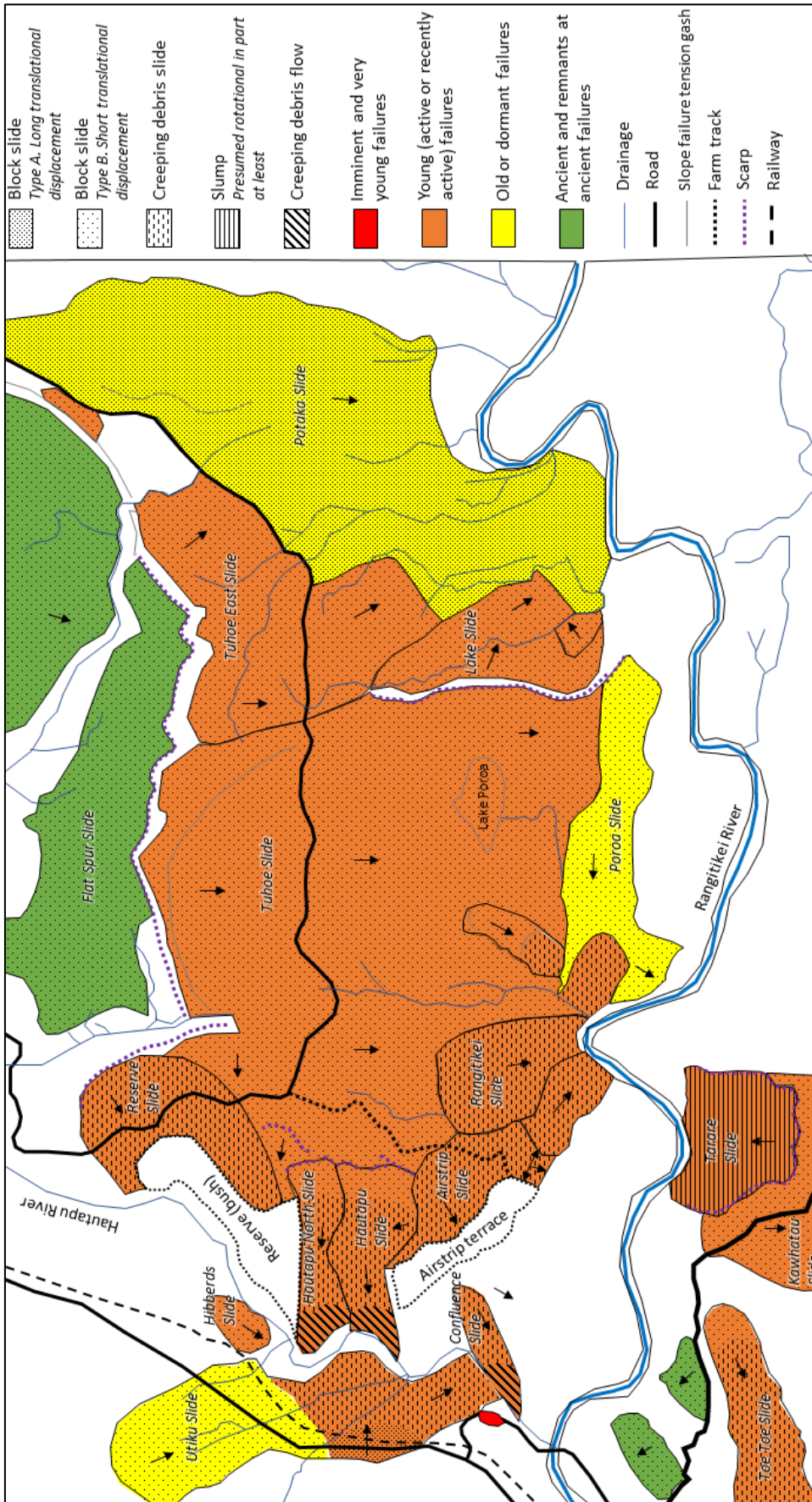
Figure 17. Slope failures of the Poroa Slide Complex, redrawn from Thompson (1982).
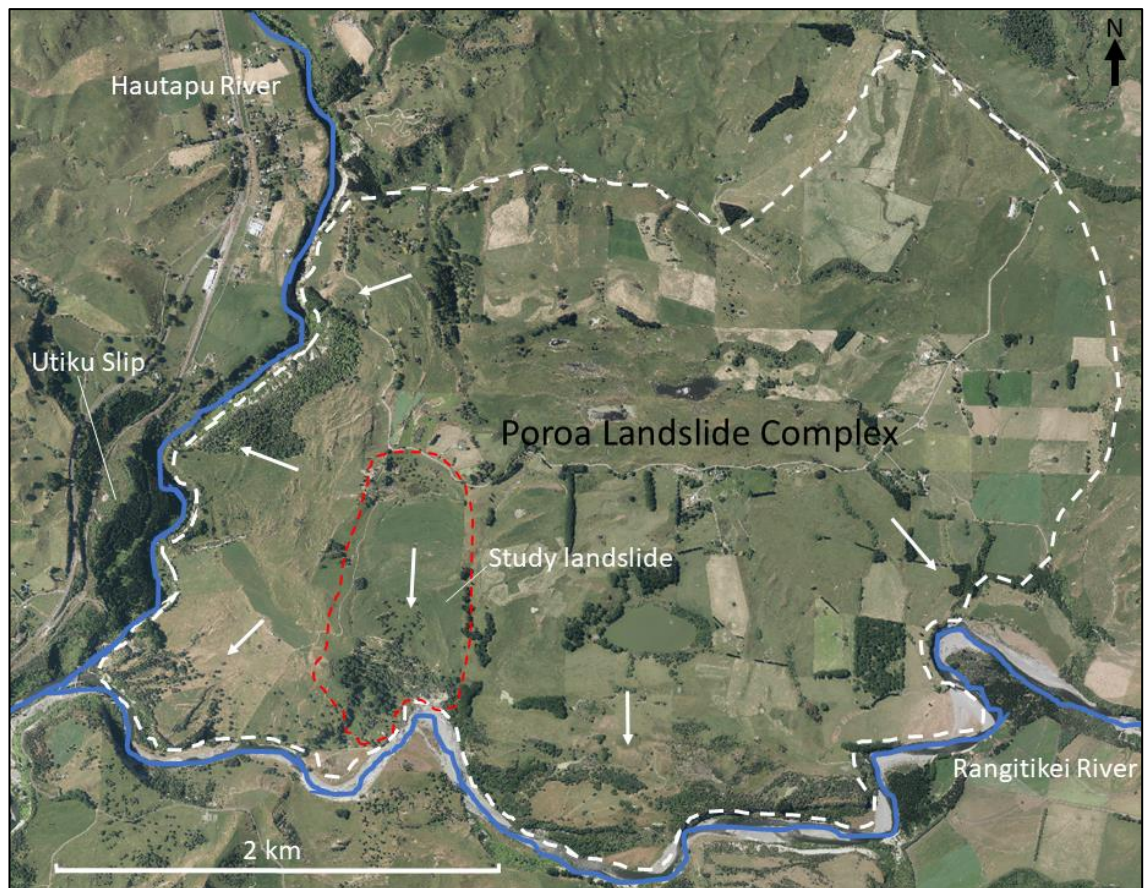
Figure 18. Poroa complex with white arrows indicating general movement directions and the white dashed line showing the boundary (modified from Thompson, 1982; Lee et al., 2011; McColl & McCabe, 2016, and using a Digital Elevation Model of the area). The red dashed line marks the boundary of the Rangitikei Slide in this study. Aerial imagery from summer 2015/2016 by Horizons Regional Council. Imagery credit: MWLASS 2016

The Poroa complex is suggested by Thompson (1982) to have formed in phases, with the initial movement site marked by the Flat Spur Slide in the northern area of the complex. Based on the presence of some Kawakawa Tephra exposed nearby, the slide is possibly older than 20,000 years old. The Tuhoe Slide, running through the complex centre, marks the second phase of movement in the complex (Thompson, 1982). This slide is 2 km^2 in size and moving southwards, and Thompson included smaller block slides and debris slides in this slide including the Rangitikei Slide. The last recorded major movement of the Tuhoe Slide was around 1925 (Milne, 1973), and reportedly dammed Lake Poroa, although the lake is believed by local iwi to be much older than this. Some landslides in the complex are estimated to be over 20,000 years old, but most of the currently active landslides are less than 1,800 years of age (Thompson, 1982). Based on personal communications, most movement was reported in the summer months when the land dries (Thompson, 1982), although this contradicts more recent landslide studies. This was also reported by landowners rather than investigated using objective methods, and without consideration for wider controlling factors such as high flows which can be common in summer months.

The Poroa Slide truncates the Tuhoe Slide, cutting across the toe at right angles and moving on a surface with a very low dip angle (Fig. 13). The boundary to the north is marked by a swampy drainage area, and the southern edge is bounded by a middle Ohakean river terrace (14,000 years BP) which separates the slide from the Rangitikei River (Thompson, 1982).

2.5   Rangitikei Slide

The Rangitikei Slide is situated on a dry stock farm in the Taihape region, New Zealand. The Rangitikei River cuts the toe of the landslide, and movement is understood to have been ongoing for generations according to the Farm Manager. First impressions of the site indicated that there was nothing markedly different to other large, slow-moving landslides in the region regarding geology, geomorphology, seismicity, and climate. Most noticeable was the position of the Rangitikei River, flowing at the toe of the landslide, which is a significant river in the North Island, New Zealand. The river enters a sharp true-left bend at the landslide toe, increasing the likelihood of bank erosion.

3 Methodology

The objectives of this research are to assess the movement patterns of a large, slow-moving landslide, and identify the primary movement drivers. To achieve these objectives, several surface monitoring techniques were adopted to achieve the temporal and spatial resolutions required to capture the different movement patterns, such as seasonal and daily movement. Numerous methodologies are employed by different landslide studies to monitor displacement and evolution through time, with the approach taken dependent on the desired data resolution and collection frequency. Each methodology yields different spatial and temporal resolutions, with associated advantages and disadvantages (Table 1).

Table 1. Advantages and disadvantages of the different methods of measuring displacement, from Mansour et al. (2011)

Instrumentation type	Advantages	Disadvantages
Manual inclinometers	- Can measure displacements as low as a fraction of a millimeter.	- Slope indicator casings are broken at cumulative displacements of about 130 mm. Therefore, the lifetime is short in very slow and slow slides.
	- Temporal resolution can be improved by increasing the frequency of measurements, i.e., every day or less.	- Measure the displacement versus time at a single point. Thus, there is no spatial coverage for large sites. Hence, the technique is not economically feasible for large sites.
		- Highly frequent monitoring of manual inclinometers is expensive for remote sites in terms of a technician wages.
In-place Inclinometers	- Overcome the temporal resolution drawback of manual inclinometers. The sensor is connected to a data-logger that records the displacements at intervals as short as required.	- The location of the rupture surface should be determined before the installation of the in-place inclinometers. Therefore, a slope indicator casing should be installed first.
		- Have the same drawback of the low spatial coverage as manual inclinometers.
Extensometers	- Measure the displacement by measuring the opening of cracks	- Do not measure large displacements and, hence, not suitable for measuring displacements of slow slides or the upper range of very slow slides.
	- Do not require deep installations	- Measure the displacement at discrete points and, hence, do not provide good spatial coverage for large sites.
		- Measure surface displacements rather than the displacement at the rupture surface elevation.
		- Unable to determine the location of the rupture surface.
Remote techniques (InSAR, DInSAR, TLS, etc.)	- Suitable for measuring relatively large displacements (slow and the upper range of very slow movements), which cannot be captured by inclinometers or extensometers.	- May not be able to capture extremely slow movements over the monitoring interval, which is around a month.
	- Overcome the spatial resolution drawback of the previous techniques by providing coverage to large sites as long as reflective objects are present or installed at strategic locations across the site.	- No coherence is expected to occur if no reflective surfaces exist or are installed.
		- Measure the surface displacement rather than the movement of the rupture surface.
		- Unable to determine the location of the rupture surface.
		- Unable to determine the location of the rupture surface.
Surface surveying	- Suitable for measuring relatively large displacements (slow and the upper range of very slow movements), which cannot be captured by inclinometers or extensometers.	- Extremely slow movements may fall below the accuracy of the measuring instruments (total station).
	- Overcome the spatial resolution drawback of inclinometers and extensometers by providing coverage to large sites as long as surface targets are installed at strategic locations across the site.	- Measure the surface displacement rather than the movement of the rupture surface.
	- The installation of surface targets for surveying is less expensive than installing corner reflectors for satellite imagery.	- Unable to determine the location of the rupture surface.
Geomorphologic evidence	- Very useful in quantifying long-term movements that occurred over many years and where there is no other method of measuring the movement.	- Cannot account for very slow or extremely slow movements because of the small scale of air photos.
		- Measure the surface displacement rather than the movement of the rupture surface.
		- Unable to determine the location of the rupture surface.

Cost, time, and manpower also influence the appropriateness of each methodology in a study, as a limited amount of any of these factors reduces the utility of certain methods. When choosing appropriate methods for a study, there is an interplay between external influences (e.g. budget and time) and the characteristics of the method i.e. data resolution and whether this fulfils your requirements. There is a necessary balance between, for example, the ideal spatial data resolution and time required to employ a particular method of surface surveying; for instance, repeat Total Station or GPS surveys could be used to detect mm-scale movements, but they are time-intensive, particularly if used over a large area. Alternatively, photogrammetry or airborne or terrestrial laser scanning offer relatively dense data collection over a short time-period, making them useful for large areas (Brasington *et al.*, 2000).

This study focused on surface monitoring over a large area (~50 ha), and needed a range of temporal and spatial resolutions to provide information for the different landslide areas (head scarp area vs. toe area) and produce results over different timescales. This was necessary to achieve the research objectives – identification of movement patterns and exploration of movement drivers – which can occur over a range of timescales (individual event, seasonal, or annual), and influence areas of the landslide differently due to complex interactions between intact blocks. This led to the use of a RTK-dGPS network (seasonal differences) in conjunction with pixel tracking of the toe (event-based displacements), to capture movement spatial and temporal patterns of movement for correlation with environmental factors (rainfall and flood events). Geomorphic methods (photogrammetry and geomorphic mapping) were used to further identify the active landslide boundary and the areas experiencing the most prevalent geomorphic change through time. The methods utilised in this study included equipment that was readily available for use (RTK-dGPS, time-lapse camera set-up, and UAV for photogrammetry) and only required an equipment hire cost.

This study does not address any subsurface investigations (groundwater and subsurface deformation) due to time and site access limitations. It is instead assumed that rainfall is driving pore-water pressure changes within the landslide, a well-known process (Picarelli, 2007; Massey, 2010; Nafarzadegan *et al.*, 2013), and subsurface deformation is inferred to be represented by the surface deformation as the Rangitikei Slide is considered to be a translational slide, which involves the movement of the entire mass from one location to another using a planar failure surface (Varnes, 1978; Massey, 2010; McCabe, 2013).

3.1   Geomorphic assessment of landslide movement

Two methods were used to assess the movement mechanisms of the Rangitikei Slide to define the landslide boundary and different movement zones by focusing on landslide geomorphology

to indicate movement patterns. Photogrammetry was used to create a 2-D orthophoto and Digital Elevation models (DEMs). DEM differencing was used to compare a series of DEMs of the slide over one year to highlight specific areas of geomorphic change and quantify sediment delivery to the Rangitikei River. Geomorphological mapping was completed to create a map of the slide that was verified with site visits, and was used to better understand movement patterns through deformation features. Coring was also undertaken in October 2017 at the toe during installation of piezometers to determine the depth of the failure surface, which further informed movement patterns. The piezometers were installed at the end of the study period for a different project, so were not used in this study.

3.1.1   Photogrammetry

A DJI Phantom 3 Professional UAV was used to collect nadir (vertical) and oblique photographs of the landslide on three separate surveys (October 2016, May 2017, and October 2017). The purpose was to identify the active landslide area, the movement patterns across the landslide (by filling the space between the GPS points), and quantify the geomorphic change occurring between surveys i.e. localised elevation loss and gain. The flight paths allowed for the necessary overlap (80%) of the nadir photographs. The additional collection of oblique (approximately 30° from the surface normal) photographs increased the effective overlap of photo pairs (Figure 19) and helped to better capture vertical objects (e.g. scarps). Ground control points (GCPs) were placed on the landslide and surveyed with the Trimble RTK-dGPS to georeference the model and improve model accuracy.
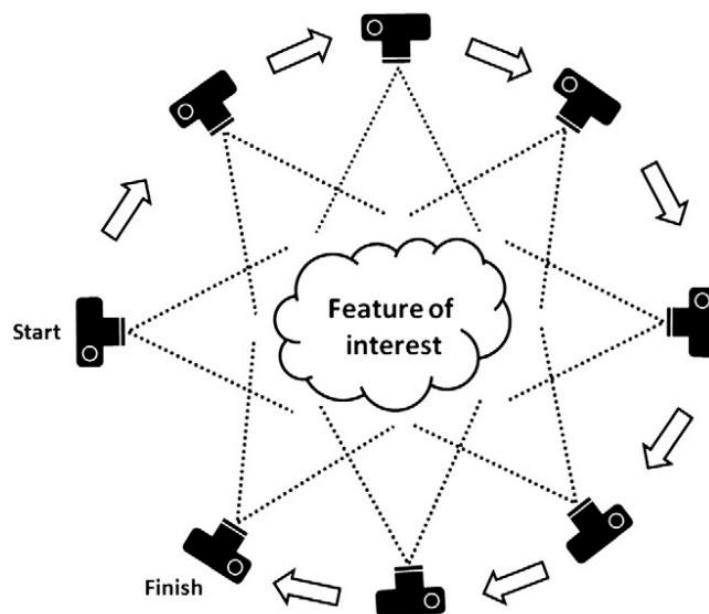
Figure 19. Diagram depicting the ideal Structure-from-Motion photogrammetry technique, where multiple photos at varying angles with overlap are needed for 3-D reconstruction (Westoby et al., 2012).

The program Agisoft Photoscan was used to process the photos into a 3-D model, using Structure-from-Motion (SfM). The SfM pipeline (Figure 20) in PhotoScan involves a series of steps to prepare the photoset for creation of a dense cloud (dense 3-D point cloud which forms the foundation of the 3-D model), including editing the point cloud using the Gradual Selection workflow to reduce noise. A DEM and orthophoto were created from the classified dense cloud, where points were classified as either ground or non-ground using the Point Cloud Classification tool, and the DEM was down-sampled to 0.2 m resolution to be consistent between models.
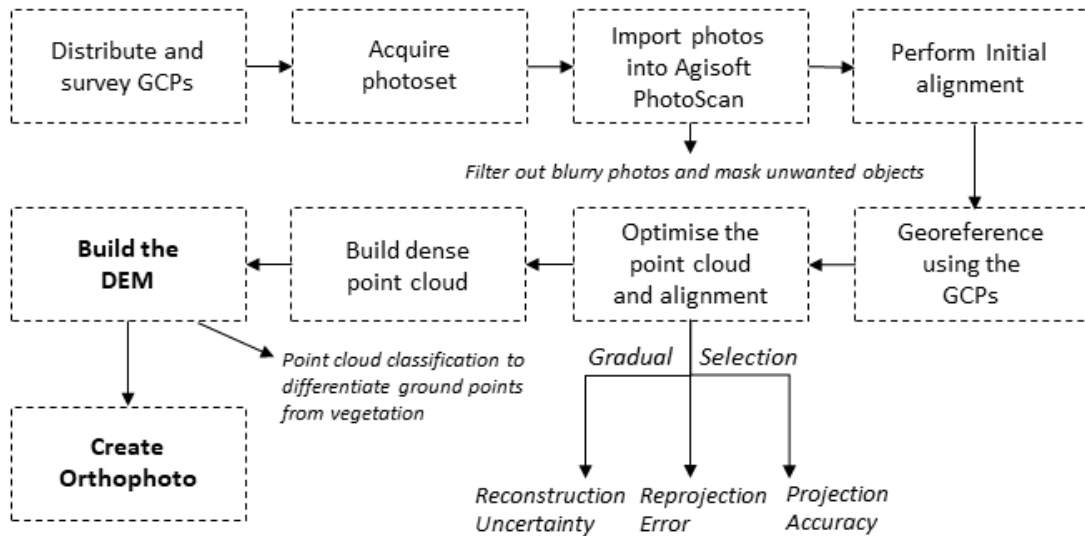
Figure 20. Structure-from-Motion pipeline used to produce the 3-D models, DEMS, and orthophotos. Adapted from Westoby et al. (2012).

Photogrammetry is influenced by GPS and model error. The photogrammetry model error is linked to the RTK-dGPS error, as the GPS was used to georeference the model. However, the model has inherent errors irrespective of the georeferencing error, causing distortion around the model edges and areas where photos are poorly aligned. There is also error in DEM generation when trees or non-ground objects are not adequately classified, creating anomalies (holes and high points). The RTK-dGPS error describes the ability of the model to estimate its position in 3-D space. During processing in PhotoScan, two GCPs were left out from georeferencing the model (Table 2), which tests the accuracy of the model in predicting its location in 3-D space. These were checked by comparing the modelled (estimated) coordinates against the surveyed coordinates, and the difference used as an error value to describe the model accuracy. As two GCPs were used as an error analysis for each survey, the two error values from these were averaged using the root mean square (RMS) error. The specifications for each photogrammetry model is shown in Table 3.

Table 2. RMS error for each photogrammetry survey, which describes the model accuracy.

	GCP label	Error (m)	RMS error (m)
October 2016	*1001*	0.0008	0.0037
	59	0.0065	
May 2017	*Little yellow 6*	0.055	0.05
	67	0.0451	
October 2017	*Rb30*	0.0269	0.016
	Yb19	0.0049	

In making the DEMs of Difference (DoDs), error was accounted for by creating error masks (error surface) of the modelled positions of the GCPs within PhotoScan, which was used to create spatially-variable error across the DoD.

Table 3. Specifications for the three photogrammetry models, gathered from the output report from PhotoScan of each project.

	Photos	Tie points before gradual selection	Tie points after gradual selection	Model res. (cm/pix)	GCP count	DEM res. (cm)
October 2016	3221	4,167,231	2,967,193	2.96	21	20
May 2017	3102	4,912,882	4,487,925	3.16	27	20
October 2017	4242	1,170,372	675,102	2.86	28	20

Any large areas of significant elevation change in the DoDs (deep red or blue areas) are likely caused by one of two factors; vegetation interference, particularly near the middle of the model, or areas not included in one of the DEMs. The area captured in each DEM is dependent on the flight path and camera angle, which were altered for each survey as the SfM method was fine-tuned for the Rangitikei Slide. This will often be shown by holes and edges visible in the orthophotos. These edges and holes can differ between subsequent surveys, and when the DEMs are differenced the holes and missing edges produce significant elevation change. As the holes are limited to near the model edges, any significant elevation change near the edges of the DoD need to be treated with caution. Vegetation interference occurs where there are areas of dense vegetation, as the point classification tool in PhotoScan may not classify ground points correctly, and the classification also differs between models. Large areas of high elevation change that is not close to the model edges can often be attributed to vegetation interference, especially if these large areas are anomalous compared to the rest of the DoD.

3.1.2   Geomorphological mapping

The Rangitikei Slide was mapped at a 1:4,100 scale using the DEM and orthophoto produced by the photogrammetry model. The features mapped were then investigated during site visits to

ground-truth observations from the imagery. Surface deformation features were mapped to inform understanding of landslide movement. These deformation features include scarps, grabens, tension cracks, and ridges. The mapping process was undertaken in ArcMap over contour lines generated by the first Photogrammetry DEM (October 2016) and the orthomosaic.

The western landslide boundary was identified using primarily by site visits, aerial imagery, and a DEM (produced through photogrammetry). There was no single morphological feature such as a drainage line or distinct network of tension cracks on which to base the boundary, so the space between movement features was used to infer the boundary location – i.e. ridges and scarps. There are many factors that affected the location of the entire landslide boundary within the geomorphological map, including knowledge from the farm manager, RTK-dGPS monitoring, photogrammetry, and site visits to produce the geomorphological map.

3.1.3   Coring at the toe

A percussion corer – an impact-driven corer that uses a jackhammer to drive the chamber into the ground – was used at two sites on the landslide toe on the 10th October 2017 (Figure 21). Extension rods are used on top of the coring chamber to extend the reach of the corer, with site 1 reaching 2.5 m and site 2 reaching 11 m. Recovery can be difficult, particularly further from the surface, and require a hydraulic jack to lift the chamber back to the surface.

Figure 21. Photograph of the percussion corer at site 1, showing the generator (yellow), jackhammer (yellow, in use), and hydraulic jack to lift the cores back to the surface (orange). Taken on the 10th October 2017, starring David Feek (Technician) and Sam McColl (Supervisor).

The aim of drilling was to install piezometers for a following project, but was also used to determine the approximate depth of the failure surface influencing the landslide, as it was initially assumed that the clay seam visible in the landslide toe front was the primary failure surface.

3.2 Movement monitoring

Technological advances have enabled capture of higher-resolution movement events, such as the increased use of Total Stations and Real-Time Kinematic Differential Global Positioning System (RTK-dGPS) which revolutionised geomorphic monitoring (Brasington *et al.*, 2000; Fuller *et al.*, 2011; Fuller & Basher, 2013). Monitoring data of varying temporal resolutions were needed in this study to investigate movement initiation, duration, rate, bearing, location, and the interaction between slide blocks. High temporal resolution data (Time-lapse imagery and pixel tracking) was required for event-scale (hourly) movement.

3.2.1 RTK-dGPS surveys

A survey network was installed on the landslide in July 2015, consisting of short waratahs hammered into the ground across the landslide. Ten surveys were completed of the site, although the July 2016 survey data from the R10 Trimble rover was found to be missing, and spanned July 2015 to October 2017. Survey mark location (Figure 22) was determined strategically by looking at aerial imagery of the site and attempting a good representation of each landslide block while avoiding localised movement (erosion). These landslide blocks (upper area, middle, and toe) were hypothesised based on local knowledge from the land manager, site visits, and previous studies in the area, which highlighted different movement rates based on geomorphic features. On the second visit for survey 2, two more survey marks were added off the proposed active landslide area. A Trimble RTK-dGPS R8 and R10 base station and rovers were used to complete surveys at 3-monthly intervals, starting in July 2015. This was done to obtain information about seasonal movement patterns across the landslide in the initial phase of the project. Movement rates were calculated by measuring the location of each survey mark and differencing the position from the survey mark location within the previous survey. This provided a movement rate for the period between those surveys. The RTK-dGPS data was collected using the New Zealand 2016 Geoid model (corrected retrospectively for the early surveys) and used New Zealand Transverse Mercator grid coordinates. The base station baseline length was always within ~2 km, with the base station placed over a LINZ benchmark survey peg (code B47B). This benchmark is an Order 3 survey mark, meaning it is considered 'survey accurate' (see http://apps.linz.govt.nz/gdb/index.aspx?code=B47B). The RTK-dGPS survey method had a wide spatial extent and a low temporal resolution (3-monthly).

To assess survey point measurement quality, a survey mark was reoccupied at the beginning and end of the survey to provide an indication of the horizontal measurement precision (δxy) (Retimana *et al.*, 2004; Brasington *et al.*, 2000), which was then used as the inherent measurement error for each survey. This indicates the repeatability of measurements within

each survey, of which the maximum error was ± 50 mm. This value includes the RTK-dGPS instrument internal error and user error (e.g. pole tilt), but other errors such as multipath errors may not be accounted for, so should be treated as a minimum value.

The calculation of error for movement rates (δu) was calculated using a quadrature sum (square root of the sum of squares) to propagate the precision errors from individual surveys (δxy_1 and δxy_2) using Eq. 1 (after Brasington *et al.*, 2003; Neverman *et al.*, 2016):

$$\delta u = \sqrt{(\delta xy_1^2 + \delta xy_2^2)} \qquad\qquad (\text{Eq.}\,1)$$

This combines two sources of error, providing a propagated error for the comparison between the two surveys. The highest cumulative error was ± 58 mm, indicating that there was approximately 6 cm of error between surveys. This measure of error was favoured in this study over the reported precision estimates provided by the Trimble RTK-dGPS software, as the reported precisions were calculated for each peg and were not a propagated error between each survey. Cumulative error is needed for movement analysis between surveys, rather than a single survey error. Total horizontal movement error margins were calculated by propagating the precision errors for each survey included in the survey period for every peg (using Eq. 1).
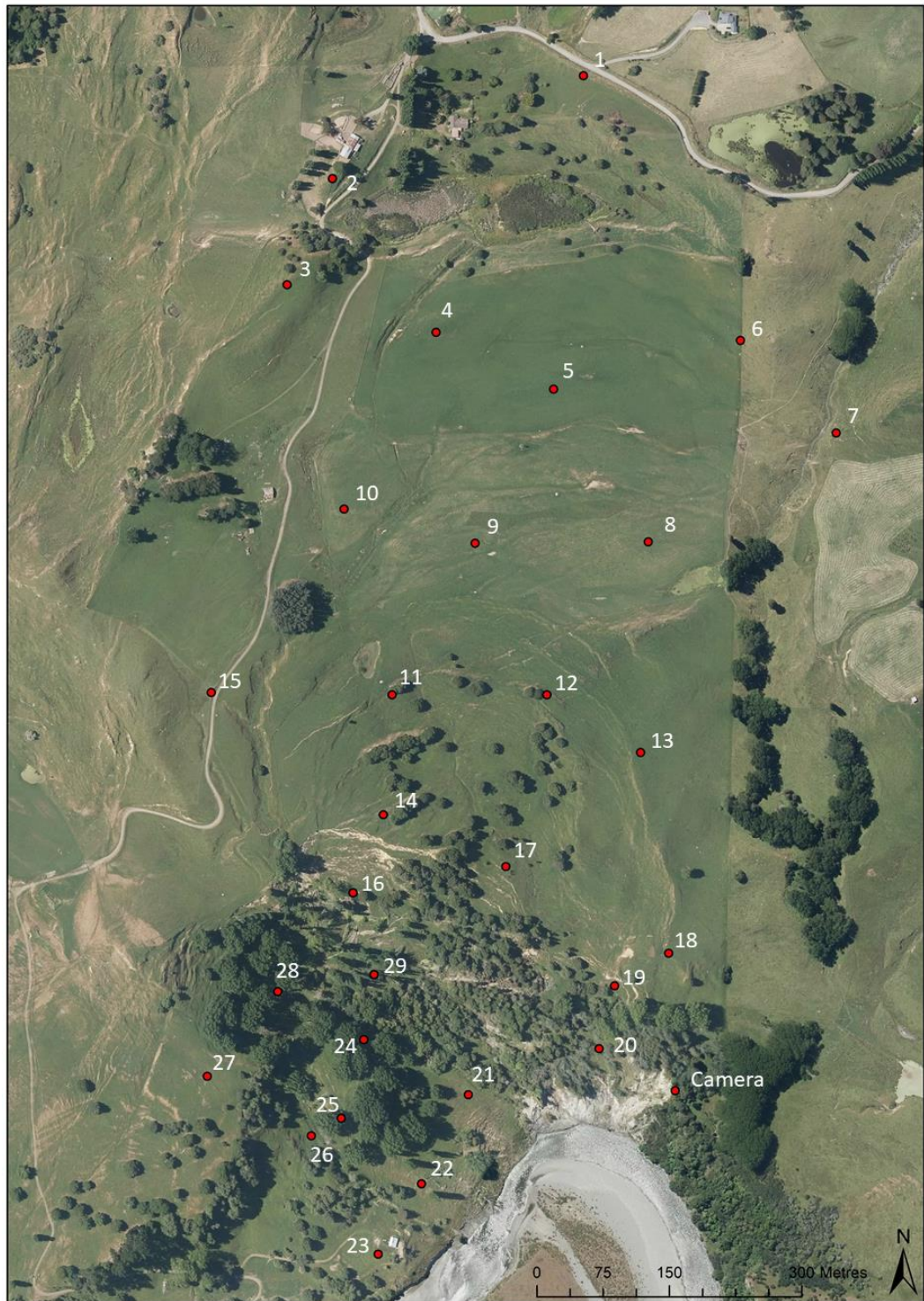
Figure 22. RTK-dGPS network across the Rangitikei Slide.

3.2.2   Time-lapse imagery

A Canon DSLR camera mounted on a tripod structure (Figure 23) was used to collect time-lapse

imagery of the landslide toe, including where the toe meets the Rangitikei River. The camera is

powered by a 12-volt battery and solar panel, and is housed in a water-tight box containing the

camera and a GPS-clock which allows for photo collection at a consistent time interval, with the

interval set by a Raspberry Pi computer. Initially a 40-mm lens was used on the camera (July 2015 to September 2015), but was changed to a 24-mm lens to capture a wider view of the scene (Figure 24).

Figure 23. Time-lapse camera set-up, showing water tight casing and the solar charging panel.

The time-lapse camera takes a photo every hour during daylight hours and stores the images on a memory card (replaced during each 3-monthly survey). This method produces a relatively high temporal resolution dataset (limited to daylight hours) due to hourly photo collection, and good spatial resolution (cm – m per pixel), with the spatial extent limited by the camera frame (Figure 24).
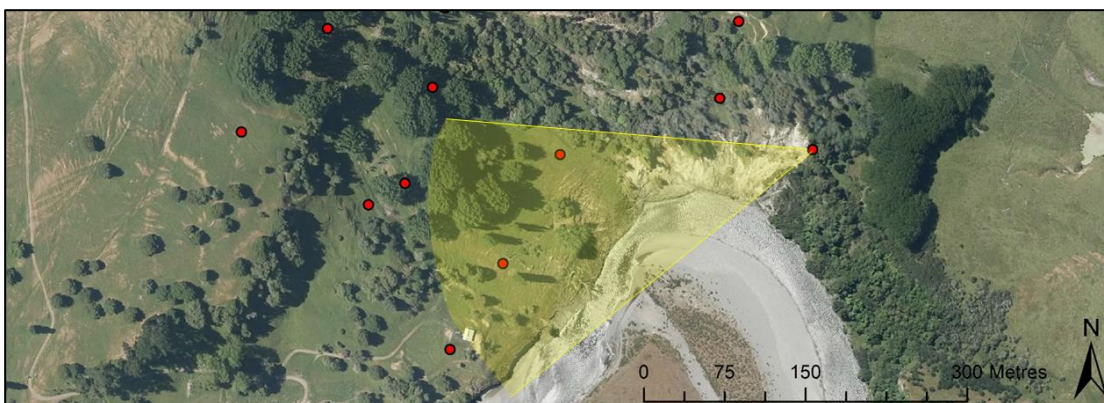
Figure 24. Diagram showing the camera view of the landslide toe.

This method was chosen for its ability to capture high temporal resolution data (hourly) semi-continuously, providing a qualitative dataset to visually explore the relationship between flood

events and toe movement rates. This visual data element allowed for further understanding of the toe morphology and how this changed (vertically and horizontally) through time. The time-lapse imagery provided significantly higher temporal resolution than the RTK-dGPS monitoring network and Photogrammetry by capturing the event-scale movement, but is restricted to the area within the frame. Combined with pixel tracking software, the time-lapse photography was used to explore the influence of floods on the landslide toe, providing a novel way to explore the role of landslide toe erosion at event-scale. While other monitoring systems, such as Ground-based SAR (Slope Radar), or a densely distributed continuous GPS or Robotic Total Station and prism system could have provided similar temporal-resolution, these methods were prohibitively expensive for this research project.

3.2.3 Pixel tracking

PointCatcher (see http://www.lancaster.ac.uk/staff/jamesm/software/pointcatcher.htm) was used to track individual pixel movement in the time-lapse photography, achieving high temporal resolution data (during daylight hours) of toe movement compared to the RTK-dGPS (3-monthly) temporal resolution. Weekly and hourly pixel tracking was completed, but tracking of the first 3-months of the study period was difficult due to the change in camera lenses. DEMs produced through photogrammetry can be imported into PointCatcher to gather 3D pixel tracking data and georeference the pixel distances to determine real-world displacements.
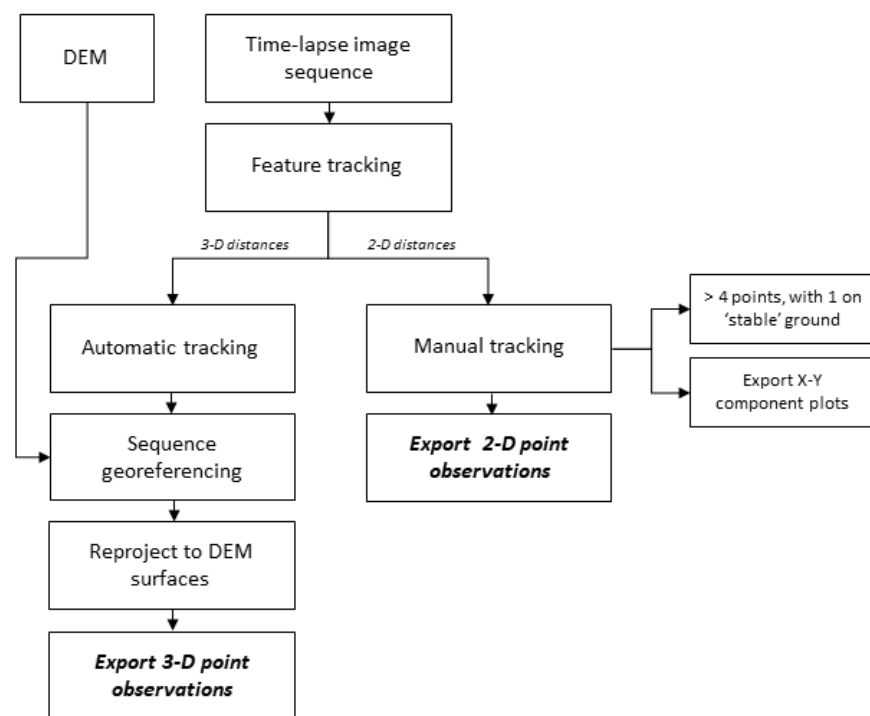
Figure 25. Common pixel tracking workflow, showing a combination of 3-D data (for monthly tracking) and 2-D data (for event-scale data). Only the workflow for 2-D data was used in this study. Modified from James et al. (2016).

There is error associated with aligning the DEM as this is done visually, and would require boundary signatures (e.g. symbols) to better match the scene and reduce this error. DEMs were not used for the pixel tracking in this study, but are an increasingly useful tool in high temporal resolution monitoring studies.

Several points were identified within the scene to track, and were strategically placed to cover the main features (Cliff, toe front, stable terrace). The process for manual pixel tracking (Figure 25) was used to investigate individual flood events, and had a high temporal resolution (hourly). This requires that each point observation (pixel in each image) is manually chosen by the user throughout the image sequence (photo set), and the 2-D point observations processed in Microsoft Excel (see http://www.lancaster.ac.uk/staff/jamesm/software/pointcatcher.htm). Automatic tracking allows the software to utilise its normalised cross-correlation-based tracking (James *et al.*, 2016) by comparing the image template to the current image to match pixels. However, due to the large displacements and variation in lighting, automatic tracking often eventually fails over long monitoring periods (James *et al.*, 2016).

3.2.4   DEMs of Difference (DoDs)

DEMs created from the dense point clouds were compared at a down sampled resolution of 0.2 m to see where the geomorphic change (vertical difference) was occurring between surveys, which translates to elevation changes. When the DEMs were imported into the Geomorphic Change Detection (GCD) plug-in for ArcMap (see http://gcd.joewheaton.org/downloads) for DoD processing, the error value from PhotoScan (GCP error modelled by PhotoScan from the point cloud) was used as a spatially-variable error mask for the thresholded DEM of Difference (DoD), which is a DoD that has accounted for error. A mask (or error surface) is a layer representing the dataset area, and is used to capture the spatial distribution of elevation errors (Neverman *et al.*, 2016). An error mask was created in ArcMap of the modelled GCP errors using Thiessen Polygons from the modelled error of the GCP points (Appendix 3). This error mask was chosen as it included spatially-variable error thresholds, which provides more detailed and location-specific elevation changes compared to a blanket minimum level of detection. The DoDs were created in ArcMap and included a propagated error threshold which incorporated the error masks from both input DEMS.

3.2.5   Quantifying sediment contribution

Sediment contribution from the Rangitikei Slide was estimated using the length of movement feature movements and width of the landslide toe within the time-lapse frame (measured from Google Earth. The thickness estimate was the average depth to undisturbed material between the two coring sites on the toe, which was found to be approximately 6 m. The unit weight for

remoulded landslide debris was adopted from Massey (2010) of 20 kN/m³, which equals 2.04 t/m³. This equation provided an estimate of the sediment contribution by the Rangitikei Slide toe, assuming uniform movement, into the Rangitikei River.

3.3 Rainfall

Half-hourly rainfall data was provided by Horizons Regional Council from their Makohine Station (Figure 26), as this was the closest publicly available station to the Rangitikei Slide site recording rainfall and therefore used as a rainfall proxy for the site. The elevation for the Makohine site is 420 m.a.s.l (Horizons unpublished data) which is similar to the upper area of the landslide (430 m.a.s.l). The alternative rainfall station (Taihape Station) was at a similar elevation (433 m.a.s.l) but was horizontally further from the study site (Figure 26), and had similar records to the Makohine Station. Bar graphs were produced from this data to identify rain events for comparison against the movement data (RTK-dGPS and pixel tracking). It is assumed that the data from the Makohine Station is representative of the study site, but the on-site rainfall may differ slightly, particularly as the study site is influenced (pore water pressures) by drainage lines that have their own catchments. This information is not reflected in the Makohine Station and should be a consideration.
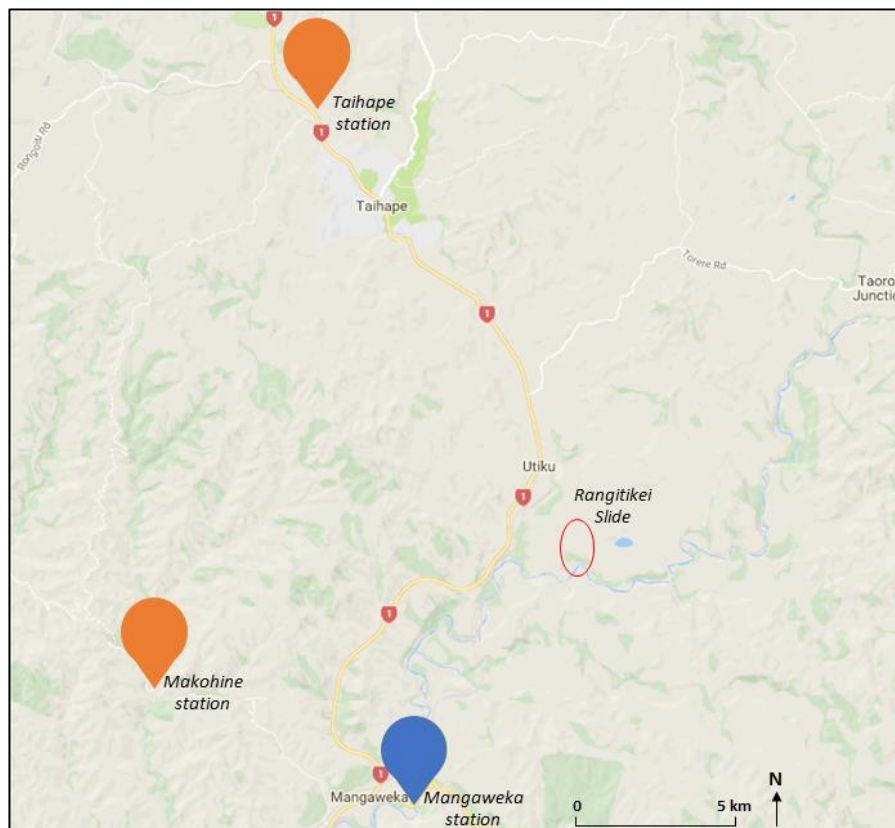
Figure 26. Locations of the environmental data (rainfall in orange and flow in blue) monitoring stations owned and maintained by Horizons Regional Council. The chosen stations were the closest to the Rangitikei Slide, shown by the red circle (image adapted from Horizons Regional Council, see http://www.horizons.govt.nz/environment-data).

3.4 Rangitikei river flows

Half-hourly flow data was provided by Horizons Regional Council from their Mangaweka station (Figure 26), as this was the closest (horizontally) publicly available station to the site recording the Rangitikei River flows. It is not expected that the rainfall and flow data correlate and represent the same events, as the Rangitikei catchment has a significant network of tributaries feeding into the Rangitikei River (Figure 27) whereas the rainfall is captured for the immediate area. This allows for the exploration of both rainfall and flow separately in relation to landslide movement. Graphs were produced from this data. It is assumed that the data from the Mangaweka Station is representative of the study site, but the on-site river flows may differ slightly as the Mangaweka Station lies downstream and includes the influence of other tributaries, particularly the Hautapu Stream. The flood events may be less significant at the study site than recorded at the Station, which should be a consideration, but should not affect the investigation into the relationship between high flows and landslide movement.

The value of 200 cumecs has been classified as the threshold for 'significant' flood events, based on the Rangitikei River flows during the study period (Figure 28). This threshold marks the upper limit of high flows (as designated by visual assessment of the flow hydrograph) within the study period, with the majority remaining below 200 cumecs. When discharge levels surpass this threshold, they are no longer categorised as high flow events for the Rangitikei River, but significant flood events.

There were 15 significant floods between July 2015 and October 2017, as well as a significant flood 'cluster' during the 2016 winter (July – September). Of these, five exceeded 400 cumecs, with three of those chosen for analysis using hourly pixel tracking due to time restrictions. The chosen three flood events had the highest quality time-lapse imagery, and occurred in April 2017 (two events) and in May 2017.
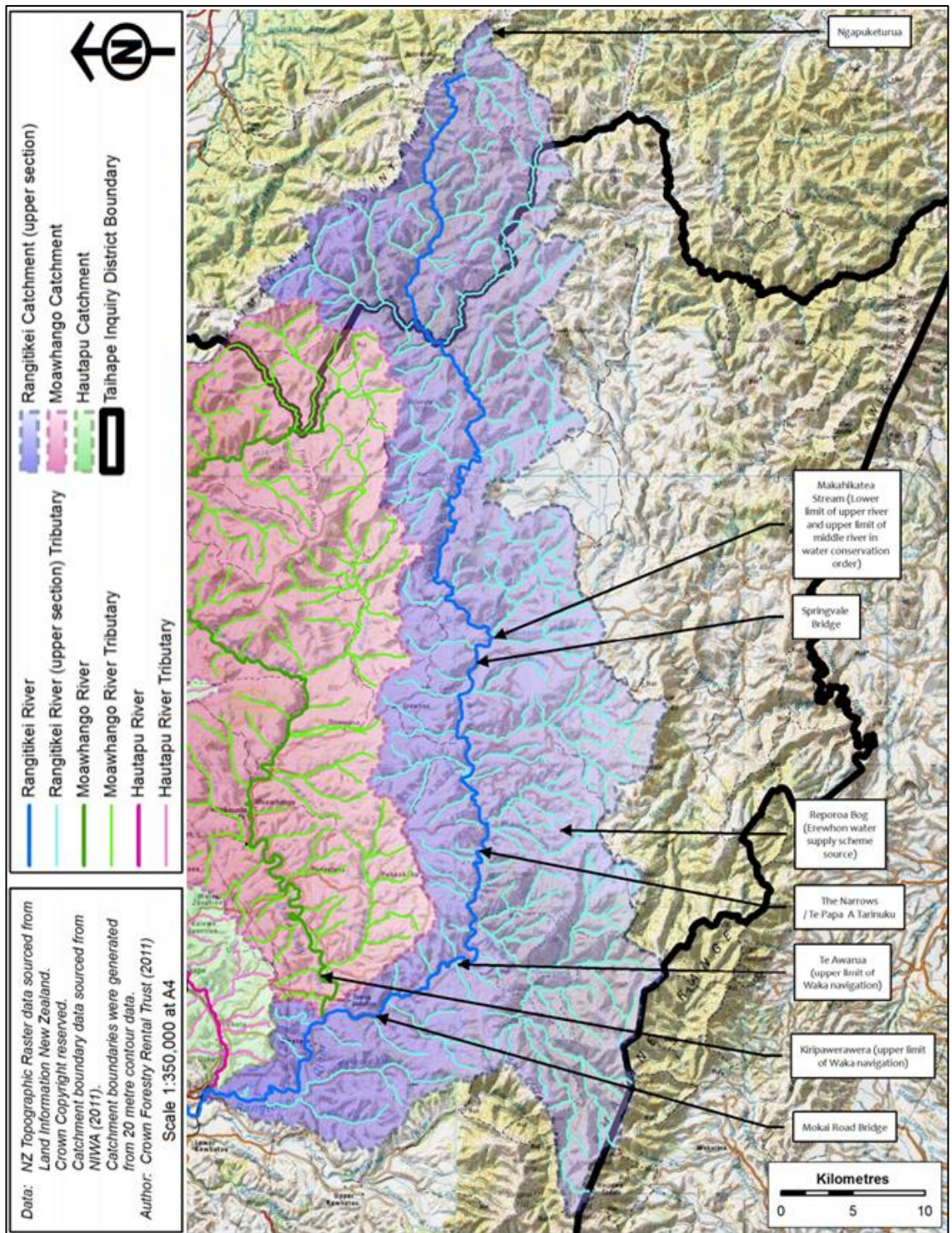
Figure 27. A map of the Upper Rangitikei Catchment (Blue area), showing the large number of tributaries feeding into the Rangitikei River (blue) (Alexander, 2012).
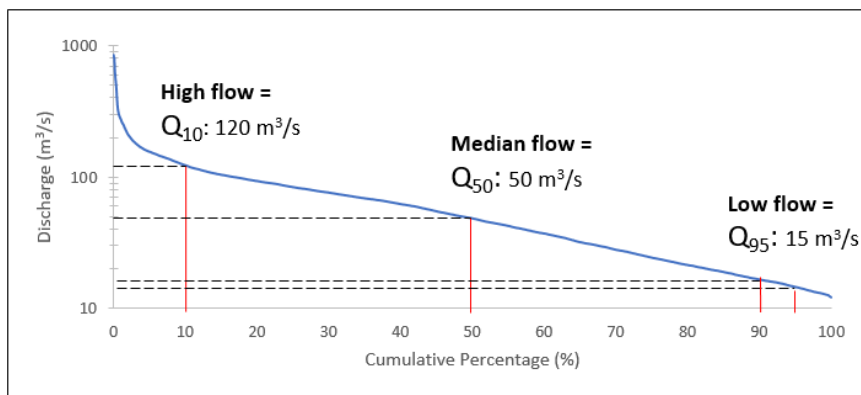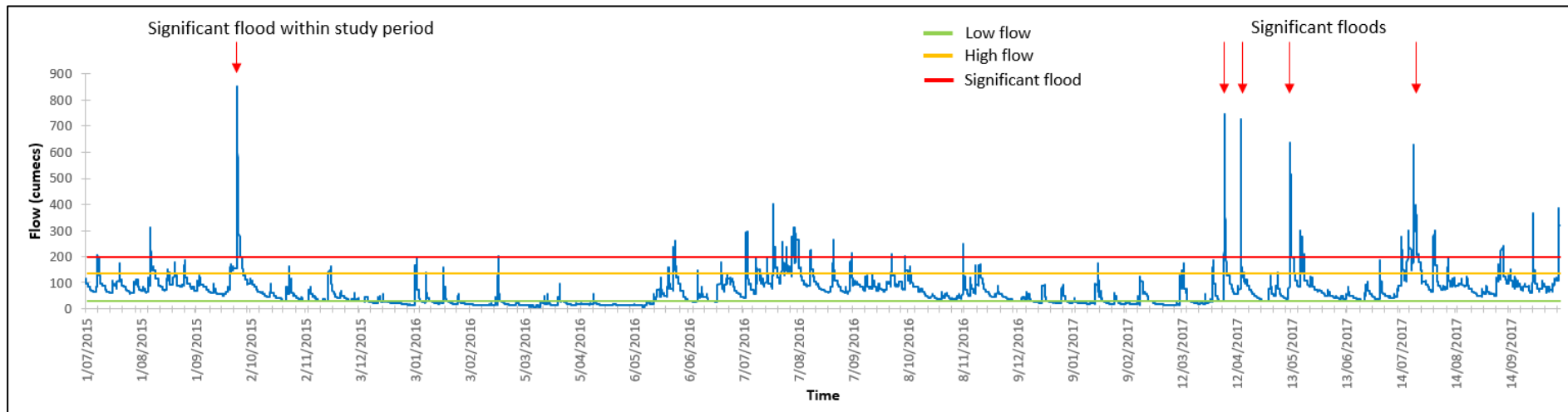
Figure 28. Flow duration curve and hydrograph informing the low, high, and significant flow discharge thresholds during the study period.

4　Results

This chapter presents analysis of surface morphology, the monitoring results for the Rangitikei Slide, and uses these datasets to re-examine the landslide extent and movement patterns. The relationship between movement and external factors is examined, and some estimates are given for the sediment delivery to the river. This landslide was previously identified by Thompson (1982) and the name (Rangitikei Slide) adopted in this study. It was hypothesised at the start of this study that the landslide had several sections (landslide blocks) with different movement rates, based on local knowledge from the land manager, previous studies in the area (i.e. Thompson (1982)), and initial site visits (geomorphic features indicative of different movement rates). This hypothesis was tested through geomorphological mapping, Structure-from-Motion modelling, and movement data.

It was also hypothesised that the primary movement drivers were groundwater fluctuations (likely driven by rainfall) and toe erosion by the Rangitikei River. This hypothesis was tested through RTK-dGPS surveys and pixel tracking (both weekly and event-based).

4.1　Spatial movement patterns

4.1.1　Geomorphological mapping

Using the Hungr (2014) classification (adapted from Varnes, 1978), the Rangitikei Slide is categorised as a translational rockslide (or block slide), assuming movement along a low angle planar failure surface as seen in similar landslides in the region (Massey, 2010; McCabe, 2013; Massey et al., 2016a). However, it could also be categorised as a complex landslide due to the earthflow-slide present at the toe (Figure 29), as determined by movement patterns and composition. The landslide has been separated into distinct zones due to morphological features indicating different movement rates (Figure 30). The upper area displays slow, translational rockslide movement, shown by the absence of broken ground and by low vertical displacements (Figure 31, photo 1), which indicates movement along a planar surface with slow displacement and lacking rotation. The central area displays a rotational element to movement and increased vertical displacement (Figure 31, photo 2 & 3). at the transition into the toe area.

The head area contains the head scarp and a graben, which is partially filled with a wetland area. Above the head scarp, outside the active landslide area, is a sharp change in slope which could represent a secondary head scarp. There were also extensional features (scarps and grabens) visible throughout the Rangitikei Slide (Figure 29), but no apparent compression at the toe. Instead, there are clear extensional features at the toe, with numerous tension cracks and mini-

horst and graben structures across the area beside the Rangitikei River and several large fallen trees.
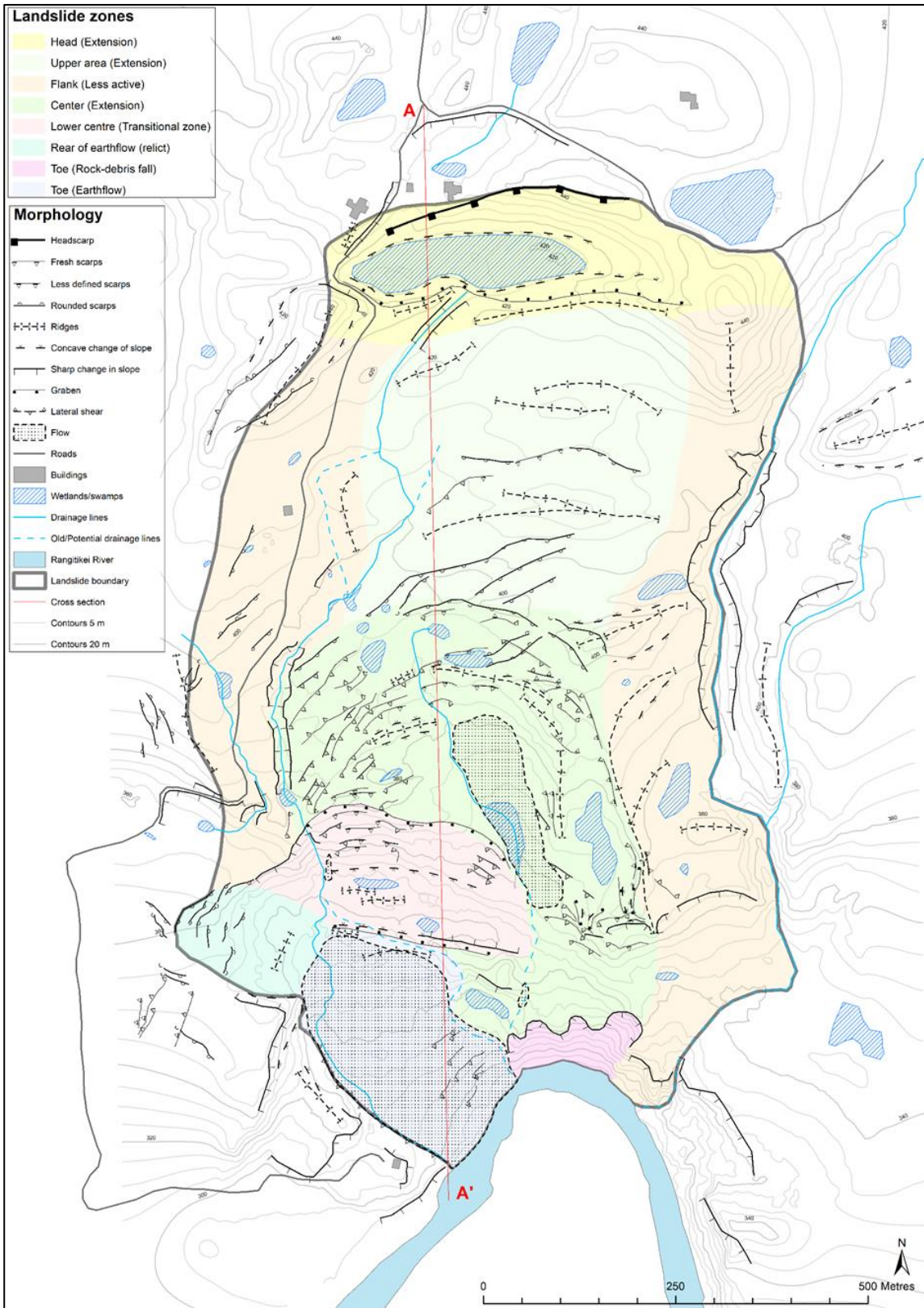
Figure 29. Geomorphological map of the Rangitikei Slide, showing morphological features, interpreted landslide zones, and the cross-section line. This map was created from site visits, a DEM, and aerial imagery.
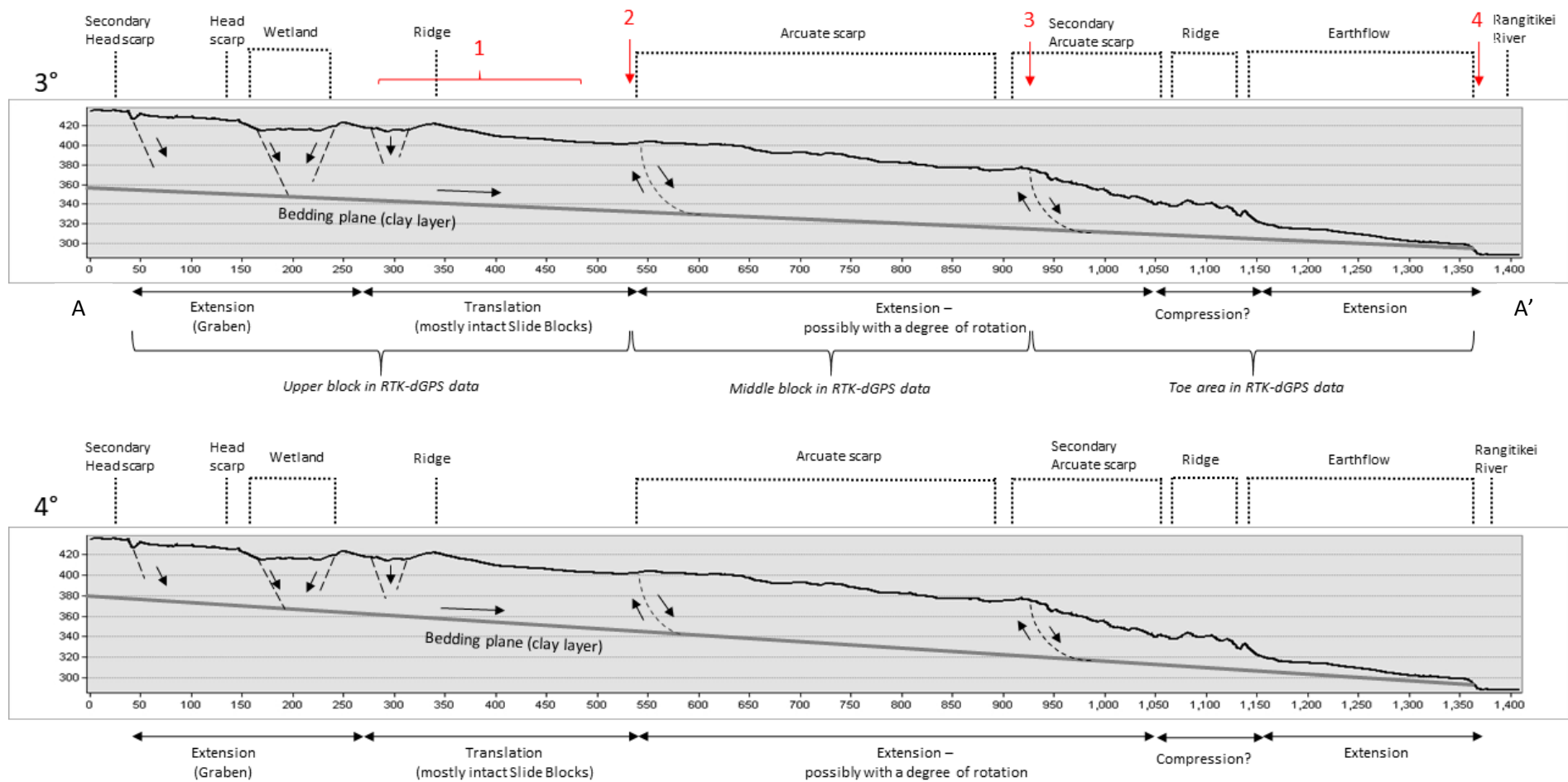
Figure 30. Cross-sections of the Rangitikei Slide with the key subsurface features for each landslide section, and showing possible failure surfaces at 3° and 4°. The red numbers refer to representative photos of the highlighted features, shown below.
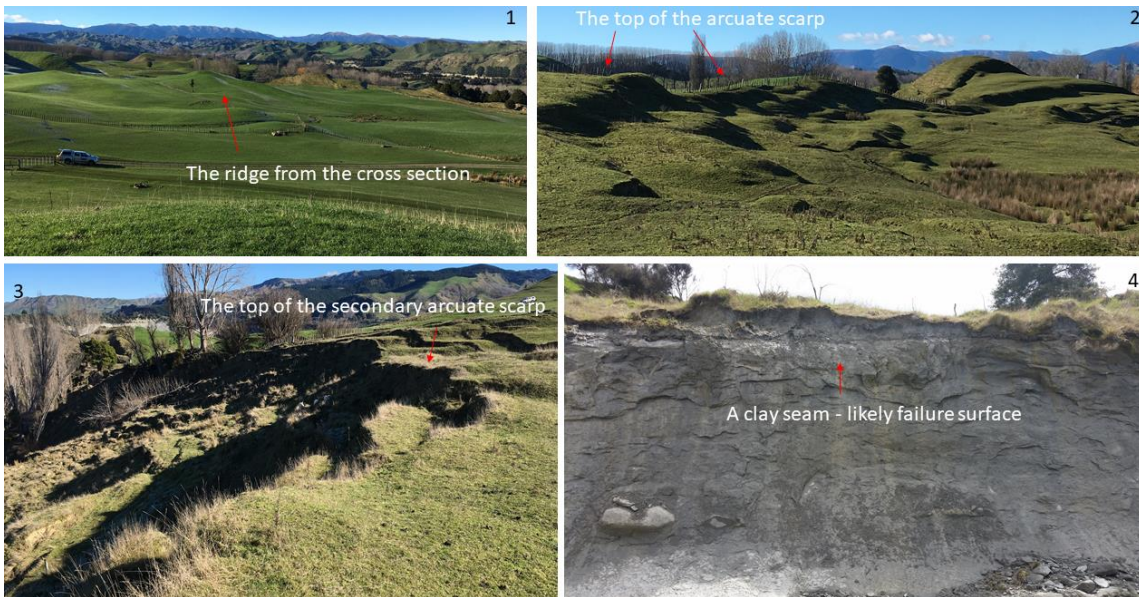
Figure 31. Photos 1-4 correlate with the numbers (in red) on the cross-sections, showing representative features of the areas identified in the cross-sections.

It is likely that the Poroa Complex has several planar failure surfaces, including the one on which the Rangitikei Slide is moving, with at least one below the uppermost failure surface (Figure 31, photo 4). This was found to be the case when coring the toe in October 2017 during installation of piezometers, which found that there was sediment disturbance down to at least 11 m below the surface on the north-east side (beside the bare rock cliff) compared to 2.5 m on the south-west side (near the shed). There was an initial assumption that the failure surface visible at the toe near the surface (Figure 32) was the Rangitikei Slide failure surface, the coring found that the remoulded bedrock exceeded the depth of the upper clay seam (~11 m). However, the Rangitikei failure surface may have actually been passed by at the second coring site (that reached 11 m), but captured in the first site at 2.5 m below the surface. The Rangitikei Slide failure surface is likely at a 3-4° angle, as shown in the cross-sections (Figure 30), which correlates with the primary surface features and the regional dip for the area (3-7° according to Massey, 2010). Two cross sections were modelled to show the differences between 3° and 4° dip, and whether it was possible to conclude based on the primary surface features what the dip was likely to be. However, it is difficult to conclude the dip angle from the cross sections without further investigation.
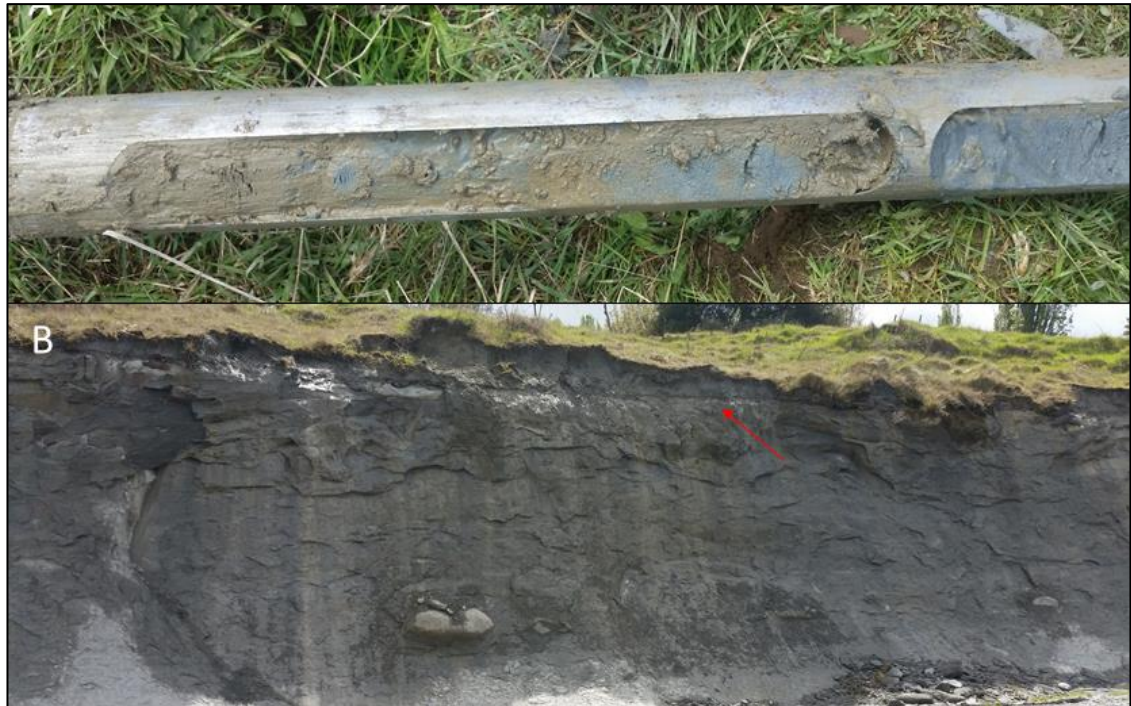
Figure 32. A) Photograph of a section of core from one of the coring sites. B) Failure surface visible at the landslide toe front during low flows.

4.1.2 Photogrammetry

The three photogrammetry surveys produced DEMs (used to create hillshade models, Figure 33), DoDs, and orthophotos (Figure 34).

The hillshade models were used with the orthophoto (Figure 34) to create the geomorphological map (Figure 29), and they show different movement zones as determined by morphology (Figure 35). Zone A contains the upper area and has a smoother surface than zone B, D, and E, and there are linear features that have a strike from a NE to SW direction (Figure 35, A). Zone B has a rougher surface than zone A, with more clear breaks in slope visible and mostly curved features (arcuate scarps). There is a divide in this zone in an E – W direction (Figure 35, B), a drainage line orientated NNW – SSE, with the western side markedly rougher than the eastern side.
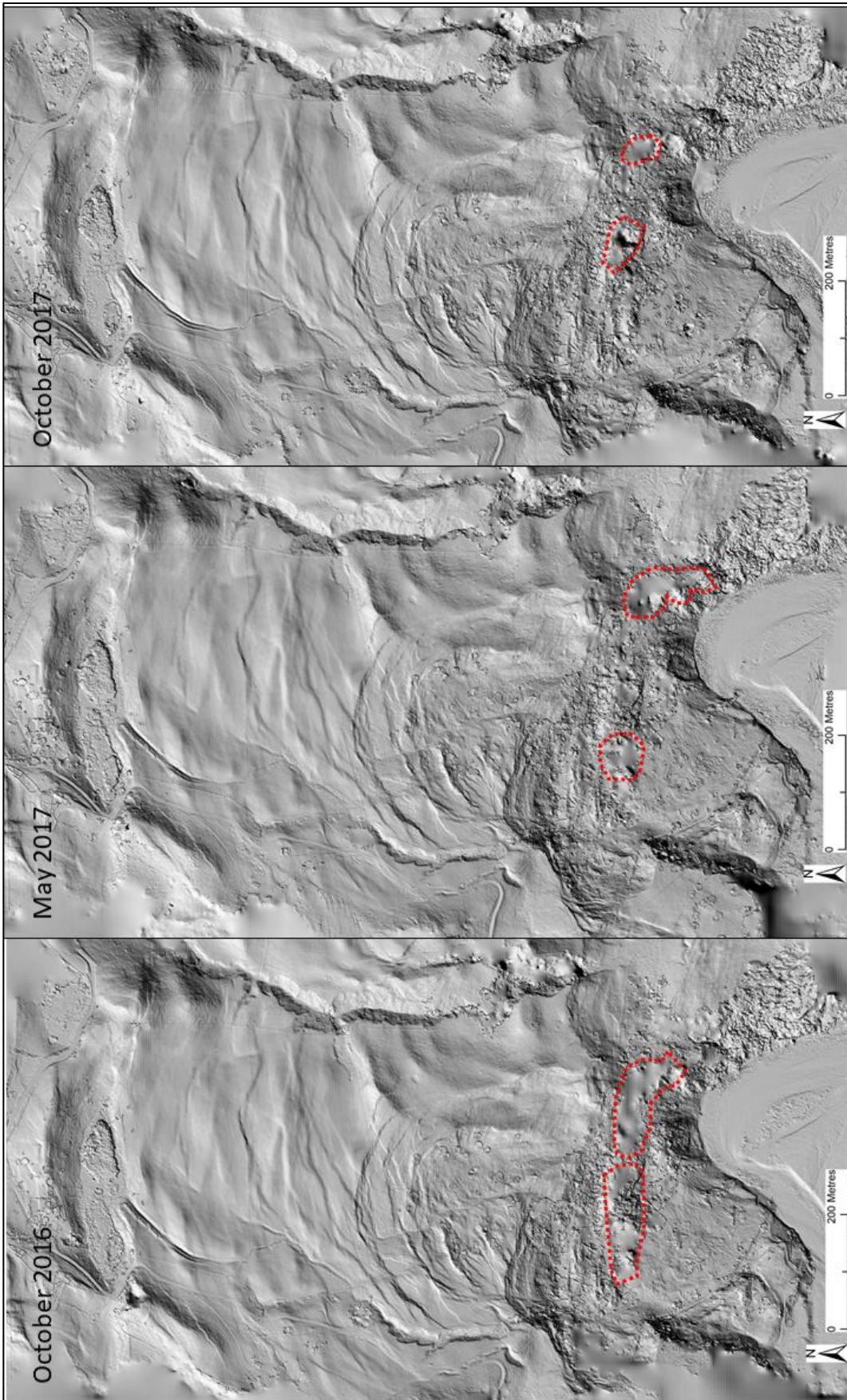
Figure 33. Hillshade models created from the DEMs for each photogrammetry survey. Vegetation artefacts are highlighted in red.

Figure 34. Orthophoto from the May 2017 photogrammetry survey, a mosaic created from the survey photos.
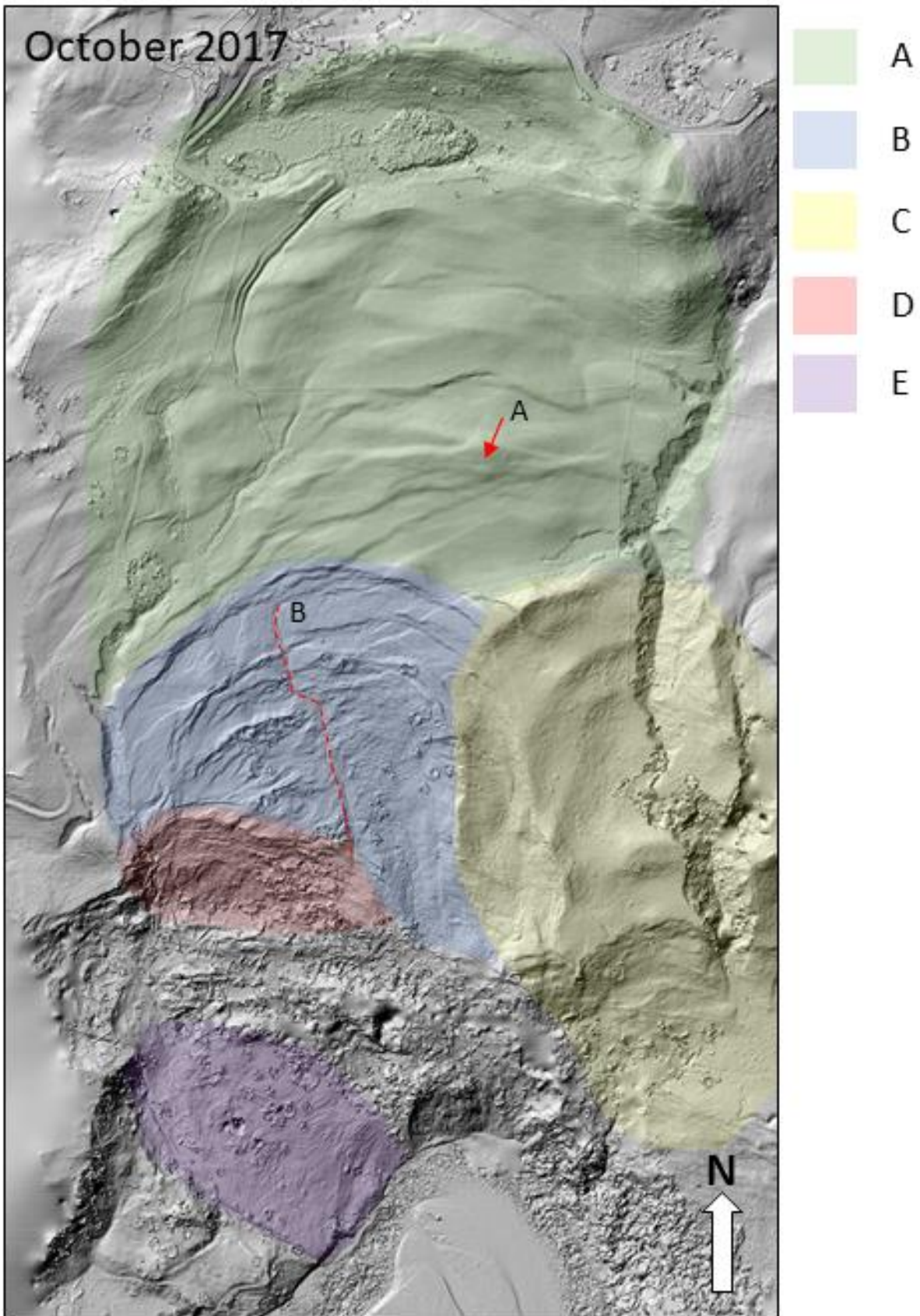
Figure 35. October 2017 hillshade model showing movement zones based on morphological features. A – B shows noticeable liner features.

Zone C has a smoother surface similar to zone A, with a number of distinctive ridges but very few sharp breaks in slope like those found throughout zone B. Zone C also has a movement direction to the SE and distinct curved parallel ridges, which could be degraded former scarps or horst blocks.
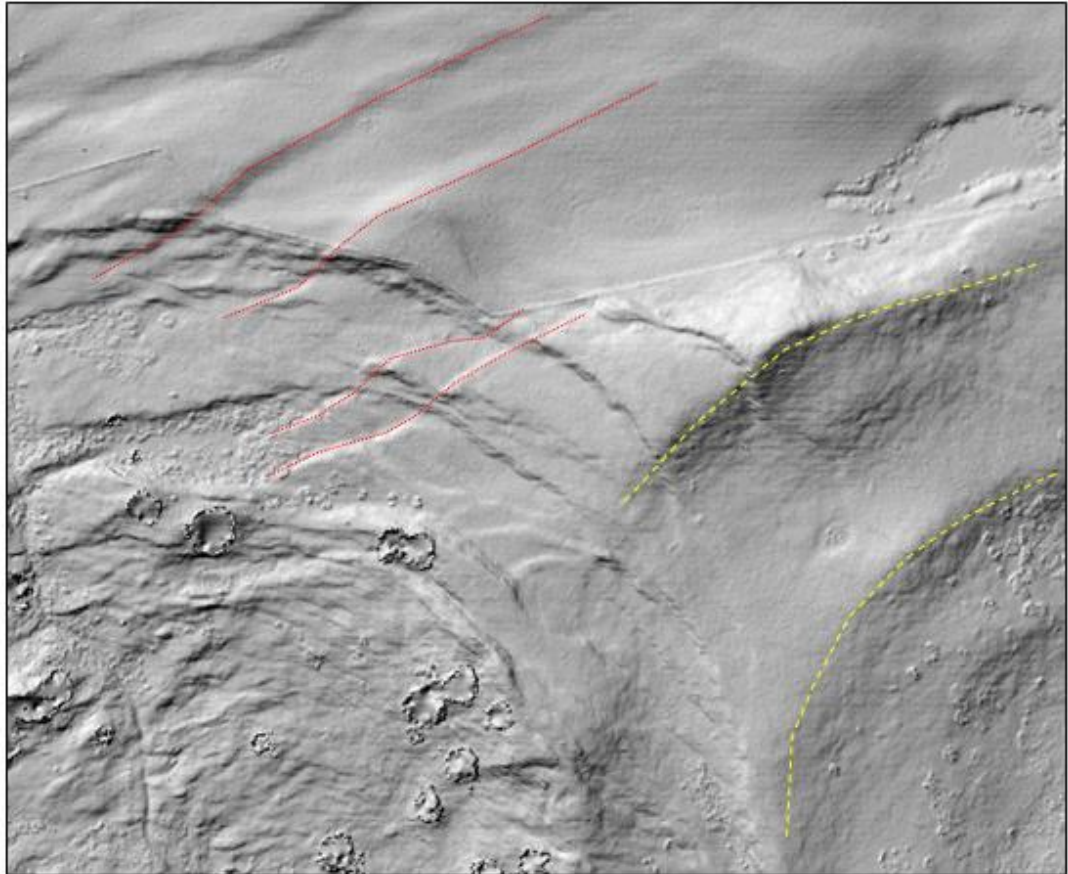
Figure 36. Close-up section of the October 2017 hillshade model, showing movement features in yellow (ridges) and red (linear features or scarps). These highlighted features are cut (or offset) by the non-highlighted features.

Zone D has the roughest surface, indicating substantial deformation and arcuate scarps similar to zone B, and is primarily composed of a graben (Figure 29). The movement features in zone B are not orientated towards zone D. The zone B features (ridges) are orientated towards the central drainage line (Figure 37), while zone D is generally orientated towards the western drainage line, which is considered the current primary drainage line within the study site and is fed from the wetland below the head scarp (Figure 29). Between zone D and zone E appears to be a graben, with fallen trees visible at the base (Figure 38), and a flow to the east.
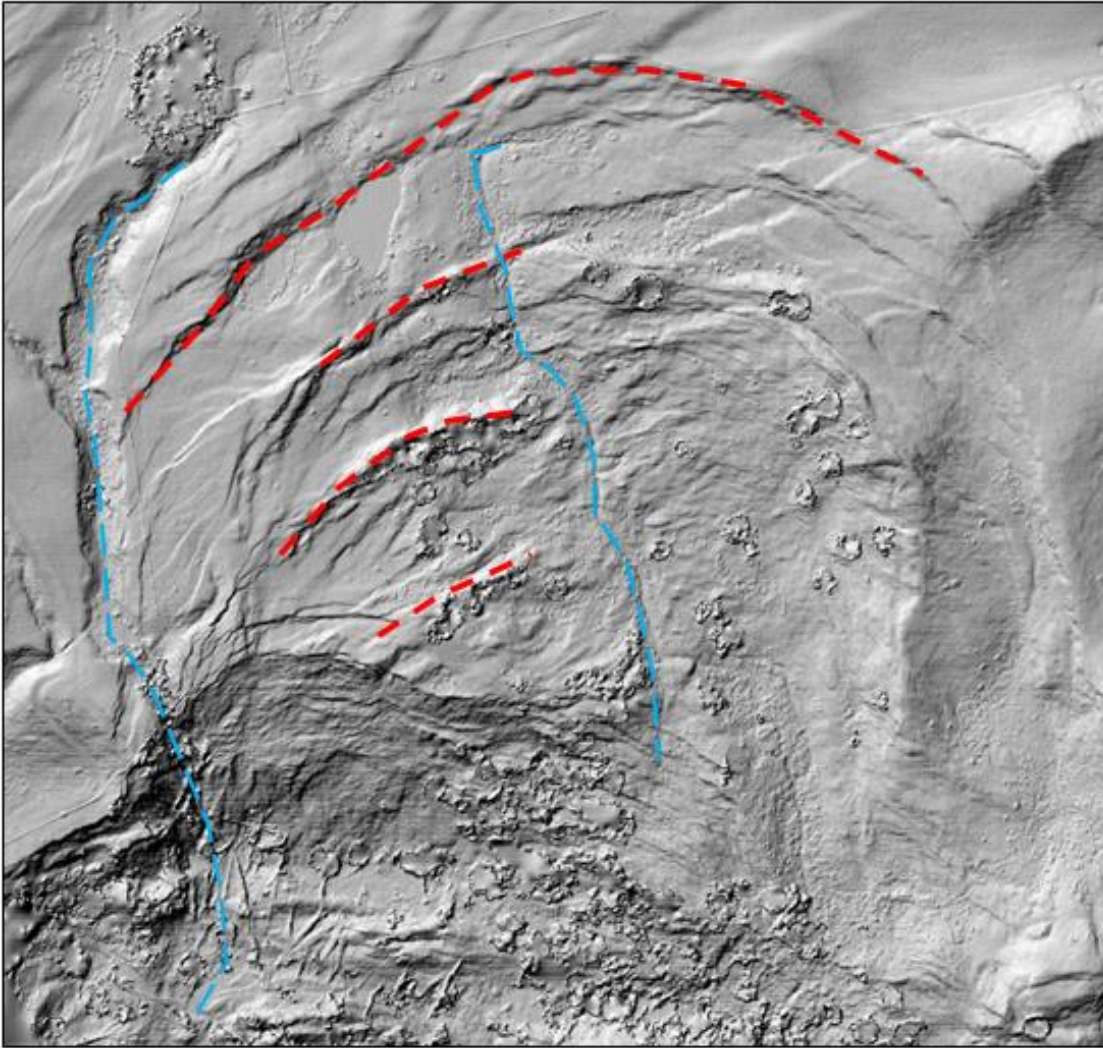
Figure 37. Close-up section of the October 2017 hillshade model, showing zone B and zone D, with ridges marked in red and drainage lines in blue.

Zone E represents the toe area, which has a relatively smooth surface (compared to the previous zones) indicating consistent movement of the entire zone (Figure 38). There are, however, smaller scarps and horst-graben features across the toe, particularly at the toe front where the material is significant remoulded and material strength is weak. There is a distinct southern boundary that is visible in the hillshade model as a line (shown by arrows, Figure 38), which represents a drainage line running down to the Rangitikei River.
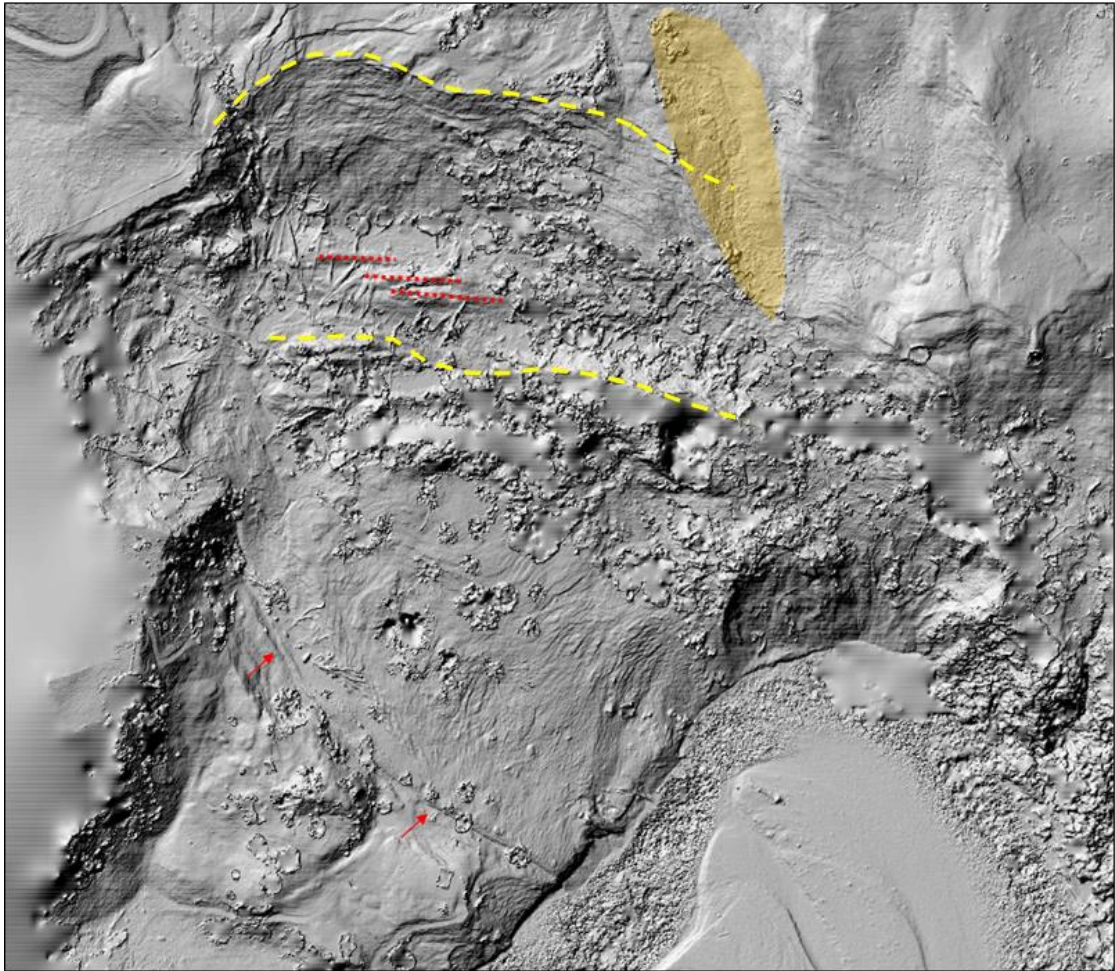
Figure 38. Close-up section of the October 2017 hillshade model, showing the zone E (toe area) and zone D. The graben edge for zone D are shown in yellow, and ridges in the graben base are shown in red. The lateral shear that marks the southern boundary of the toe area is marked with arrows and the material flow is shown in orange.

The DEMs of Difference (DoDs) show patterns of net elevation changes. The elevation changes visible in the DoDs can occur through either vertical or horizontal change. Vertical change occurs predominantly through local compression or extension. For example, local compression can increase the elevation of a feature (i.e. a ridge) with little to no horizontal change. This will be visible in the DoDs as a local increase (or decrease for extension) in elevation for the feature only. Horizontal change occurs predominantly through larger scale extension or compression, which moves features across the landscape (compression moves features together, extension moves them apart). This will be visible in the DoDs as a progression of elevation change, i.e. a ridge that is experiencing large-scale extension will have an area of elevation loss where it used to be, and an area of elevation gain where it has moved to (Figure 39).
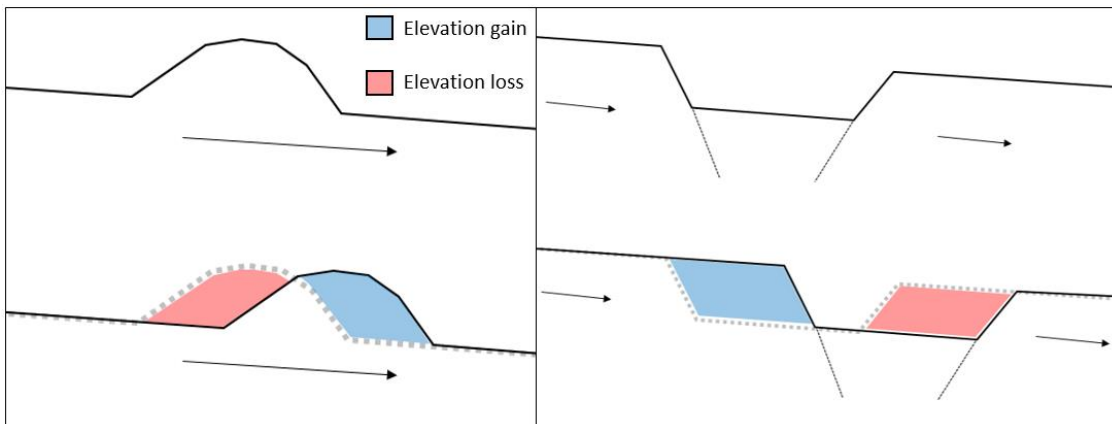
Figure 39. Schematic diagram showing how near-horizontal displacement of landslide features (in this case, a ridge and a graben) can result in elevation changes in the DoDs, which does not necessarily represent an area of significant vertical change, but rather translation of features downslope.

The October 2016 – May 2017 DoD (Figure 40), which occurred over summer, shows most significant elevation change from the central area down to the toe. The central area shows patterns of elevation loss (red) and gain (blue), which is likely influenced by patterns of extension and compression. The outline of the arcuate scarps and ridges are clearly visible in the DoD, indicating that they or the area around them experienced elevation change during the October 2016 – May 2017 period. One of the upper ridges (Figure 41, A) increased in elevation during the time-period. The next ridge (Figure 41, B) shows an area of elevation loss (red) on the northern edge (with some vegetation interference in the centre of the ridge from the large trees) and a small line of elevation gain (blue) on the southern edge. This is also shown in the next ridge down from that (Figure 41, C & D) with elevation loss to the north and elevation gain to the south as the ridge moves southwards.
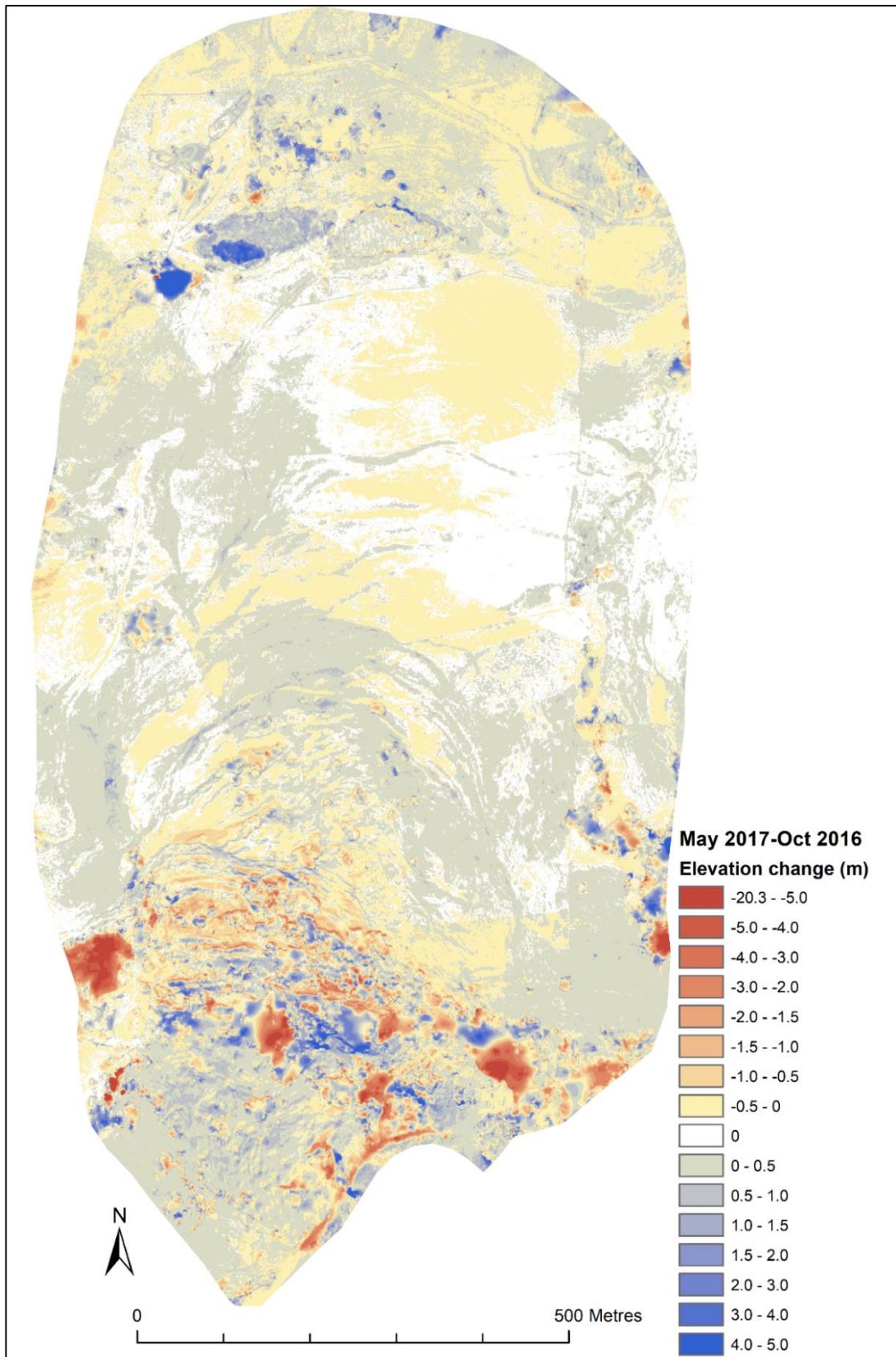
Figure 40. October 2016 - May 2017 thresholded DEM of Difference (thresholded by spatially-variable model error), showing elevation loss in red and elevation gain in blue. The scale of the vertical changes is relatively consistent except for the large elevation loss (-5 to -20 m) as they represent artefacts in the model that were not removed from the point classification tool.

The primary movement area is the south-western section of the central block (Figure 41), towards the transition zone containing a large graben.
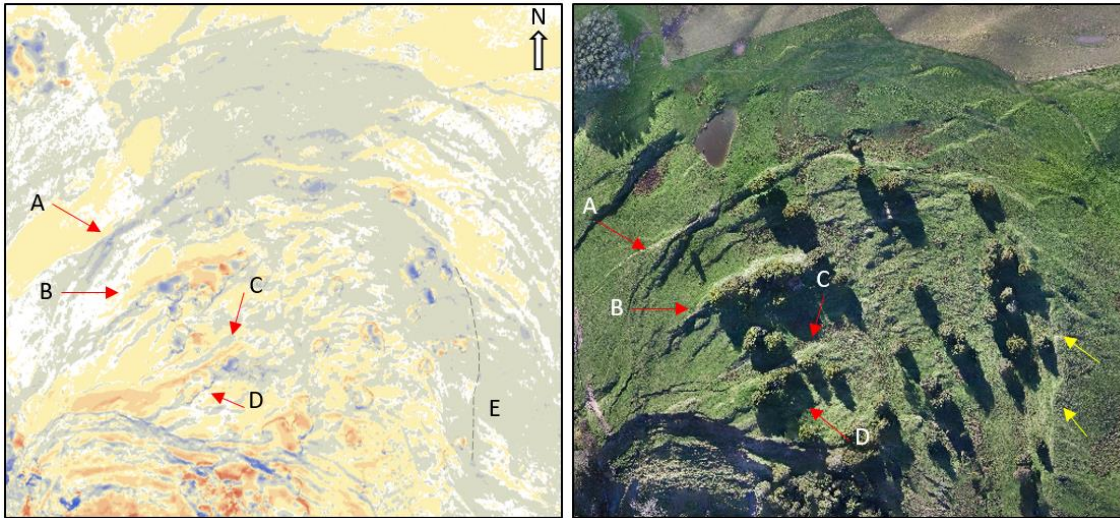
Figure 41. Comparison of the October 2016 – May 2017 DoD and orthophoto for the central area of the Rangitikei Slide, to highlight patterns of elevation change during that period. A – E are examples of notable features in the DoD, described in-text.

In the transition zone, the evolution of the graben is visible through areas of elevation loss and gain, particularly elevation loss behind the main northern edge of the graben (Figure 42, A). The graben edge itself shows elevation gain, appearing to be building up. There are blocks that have broken off and migrated into the graben (Figure 42, B) with previous positions shown in red. The eastern graben edge is also shown in blue, and below it shows patterns of elevation loss and gain as the area migrates south (Figure 42, C). The base of the graben shows significant elevation loss which could indicate that the graben is extending, and the centre is still losing elevation as it drops down. The ridges at the base of the graben show patterns of loss and gain, also indicating migration southwards (Figure 42, D).
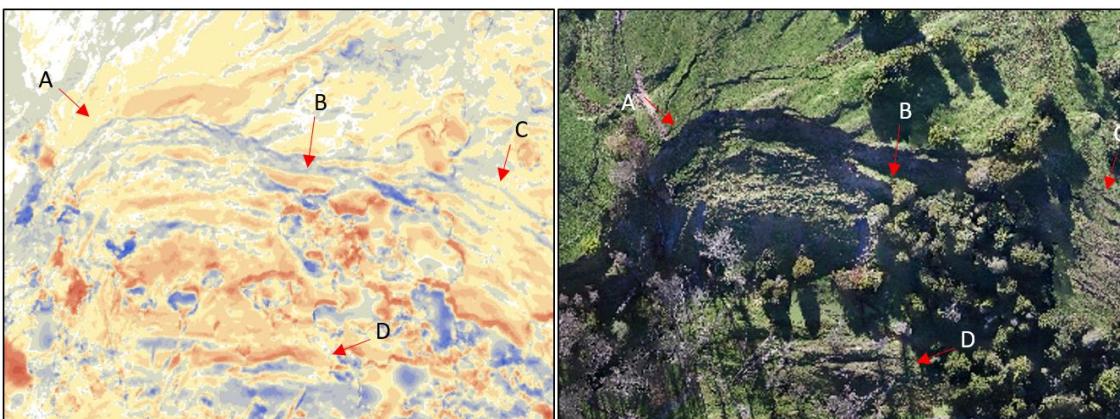
Figure 42. Comparison of the October 2016 – May 2017 DoD and orthophoto for the transition area of the Rangitikei Slide, to highlight patterns of elevation change during that period. A – D are examples of notable features in the DoD, described in-text.

The toe area shows general elevation gain on the surface, and patterns of loss and gain on the southern graben edge (Features A & B in Figure 43), indicating migration south and highlighting that this may not be as stable as initially thought. The large areas of elevation difference are likely vegetation artefacts from the densely vegetated area south of the graben edge (Feature A in Figure 43). There is also a form of vegetation interference at the toe (Figure 43, C), which represents a fallen tree. The erosion of the toe and bare rock cliff by the river is visible, which also indicates the boundary of bank cutting and the landslide movement boundary during this period (Figure 43, D & E).
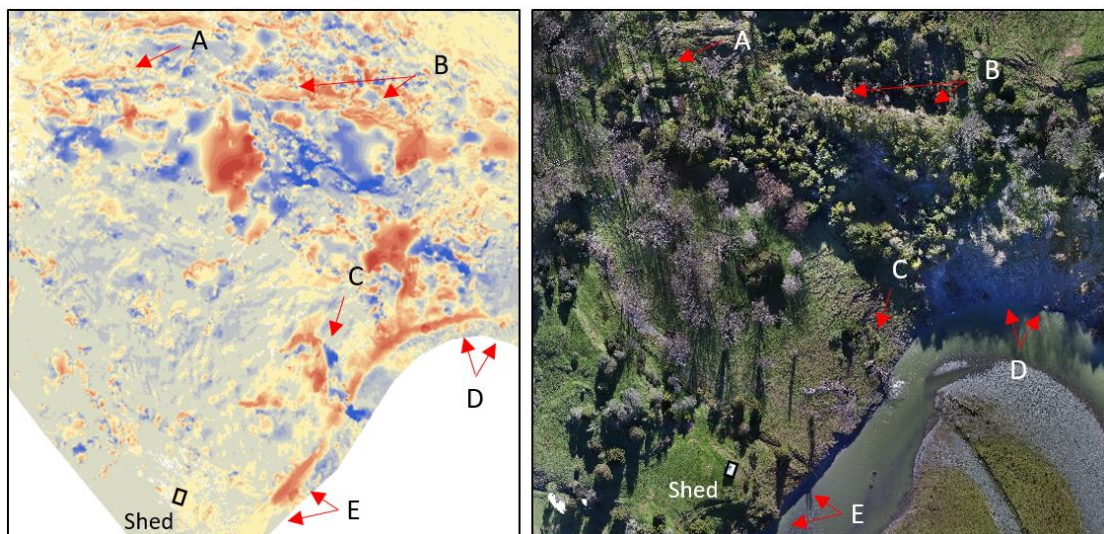
Figure 43. Comparison of the October 2016 – May 2017 DoD and orthophoto for the toe area of the Rangitikei Slide, to highlight patterns of elevation change during that period. A – E are examples of notable features in the DoD, described in-text.

The May 2017 – October 2017 DoD (Figure 44), which spans the winter period, shows a general pattern of elevation gain (blue) on the landslide.
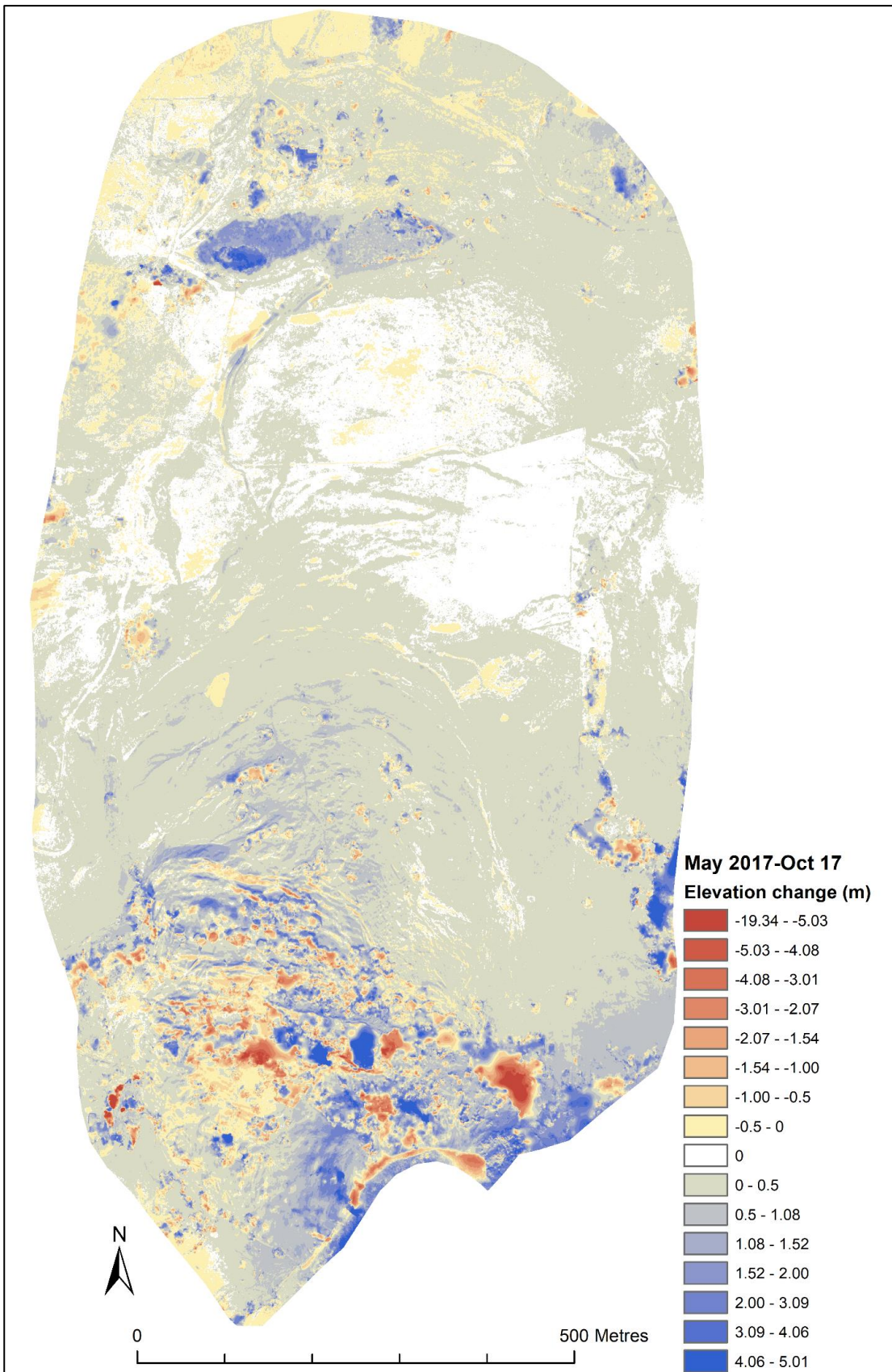
Figure 44. May 2017 – October 2017 DEM of Difference, showing elevation loss in red and elevation gain in blue.
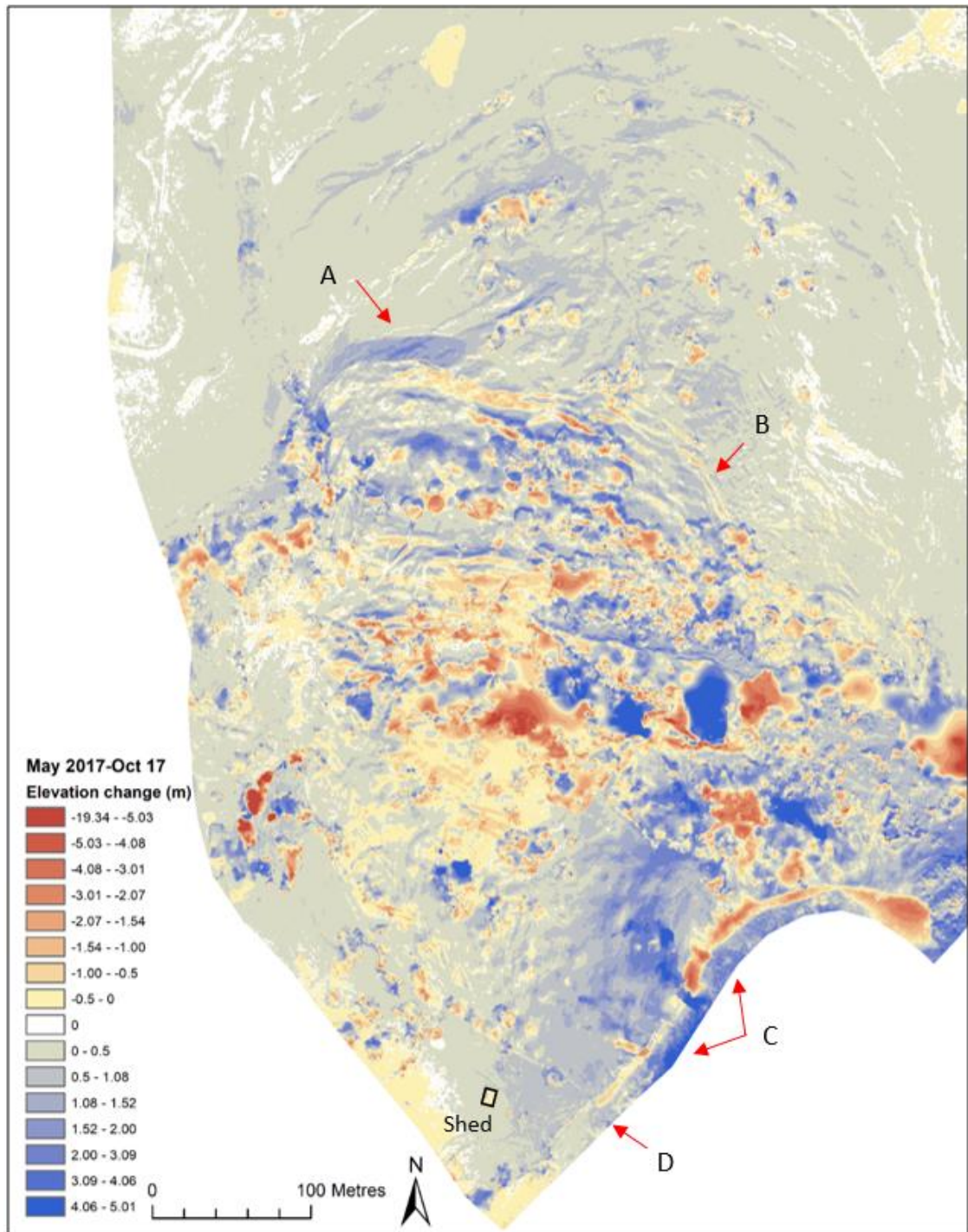
Figure 45. Close-up of the toe area in the May 2017 - October 2017 DEM of Difference, showing elevation loss in red and elevation gain in blue. A – D are examples of notable features in the DoD, described in-text.

There are areas of elevation loss on the southern side of features, which shows that southern migration has slowed or stopped (Figure 39). The northern graben edge shows a large area of elevation gain behind, and an area of loss in front representing erosion of the graben edge (Figure 45, A). This pattern, which is the opposite of the summer DoD, is visible throughout the transition zone. The eastern side of the upper graben edge shows elevation loss, which also indicates erosion of the graben edge, with the material deposited below shown by areas of

elevation gain (Figure 45, B). The lower toe area has a significant level of elevation gain that appears to be widespread across the frontal area. This represents a build-up of material, but there is still a band of elevation loss on the bank and cliff which is likely erosion from bank cutting (Figure 45, C). The erosion is not as evenly distributed across the toe front as in the summer DoD, with a lower degree of erosion occurring on the western half of the toe. The toe boundary is still clear, and the line of the lateral shear is clearly visible (Figure 45, D). There is some erosion on the bank in front of the shed, but is much less significant than on the active landslide bank, and there is also some elevation gain.

The October 2016 – October 2017 DoD (Figure 46) shows a more general trend of the landslide through time, and does not capture the seasonal trend apparent in the other two DoDs. The head graben has an area of apparent elevation loss, as shown by the larger areas of yellow and smaller patches of red. Of note in this DoD is the clear definition of the lower graben edge, highlighted by distinct elevation loss on the northern side (Figure 47, A). This elevation loss is supported by photos of the site (Figure 48) which shows falling trees and debris at the base of the graben edge. Compared to the northern graben edge, the southern edge is also significantly steeper. In this year-long DoD, the cliff front has overall experienced elevation gain (Figure 47, C). The same can be said for the toe front, except for a section of erosion which represents the removal of fallen trees.

Differences between hillshade models are very hard to assess visually, but are quantified in the geomorphic change detection analysis section. The vegetation removal (pixel classification) in the DEMs were not consistent between surveys and resulted in more 'noise' present in the October 2017 hillshade model (Figure 33). This is visible as a rougher surface on the Rangitikei River and the south-eastern corner. This will affect the geomorphic change detection analysis for the October 2017 survey.
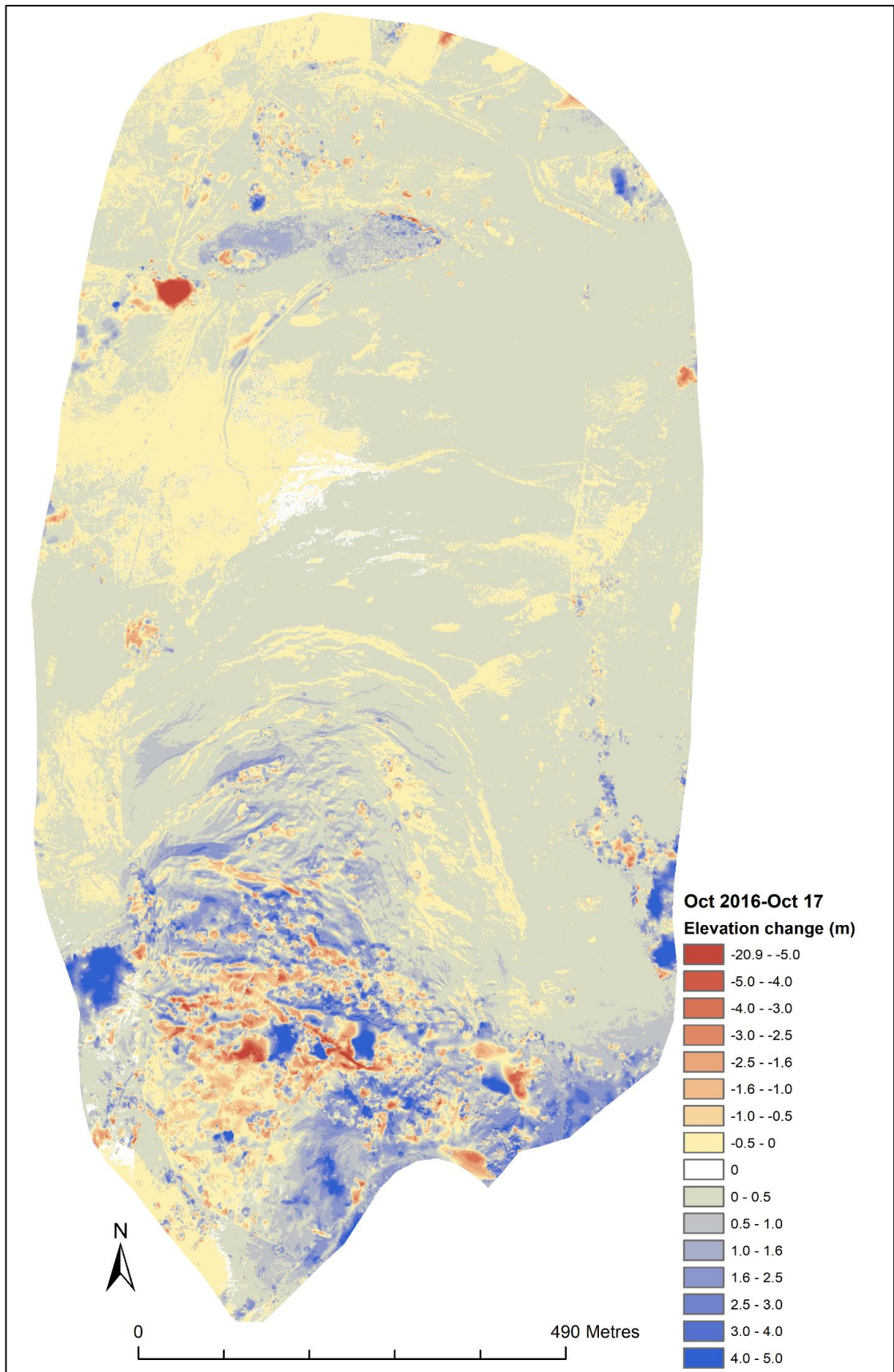
Figure 46. October 2016 – October 2017 DEM of Difference, showing elevation loss in red and elevation gain in blue.
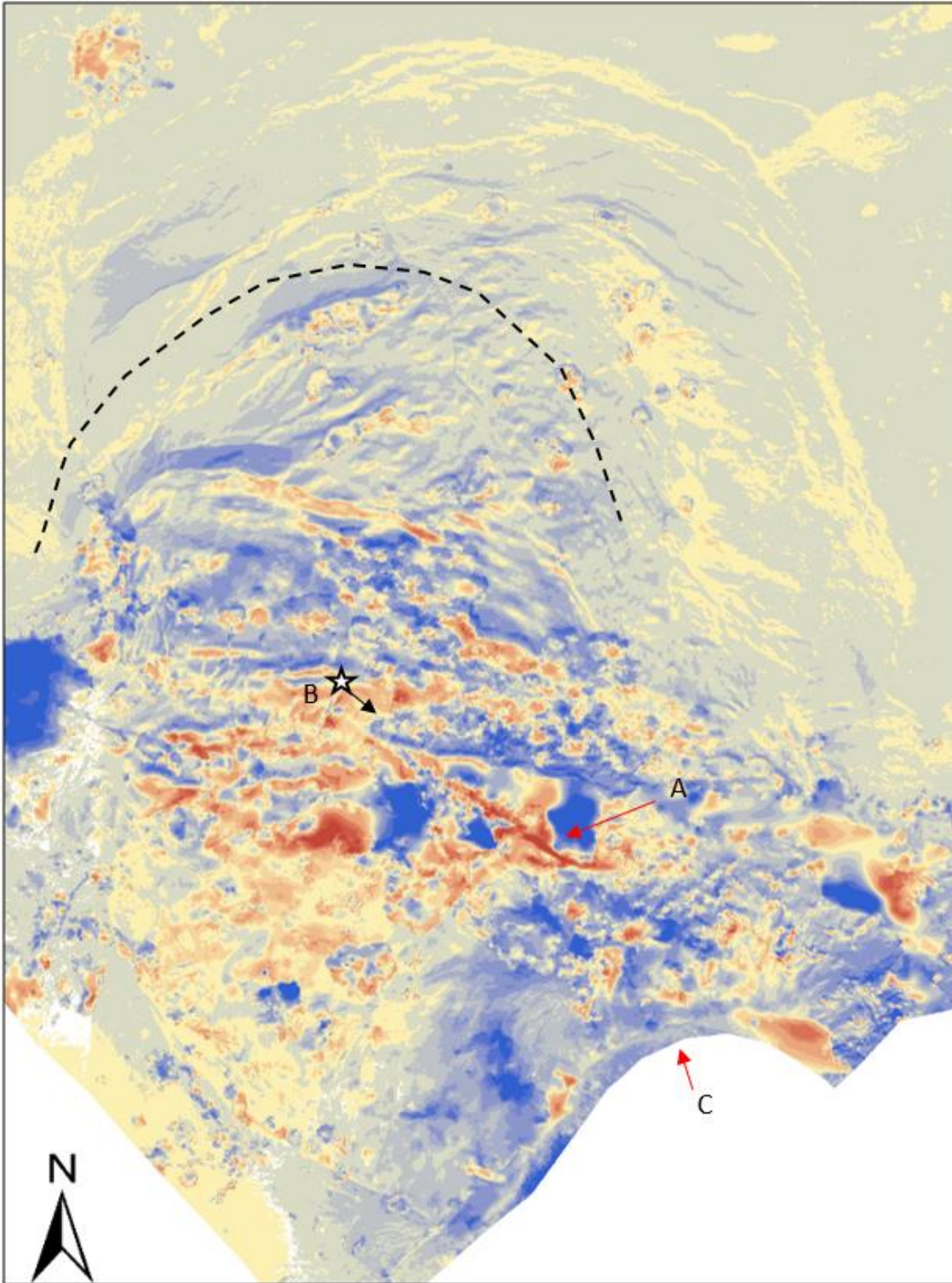
Figure 47. Close-up of the toe area in the October 2016 - October 2017 DEM of Difference, showing elevation loss in red and elevation gain in blue. A & C are examples of notable features in the DoD, described in-text, and B highlights the position and direction the photo was taken in Figure 48. The black dashed line marks the area of concentrated active movement.

Figure 48. Photo taken in October 2017 from the base of the graben, showing the southern graben edge (position shown in Figure 47).

4.1.3   Volumetric changes

GCD provides the areal, volumetric, and vertical changes that occurred within each DoD to indicate where the primary movement areas were located on the landslide. The October 2016 – May 2017 DoD indicates a higher estimate for elevation gain (labelled 'deposition' in the table) in both area and volume compared to 'erosion' (Table 4). The comparison between raw and thresholded estimates (in both Table 4 and Figure 49) highlights the importance of accounting for error, as vegetation artefacts are generally accounted for in the thresholding by classifying the point cloud into ground or non-ground points, and using only the classified ground points in each DEM. However, all vegetation artefacts are not always thresholded, resulting in small areas of large elevation differences. The percentage of elevation loss was 46% and elevation gain was 54%, which differs drastically from the May 2017 – October 2017 DoD with 20% elevation loss and 80% elevation gain (Table 5). This supports the visual analysis of the DoDs, that the winter DoD (May 2017 – October 2017) experienced more elevation gain than the summer DoD.

The histograms highlight the distribution of change, and the majority of the change is under 10 m of elevation loss or gain (Figure 49). The proportion of elevation gain and loss is clear in the histograms, particularly when comparing the summer DoD (Figure 49, graph A) with the winter DoD (Figure 49, graph B), and the stark increase in elevation gain.

Table 4. GCD output for October 2016 - May 2017 DoD, showing areal, volumetric, and vertical changes between surveys. Notable values are shown in red. In this table, 'erosion' is interchangeable with elevation decrease and 'deposition' with elevation increase.

Attribute for Oct 2016 – May 2017 DoD	Raw	Thresholded DoD Estimate:				
AREAL:						
Total Area of Interest (m²)	1,963,497	NA				
Percent of Area of Interest with Detectable Change	NA	34%				
VOLUMETRIC:					± Error Volume	% Error
Total Volume of Erosion (m³)	1,937,049	122,732	±	11,147		9%
Total Volume of Deposition (m³)	2,094,773	143,662	±	16,525		12%
Total Net Volume Difference (m³)	157,724	20,930	±	19,933		95%
VERTICAL AVERAGES:				± Error Thickness		% Error
Average Net Thickness Difference (m) for Area of Interest	0.08	0.01	±	0.01		95%
Average Net Thickness Difference (m) for Area with Detectable Change	NA	0.03	±	0.03		95%
PERCENTAGES (BY VOLUME)						
Percent Erosion (elevation decrease)	48%	46%				
Percent Deposition (elevation increase)	52%	54%				
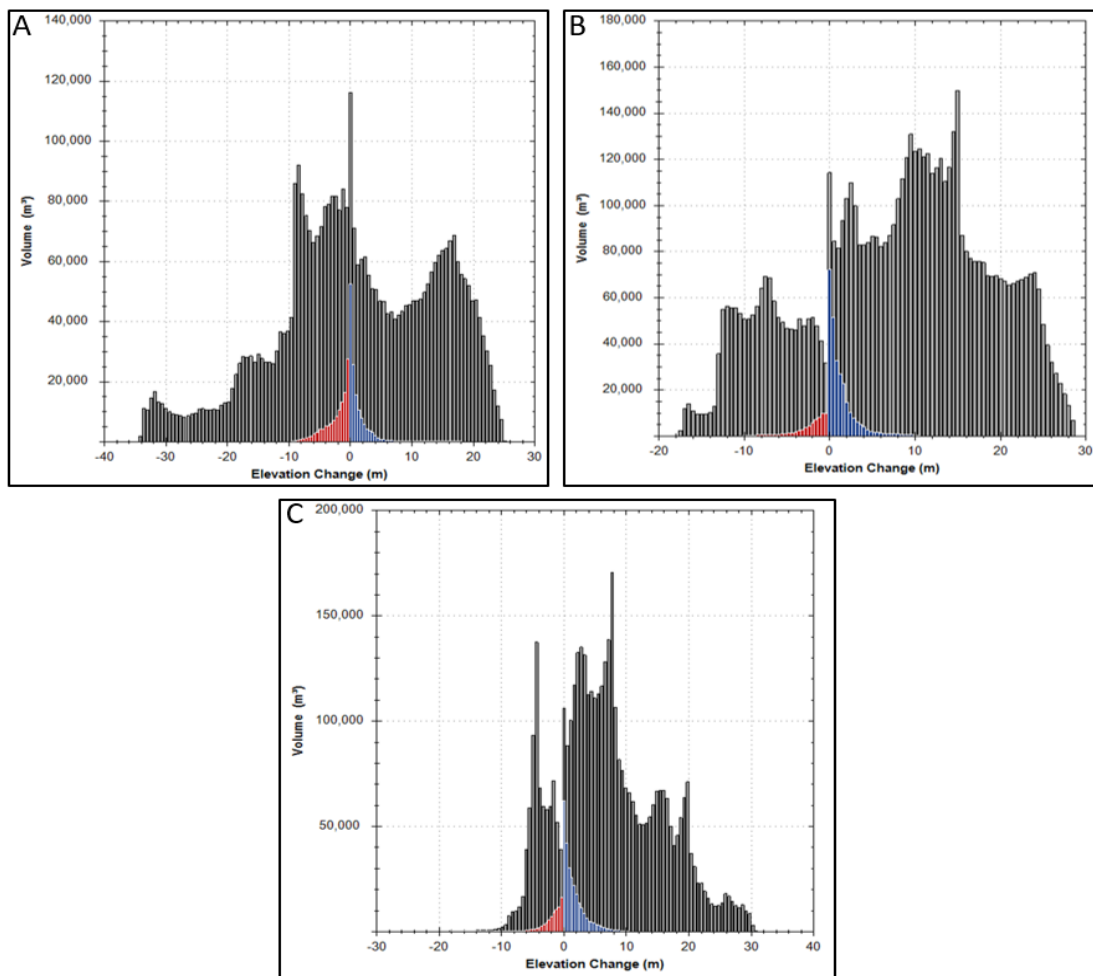
Figure 49. Histograms from all three DoDs showing the volumetric change between surveys, and the degree of thresholding in grey. A) October 2016 – May 2017, B) May 2017 – October 2017, C) October 2016 – October 2017. The histograms have different scales on both the x and y axes.

The analysis for the winter DoD (Table 5) shows a significant net elevation gain of 28 cm, compared to 3 cm in the summer DoD.

Table 5. GCD output for May 2017 – October 2017 DoD, showing areal, volumetric, and vertical changes between surveys. Notable values are shown in red. In this table, erosion is interchangeable with elevation decrease and deposition with elevation increase.

Attribute for May 2017 – Oct 2017 DoD	Raw	Thresholded DoD Estimate:		
AREAL:				
Total Area of Interest (m²)	2,002,138	NA		
Percent of Area of Interest with Detectable Change	NA	36%		
VOLUMETRIC:			± Error Volume	% Error
Total Volume of Erosion (m³)	1,437,205	66,274	± 4,134	6%
Total Volume of Deposition (m³)	4,836,562	272,177	± 26,588	10%
Total Net Volume Difference (m³)	3,399,357	205,903	± 26,908	13%
VERTICAL AVERAGES:			± Error Thickness	% Error
Average Net Thickness Difference (m) for Area of Interest	1.70	0.10	± 0.01	13%
Average Net Thickness Difference (m) for Area with Detectable Change	NA	0.28	± 0.04	13%
PERCENTAGES (BY VOLUME)				
Percent Erosion	23%	20%		
Percent Deposition	77%	80%		

Overall, between October 2016 and October 2017, almost half of the landslide experienced elevation changes (Table 6), and this amounted to a net positive volume difference of ~190,000 m³. Most of the elevation change was 'deposition' (elevation gain) during the time-period, which equates to a net elevation gain of 21 cm.

Table 6. GCD output for October 2016 – October 2017 DoD, showing areal, volumetric, and vertical changes between surveys. Notable values are shown in red. In this table, erosion is interchangeable with elevation decrease and deposition with elevation increase.

Attribute for Oct 2016 – Oct 2017 DoD	Raw	Thresholded DoD Estimate:		
AREAL:				
Total Area of Interest (m²)	1,910,865	NA		
Percent of Area of Interest with Detectable Change	NA	47%		
VOLUMETRIC:			± Error Volume	% Error
Total Volume of Erosion (m³)	805,963	84,913	± 1,367	2%
Total Volume of Deposition (m³)	3,497,968	272,650	± 5,080	2%
Total Net Volume Difference (m³)	2,692,004	187,737	± 5,261	3%
VERTICAL AVERAGES:			± Error Thickness	% Error
Average Net Thickness Difference (m) for Area of Interest	1.41	0.10	± 0.00	3%
Average Net Thickness Difference (m) for Area with Detectable Change	NA	0.21	± 0.01	3%
PERCENTAGES (BY VOLUME)				
Percent Erosion	19%	24%		
Percent Deposition	81%	76%		

4.1.4 Historical aerial imagery analysis

Historical aerial imagery from Google Earth found that some of the significant features visible on the Rangitikei Slide at present only formed in recent history. While the upper area of the landslide remained relatively static in recent history, the middle and toe areas underwent a number of changes that are visible in the imagery.

Figure 50. Aerial imagery from Google Earth of the Rangitikei River in early 2005. A - D highlights key features.

Imagery from 2005 shows that the established graben in the transitional zone (Figure 29) had not formed (Figure 50, A), but tension cracks were visible. By 2012, the graben was forming including the lower graben extent (Figure 52, A'), and in 2014 the graben appears fully formed (Figure 53, A & A').

Figure 51. Aerial imagery from Google Earth of the Rangitikei River in late 2005. A - D highlights key features.

The central drainage line was more defined in early 2005 (Figure 50, B) compared to the other imagery and at present, and fence lines were still intact in 2005 (Figure 50, C), but not visible in 2012 (Figure 52, C).

Figure 52. Aerial imagery from Google Earth of the Rangitikei River in 2012. A - D highlights key features.

The toe appears active throughout due to the fallen trees at the river edge (Figure 50, Figure 51, & Figure 52). The shed construction is visible in the 2014 imagery (Figure 53, C).

Figure 53. Aerial imagery from Google Earth of the Rangitikei River in 2014. A - C highlights key features.

Although the morphology indicates that the landslide has undergone movement in the past, which is supported by the hillshade models, the strong development of new features indicates that the landslide activity may have increased in recent years, becoming reactivated or accelerating.

4.2   Monitoring results

4.2.1   RTK-dGPS monitoring

Repeat occupations of a single point (precision error, δxy) in each survey were always within 25 mm and consistent between surveys, ranging between 12-24 mm (Table A2), suggesting that any movement >24 mm is considered to be true movement. Horizontal movement error was ≤27 mm (Table 7). Pegs designated as outside of the survey area (and peg 2 within the survey area) had movement rates <27 mm. This minimum level of detection indicates that the pegs outside the survey area (except peg 15) and peg 2 (within the survey area) showed no real movement.

There is an increase in movement rate towards the toe of the landslide, with the upper block of the landslide (zone A in the hillshades) moving <1 m (Table 7A), the middle section (zones B-C) moving <7 m (Table 7B), and the lower area (zone D-E) moving <39 m (Table 7C) in the study

period. The survey pegs within these areas are grouped as they underwent similar magnitude and direction of movement.

In the map of horizontal movement magnitudes (Figure 54), the upper block southward movement, and the middle block also shows mostly southward movement and movement towards the centreline of the landslide boundary (Figure 54, peg 19 & 28). There are pegs placed outside of the designated landslide boundary to compare against the active movement and these show similar movement magnitudes and direction to the upper area. This is because the area outside of the Rangitikei Slide is not considered 'stable' as the landslide is part of a large mass movement complex (the Poroa complex), which experiences its own movement.

The map of vertical movement magnitudes (Figure 55) shows that most vertical change occurred towards the toe and in the transitional zone between the middle block and the toe area (red and purple arrows), which are the areas with the steepest slope. In the transitional zone, vertical movement is an order of magnitude higher than the rest of the landslide and is on a similar scale to horizontal movement, which is illustrated by peg 16, which dropped ~ 3 m vertically but only moved ~5 m horizontally during the survey mark lifespan (July 2015 – March 2016). This shows a substantial vertical movement by the land in this area compared to elsewhere on the landslide.

Movement was found to be highly seasonal with greater movement in the July – December period, and lowest in the December – July period (Figure 56). The seasonal movement response is offset from the typical seasons, as the Southern Hemisphere winter is June - August and summer is December – February.

A notable feature is the response from most pegs to a cluster of flood events in April and May 2017, shown by a rapid rise in movement rates following the mid-March survey to the July survey. This increased movement precedes the 2017 winter period, and occurred outside of the usual high movement period. The RTK-dGPS data cannot be used to assess when movement is triggered within this study period due to the low temporal resolution (3-monthly surveys), but the timing and pattern of this movement is investigated further with the time-lapse imagery. Many of the survey pegs experienced more movement in the 2017 higher movement period compared to the same period in 2016, highlighting an inconsistent landslide response between the years.

Table 7 A-C. Movement statistics for the survey marks in the upper section, middle, and toe area of the landslide, including survey marks outside of the hypothesised active landslide boundary.

A Upper section	Survey mark	Survey period	Total Horizontal movement (m)	No. of days	Daily movement rate (mm/day)	Vertical movement from start point (m)	Direction
Within survey area	2	July 2015 - October 2017	0.15 ± 0.27	831	0.18	-0.04 ± 0.18	South-west
	4	July 2015 - October 2017	0.31 ± 0.27	831	0.37	0.01 ± 0.18	South
	5	July 2015 - October 2017	0.46 ± 0.27	831	0.55	-0.06 ± 0.18	South
	6	July 2015 - October 2017	0.33 ± 0.27	831	0.40	0.05 ± 0.18	South
	8	July 2015 - October 2017	0.65 ± 0.27	831	0.78	-0.13 ± 0.18	South
	9	July 2015 - October 2017	0.90 ± 0.27	831	1.08	-0.18 ± 0.18	South
	10	July 2015 - October 2017	0.30 ± 0.27	831	0.36	-0.03 ± 0.18	South
	Average		0.41 ± 0.27	820	0.49	-0.06 ± 0.18	South
Outside survey area	1	Sept 2015 - October 2017	0.16 ± 0.21	742	0.22	-0.10 ± 0.13	South
	3	Sept 2015 - October 2017	0.20 ± 0.21	742	0.27	-0.06 ± 0.13	South
	7	July 2015 - October 2017	0.24 ± 0.27	831	0.29	0.00 ± 0.18	South

B Middle section	Survey mark	Survey period	Total Horizontal movement (m)	No. of days	Daily movement rate (mm/day)	Vertical movement from start point (m)	Direction
Within survey area	11	Dec 2015 - October 2017	1.81 ± 0.19	674	2.69	-0.41 ± 0.12	South
	12	July 2015 - October 2017	1.71 ± 0.27	831	2.05	-0.66 ± 0.18	South
	13	July 2015 - October 2017	1.26 ± 0.27	831	1.52	-0.10 ± 0.18	South
	14	July 2015 - October 2017	5.45 ± 0.27	831	6.56	-1.43 ± 0.18	South
	17	Dec 2015 - October 2017	6.94 ± 0.19	674	10.29	-1.06 ± 0.12	South
	18	July 2015 - October 2017	1.08 ± 0.27	831	1.30	-0.19 ± 0.18	South
	19	July 2015 - October 2017	3.54 ± 0.27	831	4.26	-1.84 ± 0.18	South-west
	20	July 2015 - June 2017	5.06 ± 0.13	727	6.96	-1.84 ± 0.08	South
	Camera	July 2015 - June 2017	0.19 ± 0.13	727	0.26	0.10 ± 0.08	South
	Average		3.00 ± 0.27	773	3.99	-0.83 ± 0.18	South
Outside survey area	15	Dec 2015 - October 2017	0.35 ± 0.19	674	0.51	-0.02 ± 0.12	South

C Toe area	Survey mark	Survey period	Total Horizontal movement (m)	No. of days	Daily movement rate (mm/day)	Vertical movement from start point (m)	Direction
Within survey area	16	July 2015 - March 2016	4.71 ± 0.22	258	18.26	-2.82 ± 0.14	South
	21	July 2015 - October 2017	19.91 ± 0.27	831	23.96	-2.53 ± 0.18	South-east
	22	July 2015 - October 2017	38.81 ± 0.27	831	46.70	-3.33 ± 0.18	South-east
	24	July 2015 - October 2017	14.49 ± 0.27	831	17.44	-0.03 ± 0.18	South
	25	Sept 2015 - October 2017	14.48 ± 0.21	831	17.43	-0.88 ± 0.13	East
	28	July 2015 - October 2017	2.24 ± 0.27	831	2.69	-0.31 ± 0.18	South-east
	29	Mar 2017 - October 2017	4.58 ± 0.05	205	22.35	0.14 ± 0.04	South
	Average		13.53 ± 0.27	749	18.08	-1.41 ± 0.18	South-east
Outside survey area	23	July 2015 - October 2017	0.05 ± 0.27	831	0.06	0.02 ± 0.18	South-east
	26	Sept 2015 - October 2017	0.09 ± 0.21	831	0.11	0.02 ± 0.13	South-west
	27	July 2015 - October 2017	0.02 ± 0.27	831	0.03	0.04 ± 0.18	South-east
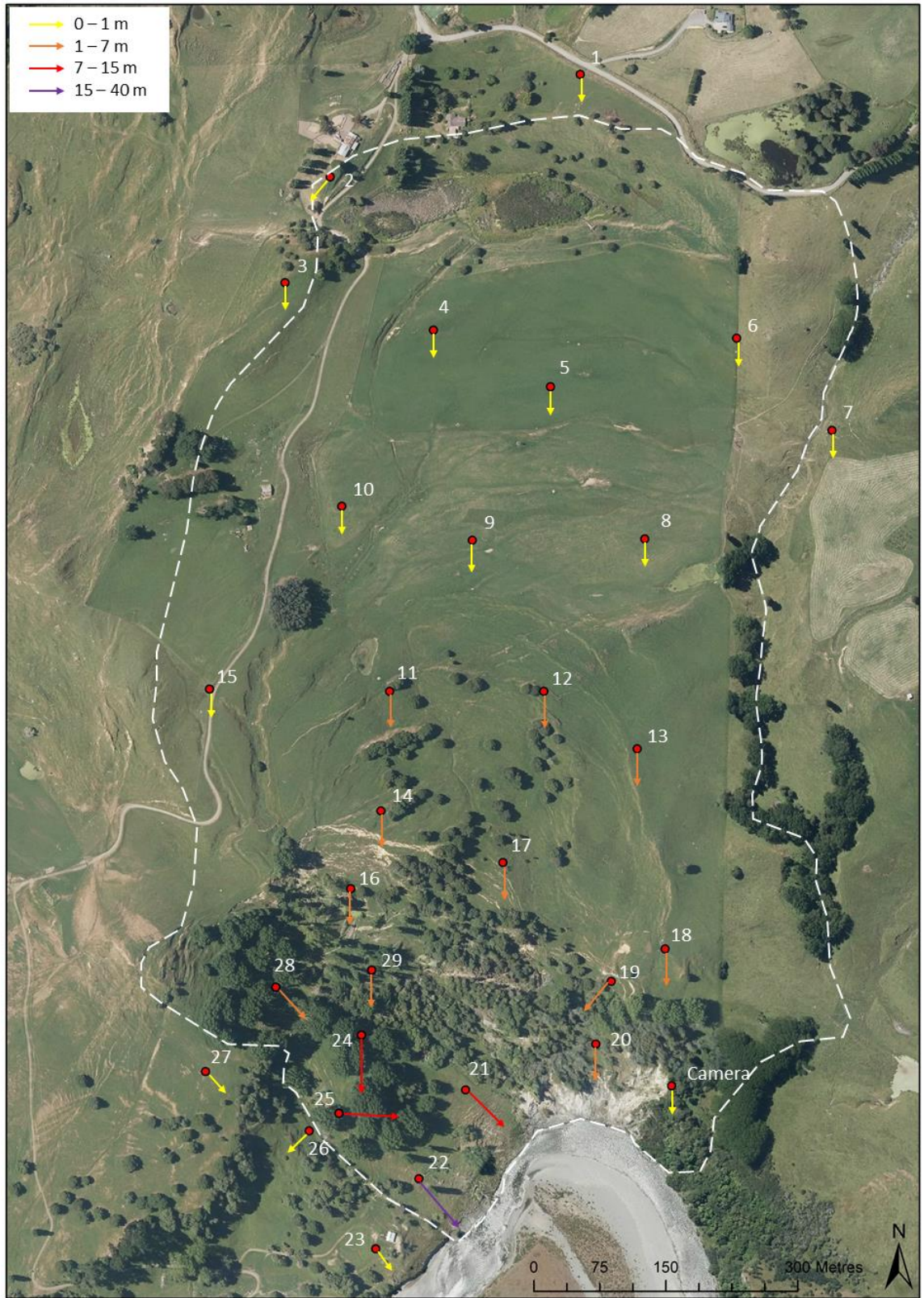
Figure 54. Horizontal movement magnitude map of the RTK-dGPS network, showing total horizontal movement from July 2015 to October 2017. Colour and arrow length indicate (roughly) movement magnitude, alongside the mapped active landslide boundary.
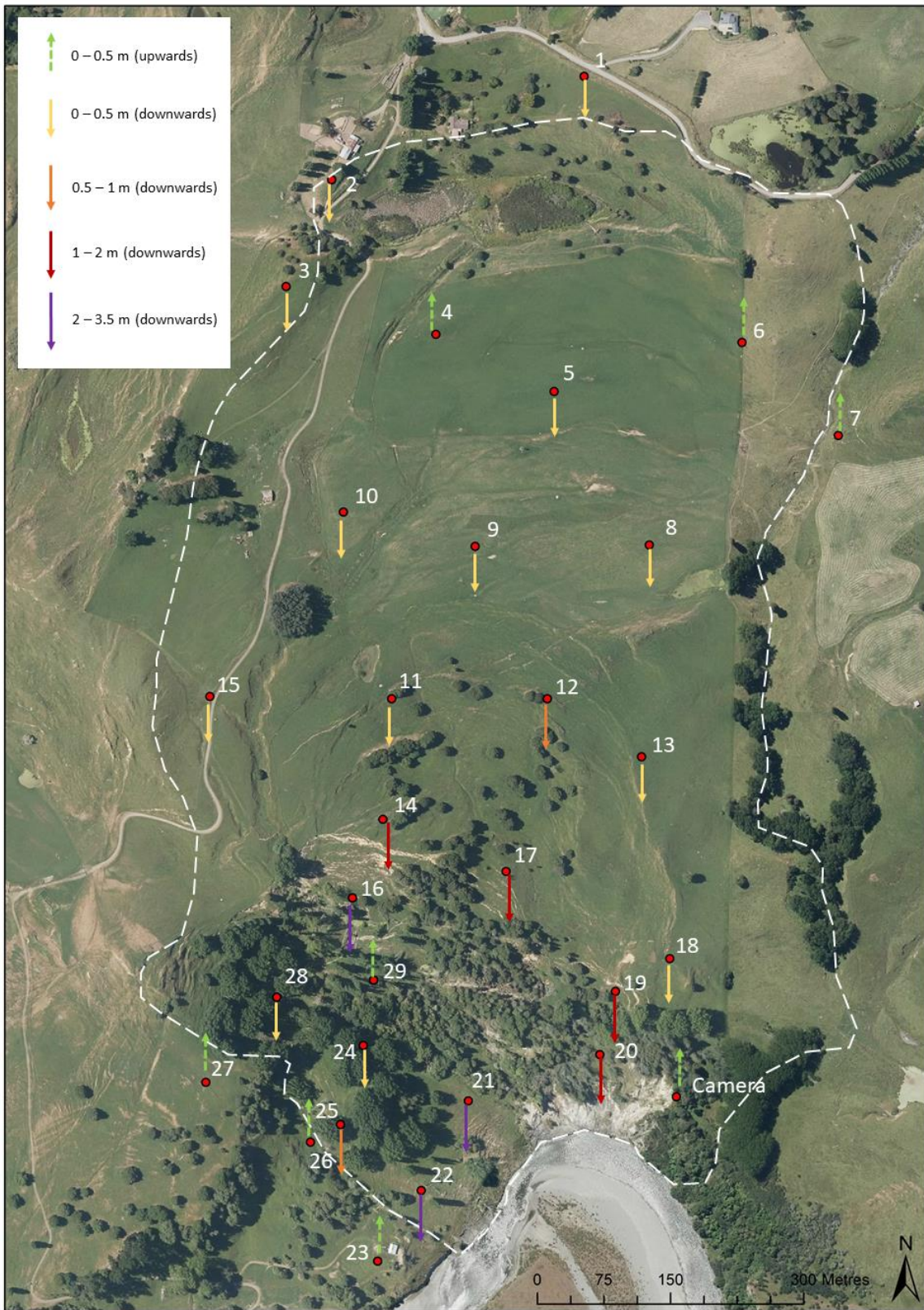
Figure 55. Vertical movement magnitude map of the RTK-dGPS network, showing total vertical movement from July 2015 to October 2017. Colour indicates movement magnitude, alongside the mapped active landslide boundary.
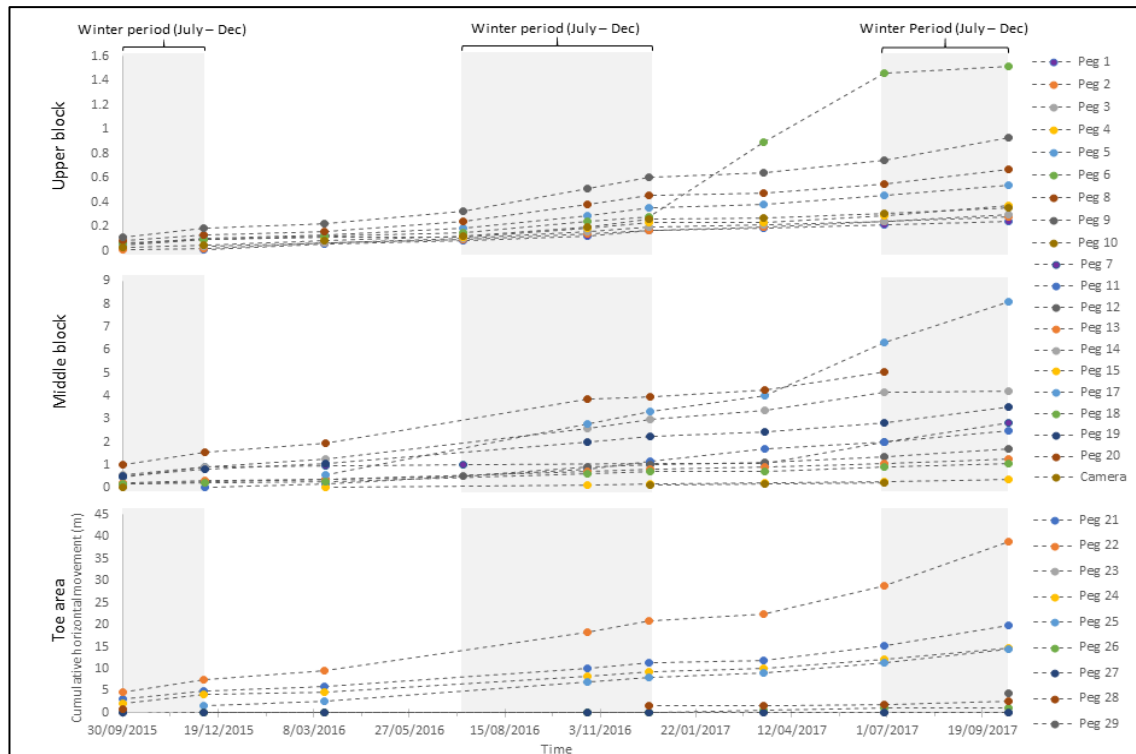
Figure 56. Cumulative horizontal movement rates for the three main areas of the Rangitikei Slide, separated by movement magnitude shown on the vertical axis, which differs for each graph. The graphs start from September as each point is the difference between two surveys, and the latter survey date was chosen as the label. This means that the first point does not start at 0 as it represents any movement between July and September 2015. The grey areas roughly signify the faster movement periods, which is difficult to accurately determine due to the 3-month resolution of the data.

Table 8. Comparison between the horizontal movement rates for representative pegs in each landslide block (peg 9, 19, and 21). The older date is differenced from the most recent date, and the mostly positive results in the table indicate that movement has increased over time. The winter periods did not span the entire designated winter season as the study period ended in October 2017, requiring the 2016 winter period to be equally shortened to allow accurate comparison. Without the July 2016 survey data for the middle and toe area, the movement rates for the start of winter 2016 were estimated by calculating the mean between the two surveys either side. The error margin was calculated by propagating the precision error (δxy) of every survey involved in the time-period.

Peg 9	Horizontal Movement difference (m)
Summer 2017 – Summer 2016	0.005 ± 0.09
Winter 2017 – Winter 2016	0.004 ± 0.08
Winter 2017 – Summer 2017	0.041 ± 0.09
Winter 2016 – Summer 2016	0.042 ± 0.08

Peg 19	Horizontal Movement difference (m)
Summer 2017 – Summer 2016	0.07 ± 0.09
Winter 2017 – Winter 2016	0.23 ± 0.08
Winter 2017 – Summer 2017	0.05 ± 0.09
Winter 2016 – Summer 2016	-0.25 ± 0.08

Peg 21	Horizontal Movement difference (m)
Summer 2017 – Summer 2016	1.72 ± 0.09
Winter 2017 – Winter 2016	2.63 ± 0.08
Winter 2017 – Summer 2017	0.91 ± 0.09
Winter 2016 – Summer 2016	0 ± 0.08

4.2.2 Pixel tracking

4.2.2.1 Weekly pixel tracking

The seasonal trend highlighted in the RTK-dGPS data is clearly visible in the time-lapse imagery, and quantified with the weekly pixel tracking data (Figure 58). There is also an event-based movement trend, which is highlighted by the landslide response to a series of significant flood events. Movement rates increase in the June – October period and decrease in the November – May period.

The 2017 winter period had a higher frequency of large rainfall and flood events than the 2016 winter (Figure 59). The 2016 winter was considered warm and mostly dry for much of New Zealand, with soil moisture levels below average (NIWA, 2016), while the 2017 winter was described as having rainfall and soil moisture levels above average (NIWA, 2017). Any increased landslide movement could be attributed to a wetter winter.

Figure 57. Weekly pixel tracking point locations on the Rangitikei Slide.
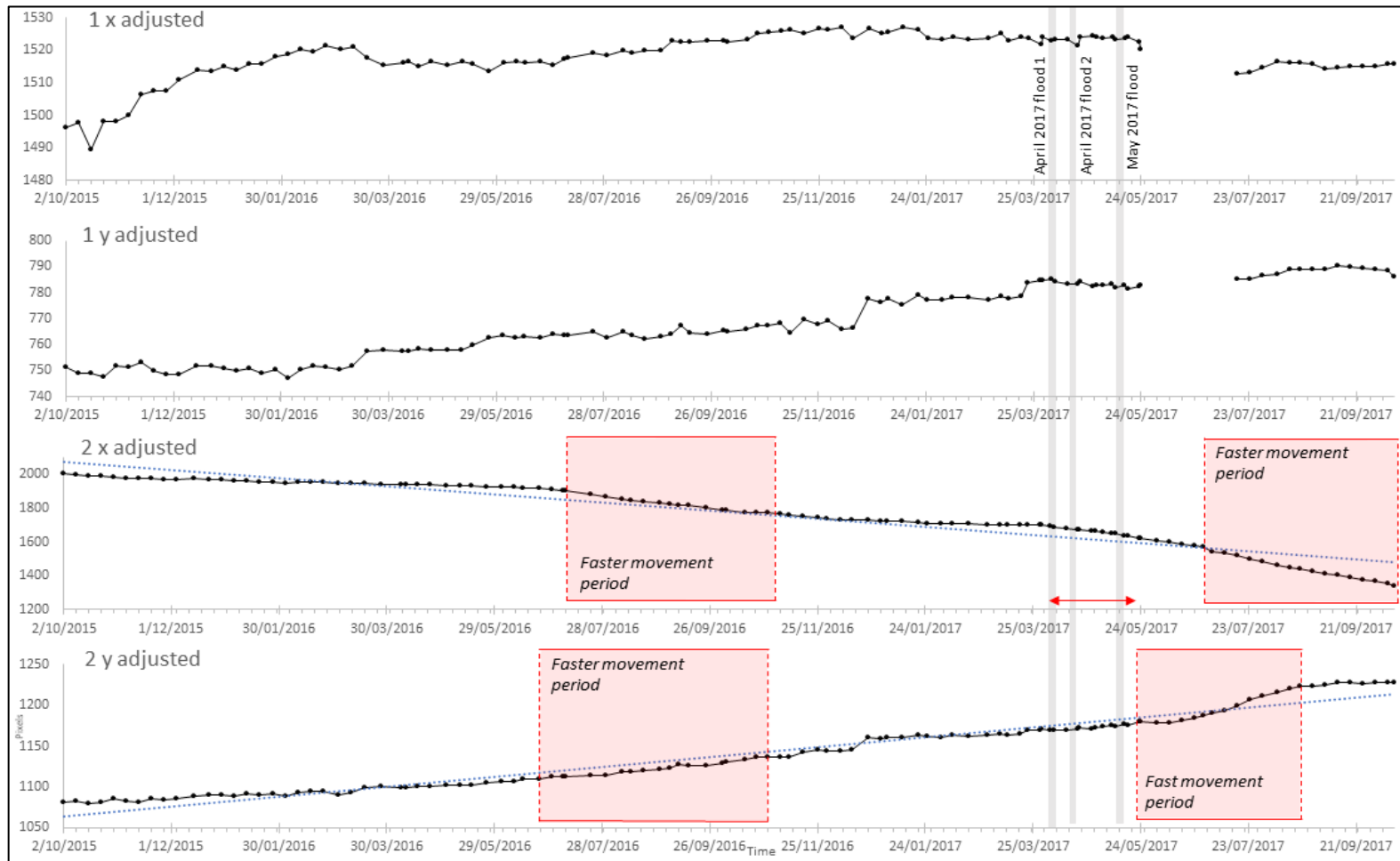
Figure 58. Weekly pixel tracking for September 2015 to October 2017 (A change in camera lens meant July – September 2015 could not be tracked on the same plot and is ignored here). X is horizontal movement (negative trend shows movement towards the river) and Y is vertical movement (positive trend shows movement downslope), and there is a significant difference in movement magnitude between point 1 and point 2. Periods of increased movement (red), the trendline (blue), and three significant flood events (investigated in more detail later) are highlighted. This data has been adjusted for distinct camera movement (verified by the time-lapse imagery) by subtracting the movement (generally vertical) from the tracking data.
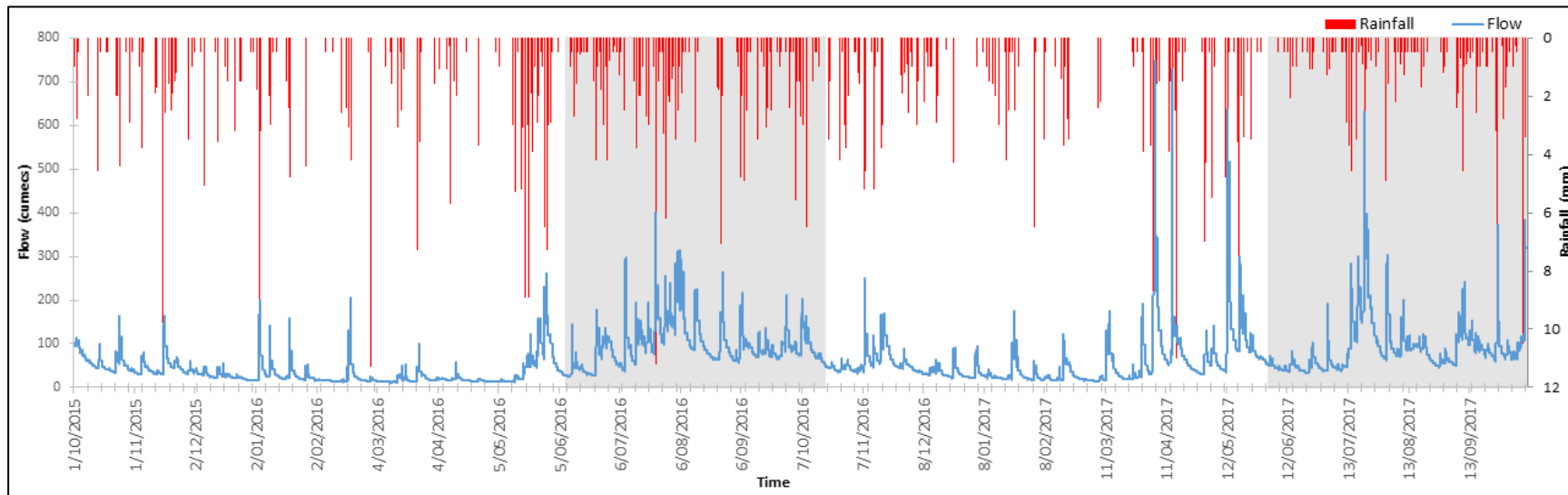
Figure 59. Rangitikei half-hourly flow and daily rainfall for the Taihape area for the whole weekly pixel-tracking period (provided by Horizons Regional Council – Mangaweka flow gauge and Makohine rainfall station). The periods of highest movement (June – October) are shown in grey.
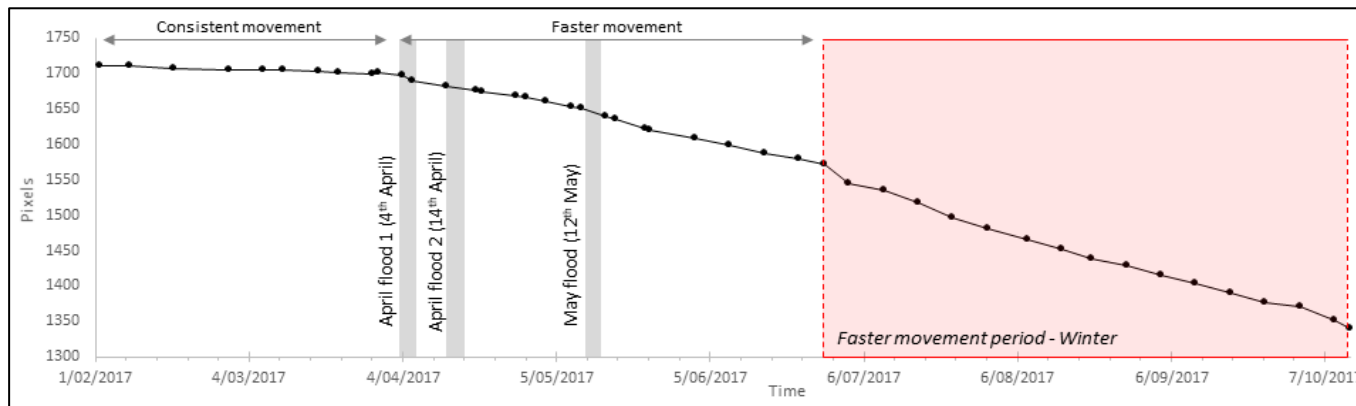
Figure 60. A segment of Point 2 x from the horizontal weekly pixel tracking, focused on the effect of flood events in 2017 (shown in grey) on movement rates.

The significant flood events (April and May 2017 floods) had a strong influence on movement rates, with a shift from a slower movement period (Figure 58, prior to the red arrow, graph 2 x) into a faster movement period. This movement period was identified in the RTK-dGPS data (Figure 56), and the weekly pixel tracking indicates that this movement was triggered by the first flood event in April (4/04/2017) and then continued through to the annual faster movement period (Figure 60). This is verified by an increased movement rate prior to winter 2017 (Table 9), which is substantial faster than the same period the previous year.

Table 9. Movement rates of the landslide toe for each time-period, determined by the weekly pixel tracking data.

	Movement rate (pixels/day)
Comparable period (April – July 2016)	0.38
Winter 2016 (July – November)	1.14
Floods 2017 (April – July)	1.48
Winter 2017 (July – October)	2.19

The increased movement during winter 2016 did not show any vertical movement patterns from initiation to stabilisation (Figure 61), but horizontally (Figure 62) shows faster movement after initiation (start of 2016 winter period) and then slower, consistent movement towards late winter. There is a period of ~2 weeks from the beginning of the 2016 faster movement period before the movement rapidly increases (Figure 62), which could be categorised as a 'lag period' as movement begins after the flow and rainfall events begin to increase. The rapid movement correlates with the highest concentration of flood events and rainfall events, and slows down after a small break (~1 week) of no substantial rainfall or flow events.

Towards the end (30th June – 13th August 2016) of the rapid movement period, the movement rate appears to increase, shown as a steeper gradient in the pixel tracking data (Figure 62).
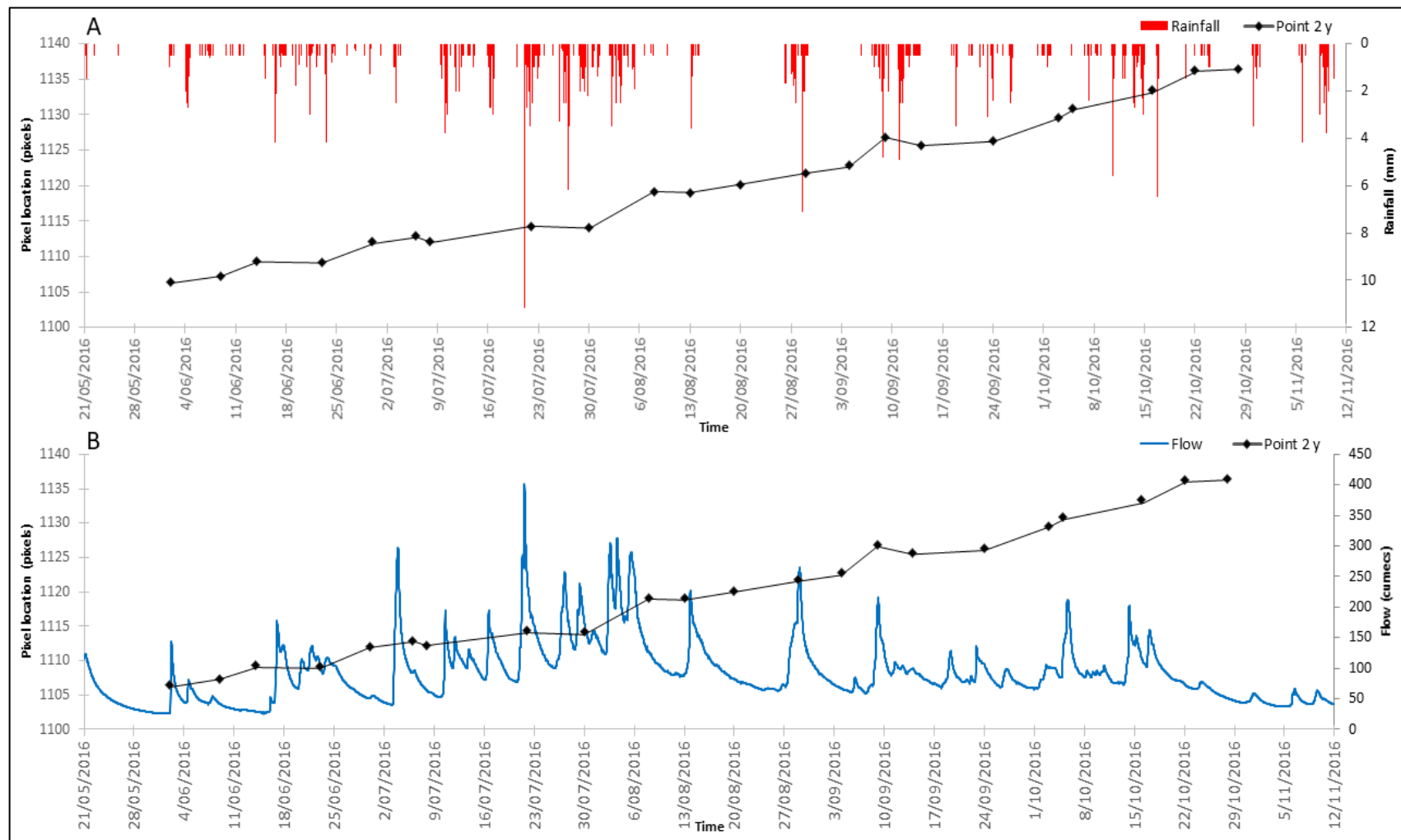
Figure 61. A) Comparison between rainfall and vertical weekly pixel tracking data for winter 2016 (Point 2 y from Fig. 2). B) Comparison between flow and vertical weekly pixel tracking data for winter 2016. A positive trend in the vertical data indicates downward movement towards the Rangitikei River, which is shown in this graph.
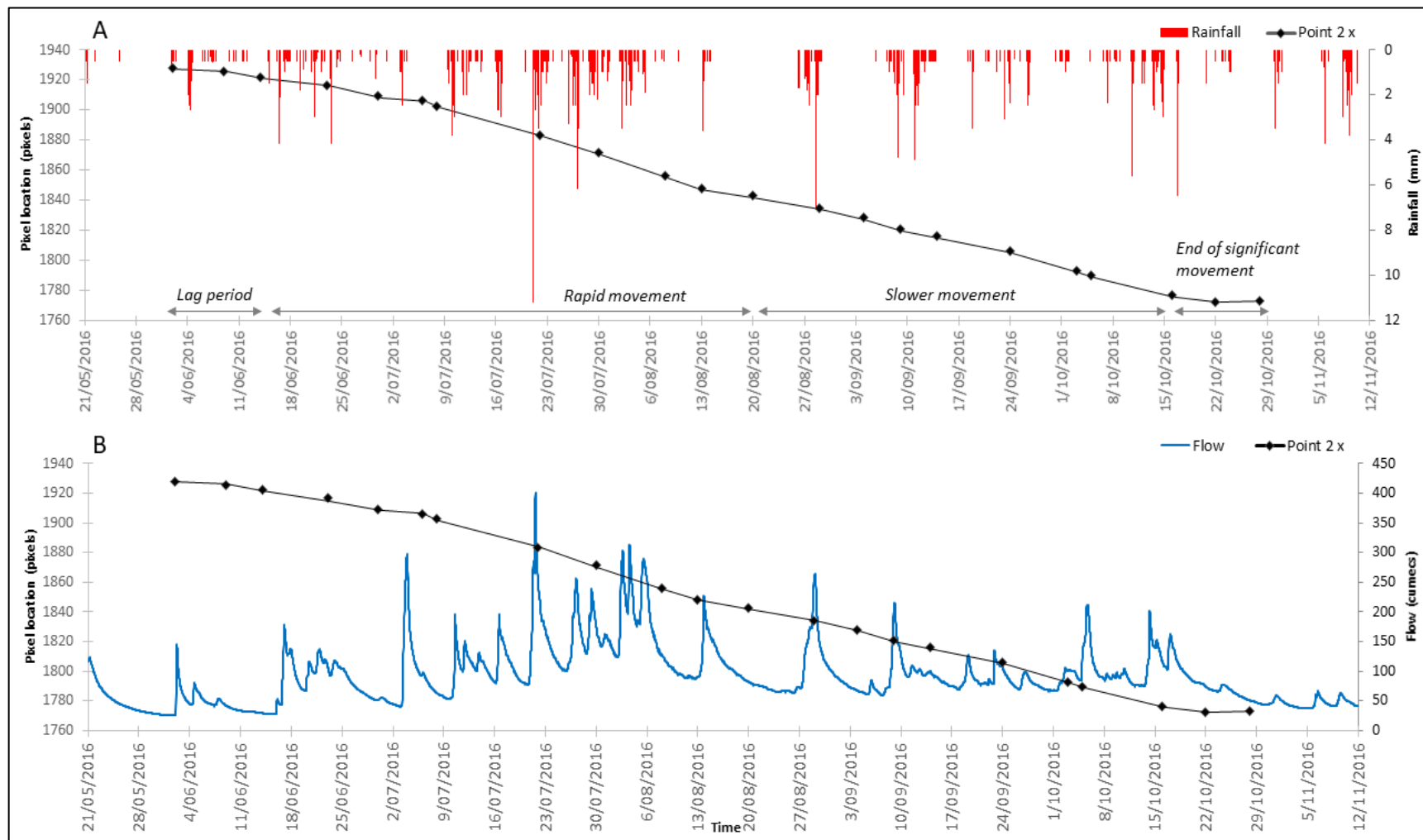
Figure 62. A) Comparison between rainfall and horizontal weekly pixel tracking data for winter 2016 (Point 2 x from Fig. 2). B) Comparison between flow and horizontal weekly pixel tracking data.

The RTK-dGPS and weekly time-lapse data indicate a possible link between significant flood events and landslide movement, with episodic movement correlating with rainfall or toe erosion at a weekly – seasonal timescale. This link is further explored through event-scale data, using hourly time-lapse pixel tracking to investigate the influence of significant flood events on the Rangitikei Slide movement rates.

4.2.2.2.1 Cyclone Debbie (4th April 2017)

One of the significant flood events occurred between the 4th – 6th April 2017, starting with a steady increase in river flow late on the 4th April due to a large ex-tropical cyclone (Cyclone Debbie) and reaching a peak of 746 m³/s (cumecs) at 5.30 pm on the 5th (Figure 63). There was a secondary peak in flow at 10 am on the 6th that rose 70 cumecs before continuing to drop.
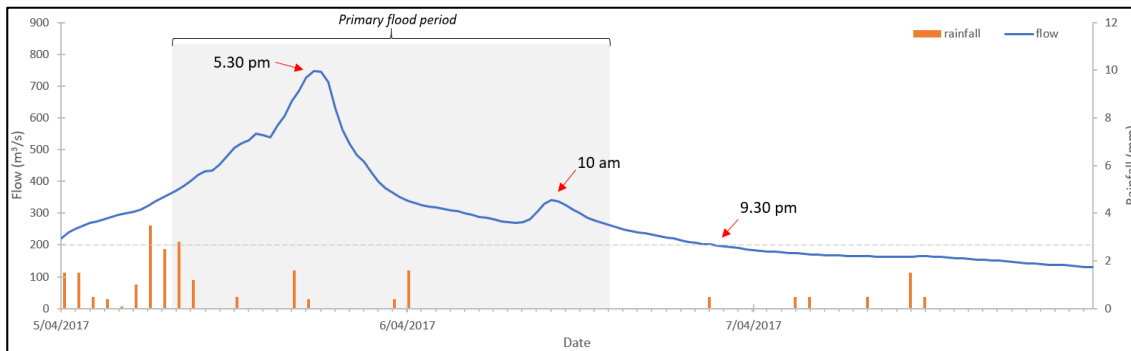
Figure 63. Rainfall and flow data for the early April flood event.

The flow receded below 200 cumecs from 9.30 pm and continued to drop throughout the 7th April. The rainfall near to the landslide site (Figure 63) was not significant during or leading up to the flood event, indicating that rainfall in the catchment upstream from the landslide site was more influential. According to the pixel tracking data, accelerated movement was initiated ~5 pm on the 5th April and correlates with the flood peak (Figure 63). The initial movement was substantial, appearing as a sudden pulse of movement resulting in a relatively consistent downslope movement by all points (Figure 64, points 2x – 4x), located to represent different areas of the lower section of the landslide (Figure 65).

The bank erosion map for the flood shows the erosion of the toe in relation to the bank position at the flood peak (Figure 66). The main flood peak was chosen as the starting position because the significant toe movement occurred at or following this. The landslide response is highlighted in the changes to the bank, which shows areas of bank fill (where the bank has slumped or flowed into free space) on the downstream bank edge, and a significant section of erosion at the base of the bare-rock cliff (Figure 66, B). This eroded area is exacerbated over time as flow levels drop, while the bank fill areas hardly change.
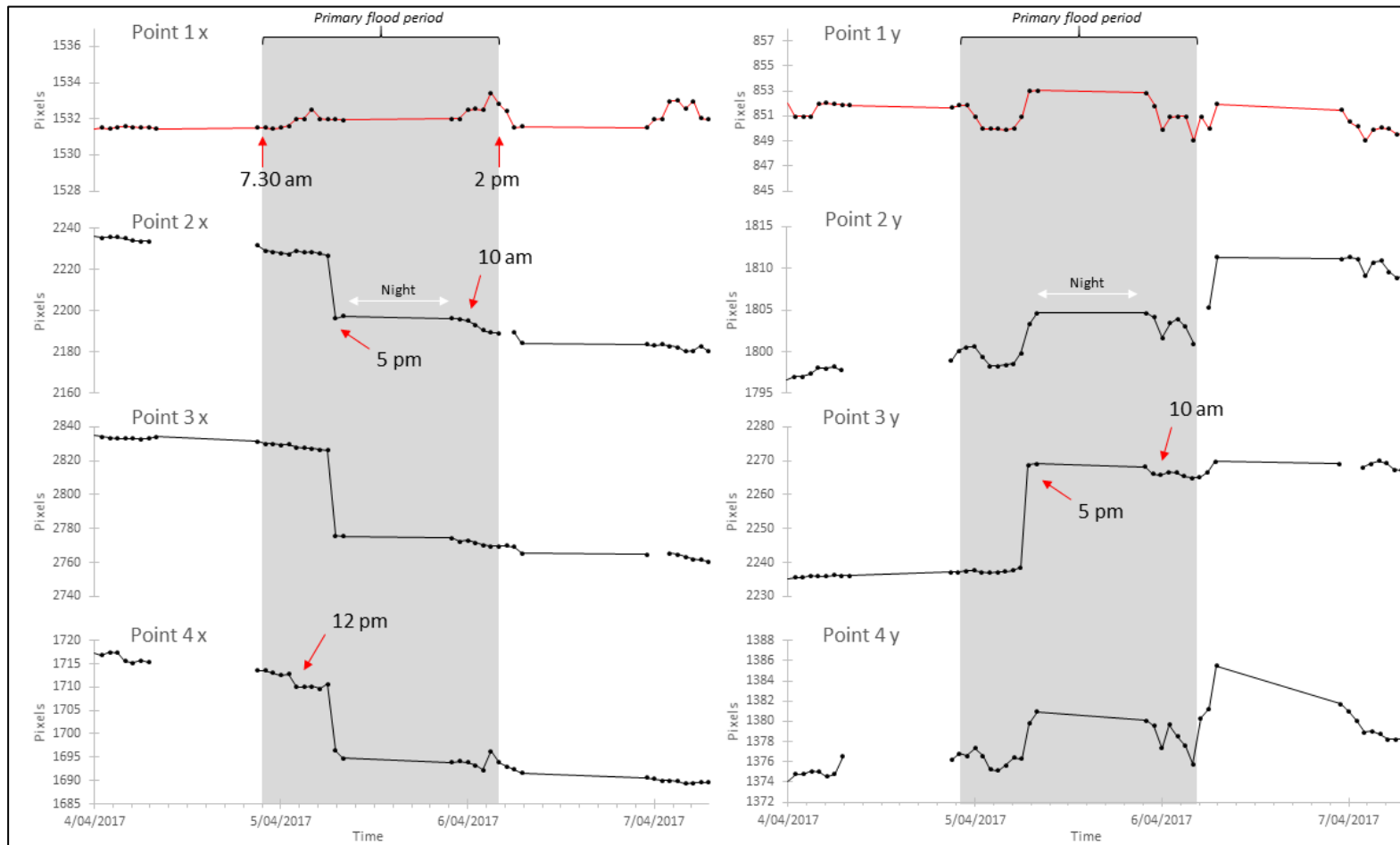
Figure 64. X-Y component plots for early April 2017. For point locations refer to Figure 65: Point 1) Centre of roof gable (i.e. control point); Point 2) Soil/grass clump near landslide toe; Point 3) Rock on cliff face of landslide; Point 4) Tree stump near landslide toe. Point 1 is on a 'stable' area of land and was used to identify camera movement. The primary flood period refers to the time above 200 cumecs, where the flow drastically exceeds normal flow levels. The long gaps (time) between points represents the night time, where photos are too dark to use. The rate of pixel change is the focus here, so the real-world displacement (metres) are not important for interpretation. It should be noted the scales for each point are drastically different, so Point 1 has very little movement (maximum of 4 pixels movement).

Figure 65. Pixel tracking point locations for the April 4th – 6th flood event.

The most significant changes occurred between the flood peak at 5 pm on the 5th and 8 am on the 6th (Figure 66, red dashed line). It is difficult to determine the timing for the initiation of movement and subsequent bank changes, as this appears to occur on the evening of the 5th, which cannot be monitored due to limited camera visibility (night-time).
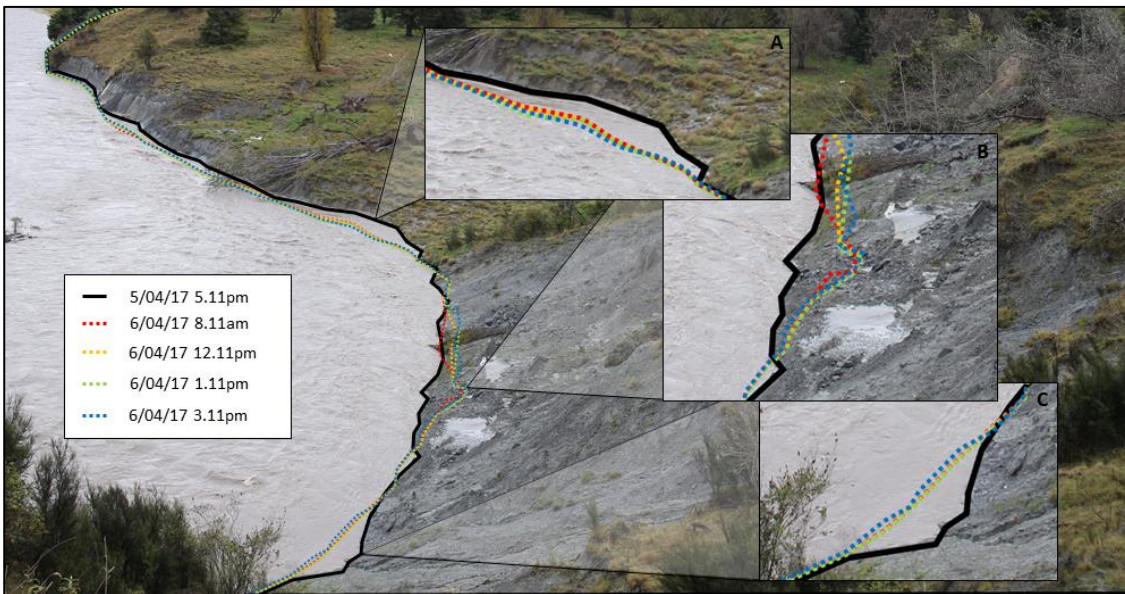
Figure 66. Bank erosion mapping showing the localised bank cutting and bank filling during the early April flood event. The map shows the cutting and filling that occurred during and an hour after the designated primary flood period.

There is a second phase following this initial movement, which correlates with the secondary peak at 10 am on the 6th (Figure 63) and is a further adjustment period in the pixel tracking. The pixel tracking shows that the landslide toe movement appears to slow and return to the movement rates prior to the flood event from the 7th. However, bank changes still occurred on the 7th, with further erosion of the bare-rock cliff base and small areas of bank fill (Figure 67). The small amount of bank fill after the primary flood period could represent some small residual movement from a particularly active section of the landslide toe (Figure 67, A).
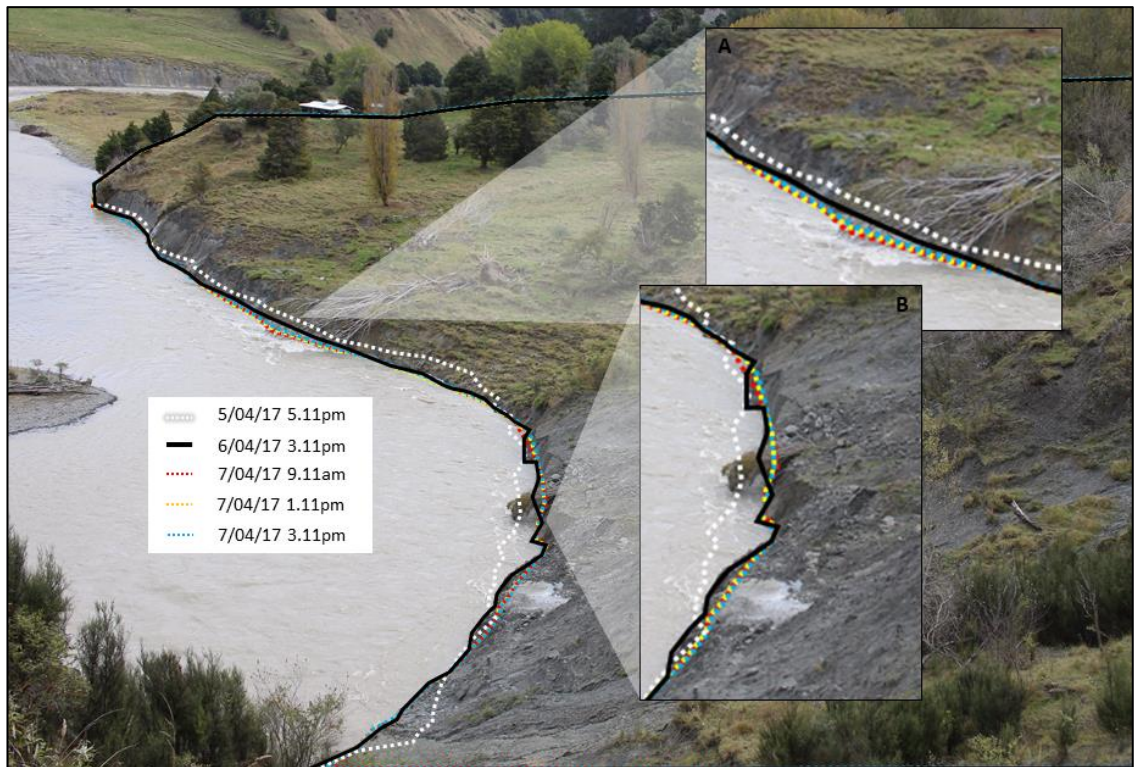
Figure 67. Bank erosion mapping showing the localised bank cutting and bank filling during the early April flood event. The map shows the cutting and filling that occurred after the designated primary flood period, highlighting the continued influence of a flood after the water has receded to much lower levels. The while dashed line represents the initial bank position at the primary flood peak.

4.2.2.2.2   Cyclone Cook (14th April 2017)

The second significant flood event (caused by ex-Tropical Cyclone Cook) began early on the 14th April 2017 with an extremely rapid rise in flow from midnight until 3 am, reaching 716 cumecs at the flood peak (Figure 68). There is a secondary peak at 4 pm on the 14th, increasing by 8 cumecs before continuing to recede. The end of the primary flood period is 1 am on the 15th April. There is a large rainfall event at 2 pm on the 16th, which appears to have no impact on river flows so is likely limited to the site. The pixel tracking shows movement being initiated on the 12th (Figure 69). Point 3 x shows a strong influence from prior to the second flood event, while point 4 x has a more definitive response to the flood.
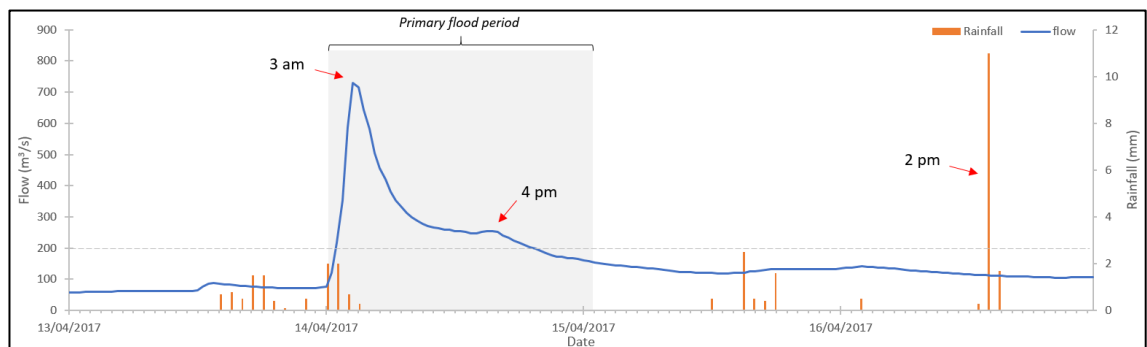
Figure 68. Rainfall and flow data for the mid-April flood event.
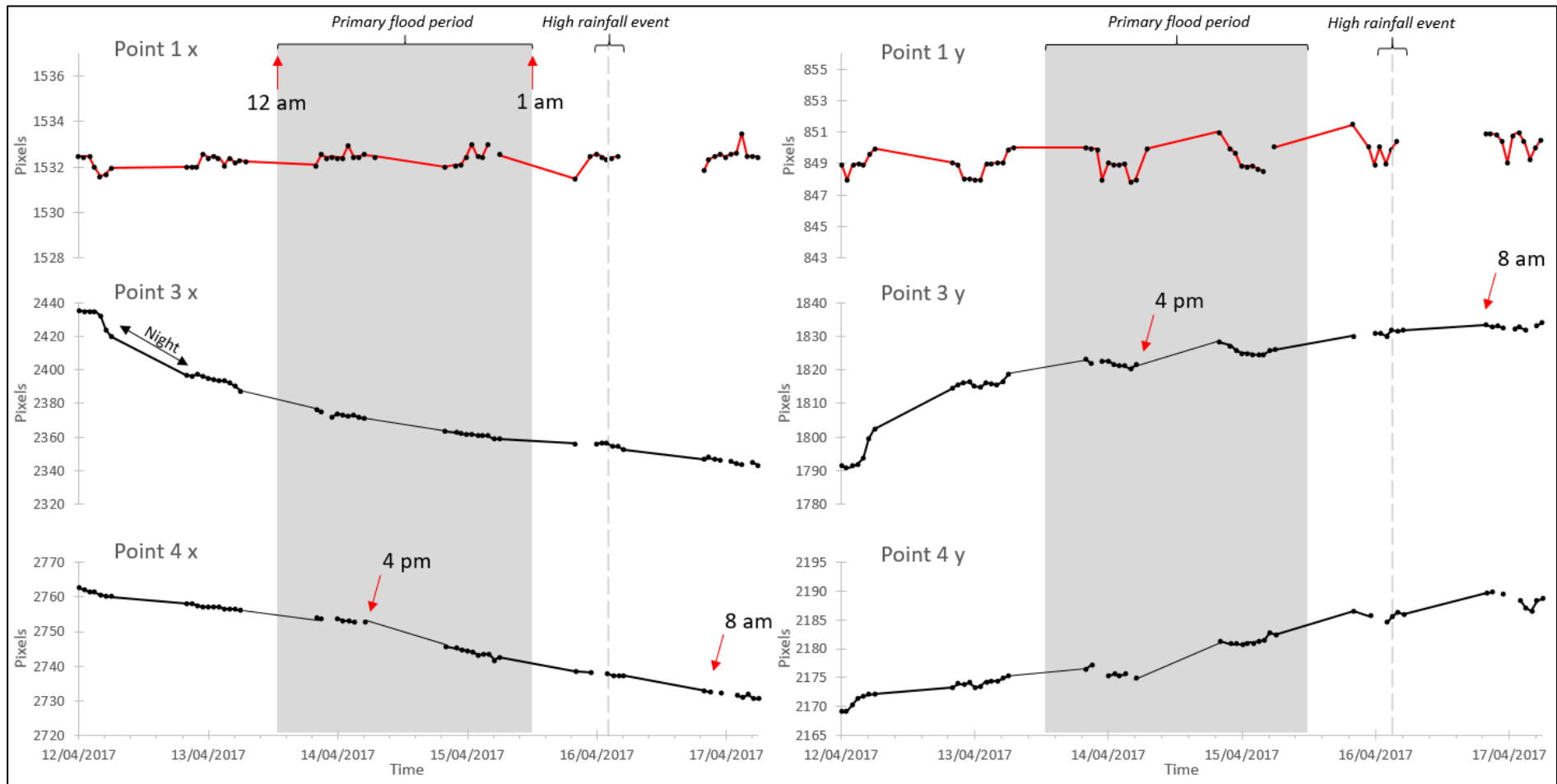
Figure 69. X-Y component plots for mid-April 2017. For point locations refer to Figure 70: Point 1) Centre of roof gable (control point); Point 3) Soil/grass clump at landslide toe; Point 4) Rock on cliff face on landslide. Point 1 can be used as an error analysis tool as it is on a 'stable' area of land.

The response of point 4 x shows a shift into a higher movement rate at 4 pm on the 14th which correlates with the secondary flood peak (Figure 68). There does not appear to be any response to the primary flood peak at 3 am on the 14th (just after the start of the primary flood period). The movement rate decreases with the lowering flow rate until the high rainfall event at 2 pm on the 16th, which caused a smaller period of increased movement at the toe. Point 2 (Figure 70) was left out of the pixel tracking results as the captured data was sporadic and lacked most of the data points. This was due to lighting of the tree base, which fluctuated too much at this point in time to be useful.
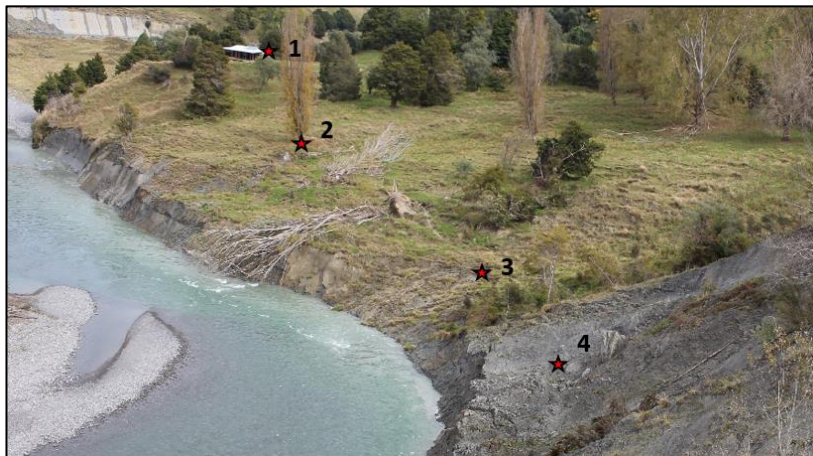
Figure 70. Pixel tracking point locations for the April 14th flood event.

The bank erosion mapping showed that erosion cut back the bank around most of the river bend, with the exception of the most upstream section of the bare-rock cliff (Figure 71, bottom of bank erosion map). The most significant erosion occurred on the sharpest section of the bend (Figure 71, B), which was consistently eroded and caused a smoother bank base than prior to the flood. The map shows the original bank outline from the 12th April, a day and a half before the flood event, which is due to time-lapse image quality in conjunction with the short lead-up to the flood peak (it took 3 hours to rise by 640 cumecs).
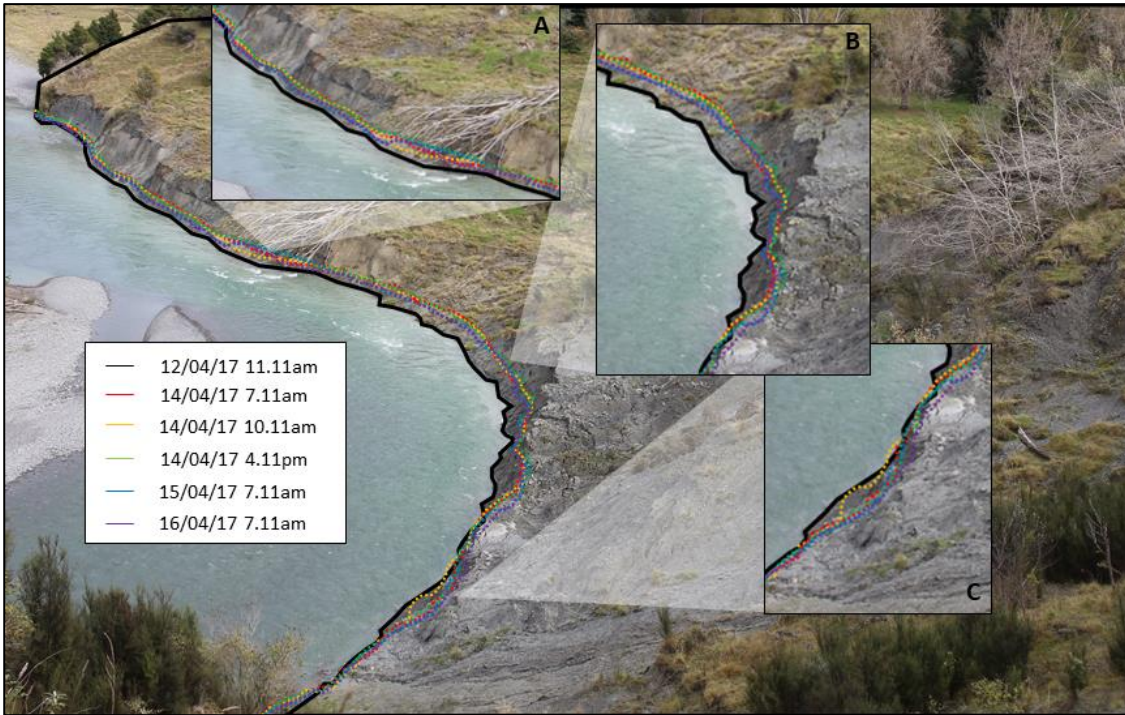
Figure 71. Bank erosion mapping showing the localised bank cutting and bank filling during the mid-April flood event.

4.2.2.2.3   May 2017

The last significant flood event in the study period began at 9.30 pm on the 11th May 2017, rising slowly at first (12.5 cumecs per hour) and then rising rapidly at 5.30 am on the 12th (102.8 cumecs per hour). The first flood peak occurred at 10 am on the 12th, and the highest flood peak reached 636 cumecs at 6 pm the same day. The flood stayed above 500 cumecs for ~18 hours before receding. From 2 am on the 13th, the flow receded below 500 cumecs and dropped consistently towards normal flow levels, passing 200 cumecs at 1 am on the 14th. The rainfall prior and during the flood event was significant, indicating almost two days of consistent rainfall.
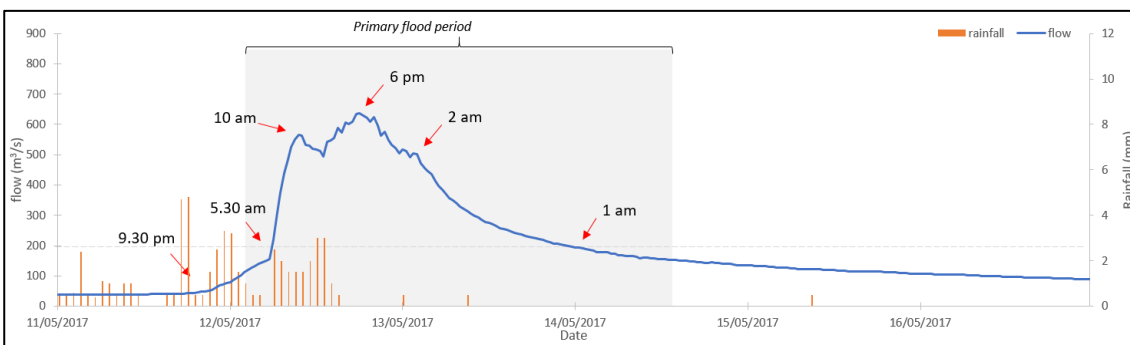
Figure 72. Rainfall and flow data for the May flood event.
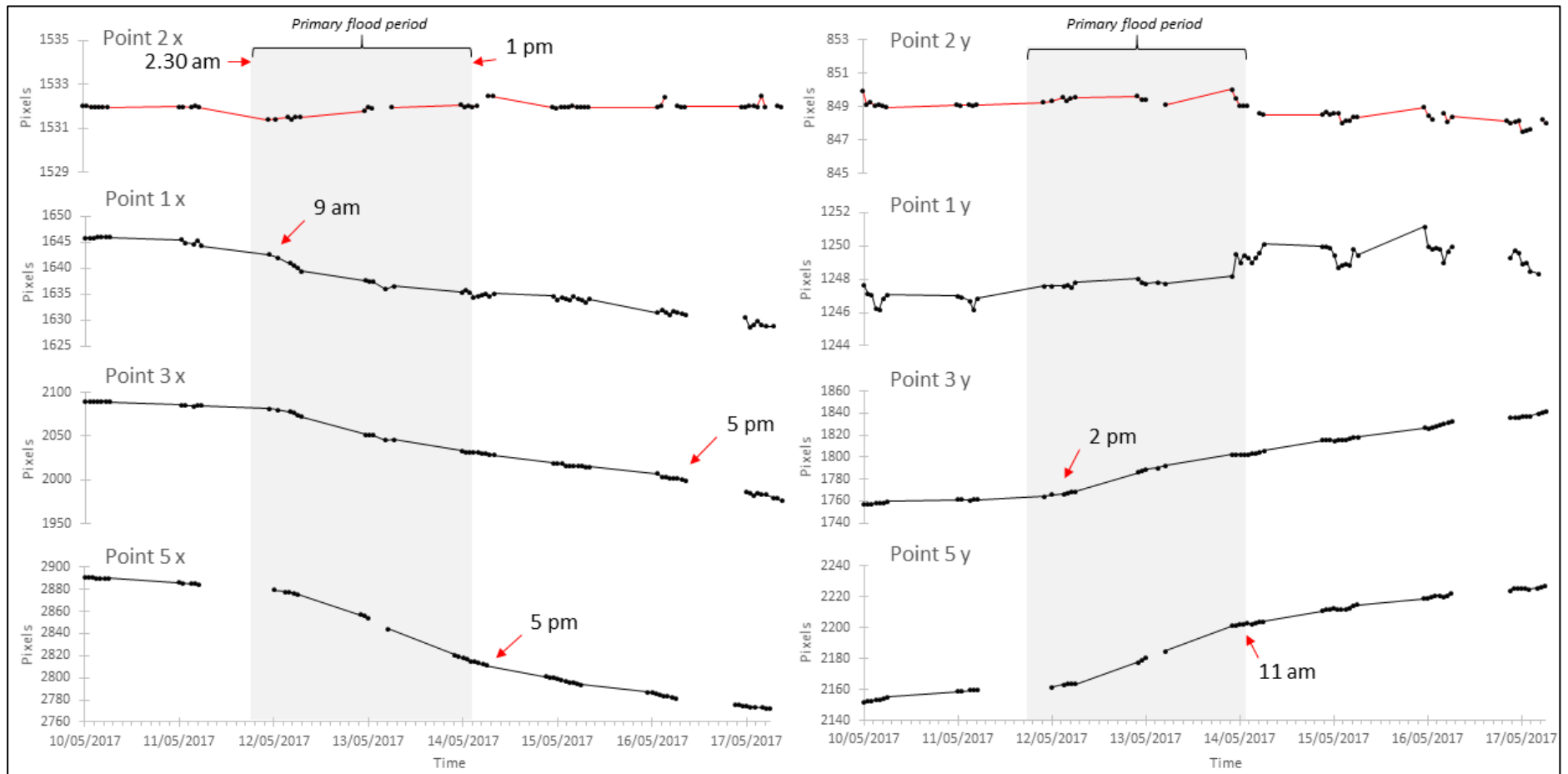
Figure 73. X-Y component plots for May 2017. For point locations refer to Figure 74: Point 1) Base of tree; Point 2) Centre of roof gable (control point); Point 3) Soil/grass clump at the landslide toe; Point 5) Rock on cliff face on the landslide. Point 2 can be used as an error analysis tool as it is on a 'stable' area of land.

The pixel tracking shows landslide movement was initiated from 9 am on the 12th, an hour before the first flood peak (Figure 73). Following this initiation point, movement was consistently rapid towards the Rangitikei River, in both horizontal and vertical directions. Point 4 (Figure 74) was not used in the pixel tracking results for similar reasons as point 2 in the April 14th flood event; namely lighting issues, which prevented the point from being accurately and consistently tracked.

Figure 74. Pixel tracking point locations for the April 14th flood event.

Point 5 shows a distinct movement pattern, showing a wave-like pattern of initial rapid movement followed by a steady decrease as movement starts to slow back to the original rates. Horizontal movement (Point 5 x) has a different timing to vertical movement, where horizontal movement starts decreasing around 5 pm on the 14th, while vertical movement starts decreasing around 11 am on the 14th. This occurs once the flow has receded substantially, and bank erosion has ceased. This is shown in the bank erosion mapping, which shows primarily bank accretion, between the 13th and 15th (Figure 75).

The flood effects on the bank shows progressive stages of bank erosion from the bank position prior to the primary flood period. The bank of the toe was cut back during the initial flood stage, and then entered a phase of gradual bank accretion during the rest of the event (Figure 75, A). The bank of the bare-rock cliff experienced the most erosion of the area, and continued to erode after the initial flood (Figure 75, B).
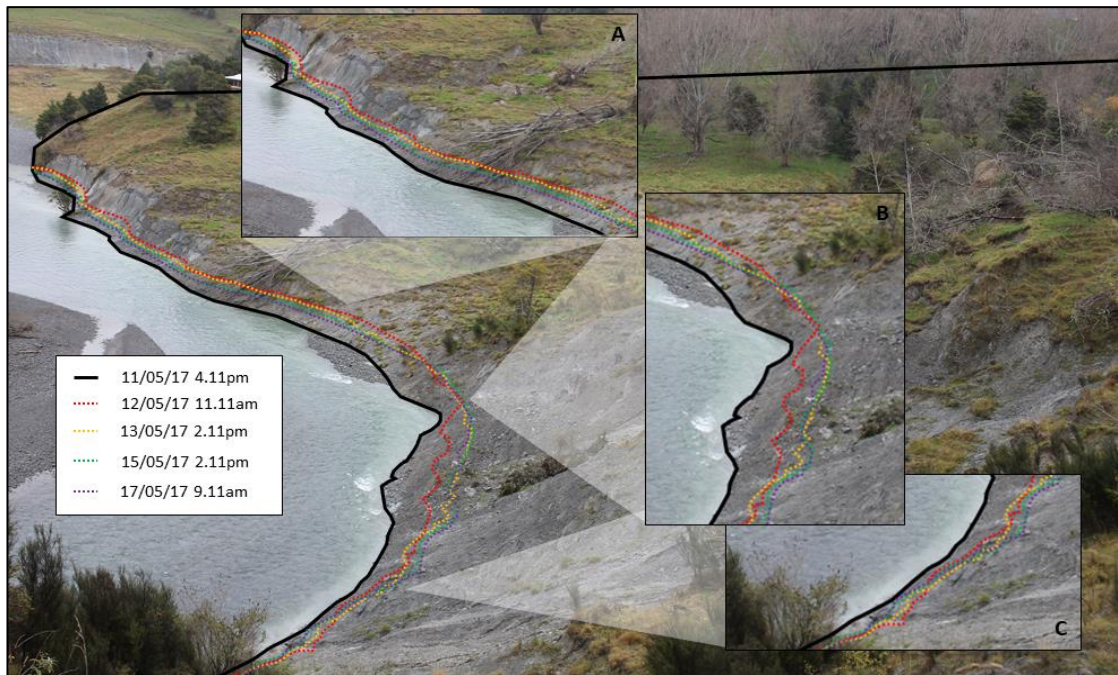
Figure 75. *Bank erosion mapping showing the localised bank cutting and bank filling during the May flood event.*

4.2.2.2.4 Comparison of flood events

When comparing the three significant flood events, the first flood event in the beginning of April (Flood 1) reaches the highest discharge and has the longest duration above 200 cumecs (Table 10). Flood 2 has the intermediate discharge of the three but the duration above 200 cumecs is the shortest of the flood events. It also follows closely behind flood 1, with only 10 days between the beginning of flood 1 and the beginning of flood 2. Flood 3 has the lowest discharge, intermediate duration, and occurs almost a month after the beginning of flood 2.

Table 10. Comparison between the three significant flood events analysed against hourly pixel tracking.

	Peak discharge	Duration above 200 cumecs	Time after last significant flood
Flood 1 (April 4th 2017)	746	45 hours	148 days
Flood 2 (April 14th 2017)	716	18 hours	10 days
Flood 3 (May 11th 2017)	633	43 hours	27 days

The differences in flood impacts between each significant flood event shows a pattern of increasing erosion over time (Figure 76). Flood 1 shows a mix of cutting and filling across the toe, while flood 2 shows consistent erosion, and flood 3 shows consistent increased erosion. There is an increasing lag in the start of the adjustment period following each flood, with flood 1 responding quickly and entering an accretionary phase before the flow has receded below 200 cumecs, and flood 2 and 3 experiencing a lag before exhibiting a strong accretionary phase. It is also noticeable that the 'after' lines in Figure 76 generally reach the same point on the bank, while the bare-rock cliff has a similar morphology after each flood except for flood 3, which cuts

back substantially. The local recorded rainfall for each flood did not appear to be an important factor in the flood events or the landslide response.
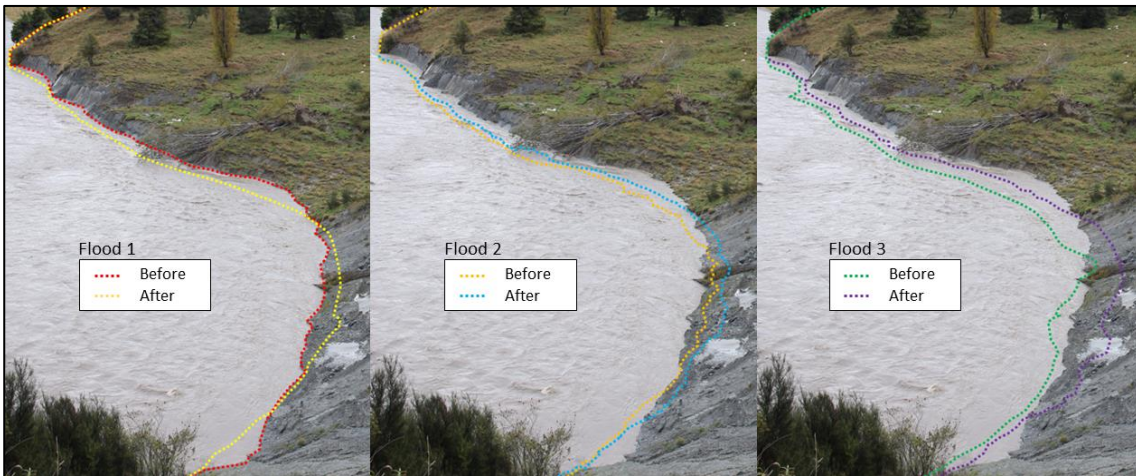
Figure 76. Comparison between flood events, showing the before and after positions of the bank for each flood. The image is from before the flood peak of the first flood (April 4th, 2017), to show the change in bank morphology over time. Flood 1 after boundary, 7/04/17, 9.11 am; flood 2 after boundary, 16/04/17, 7.11 am; flood 3 after boundary, 15/05/17, 2.11 pm.

Between flood events the landslide continued to move, with more movement occurring between flood 2 and 3 (Figure 77). The movement is relatively substantial in some areas such as at the border of the toe area and bare-rock cliff (Figure 77, yellow arrow), and is generally consistent across the toe front.
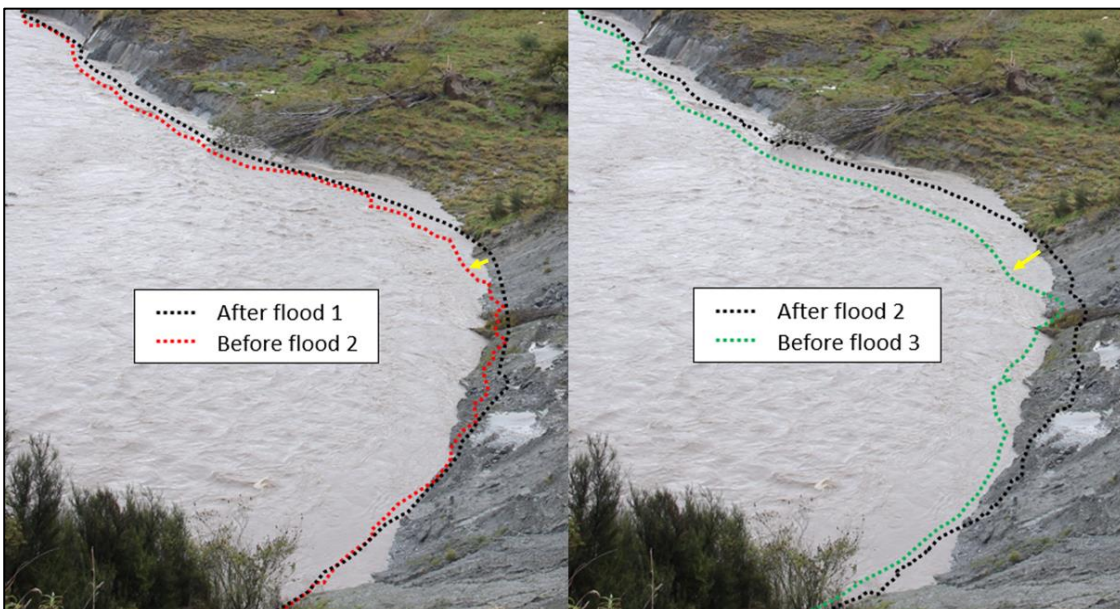
Figure 77. Comparison between flood events, showing the bank evolution that occurred between flood events, with the time between flood 1 and 2 on the left and flood 2 and 3 on the right.

4.2.3   Sediment contribution

The recorded landslide movement has delivered sediment to the Rangitikei River, and time-lapse imagery has helped to quantify this. Analysis of the landslide toe evolution using the time-lapse

imagery can provide a rough estimate of the sediment contribution to the Rangitikei River between July 2015 and October 2017. Using Google Earth, 2015 imagery was measured to gather the width and length of the toe area visible in the time-lapse frame for a sediment contribution estimate, and the time-lapse imagery compared to find start and end positions of features (i.e. trees) within the study period (Figure 78, A-E). The features show a movement gradient across the toe, with Point A (likely on the other side of the boundary) moving an indistinguishable amount while Point E moved around 50 m in just over 2 years.

The estimated sediment contribution equation (shown in Figure 78) includes the unit weight (2.04 t/m^3, which equals 20 kN/m^3) from Massey (2010) for remoulded landslide debris (Silty, fine sand, medium dense), which is the assumed composition of the landslide toe. The measurement of the material unit weight was beyond the scope of this study, and to provide a realistic estimate the value was taken from literature on nearby landslides (i.e. Massey, 2010). The movement of Point D was used as a conservative figure, as the 50-m movement experienced by point E could include significant extension and generation of fractures within the materials, which reduces the bulk density and over-estimates the sediment contribution. The landslide thickness was a conservative average between site 1 and site 2 (11 m + 2.5 m / 2 = 6.5 m). Based on the sediment contribution equation (Figure 78), approximately 19,000 tonnes of sediment are estimated to be entering the Rangitikei River from the landslide each year, assuming a similar bank position.
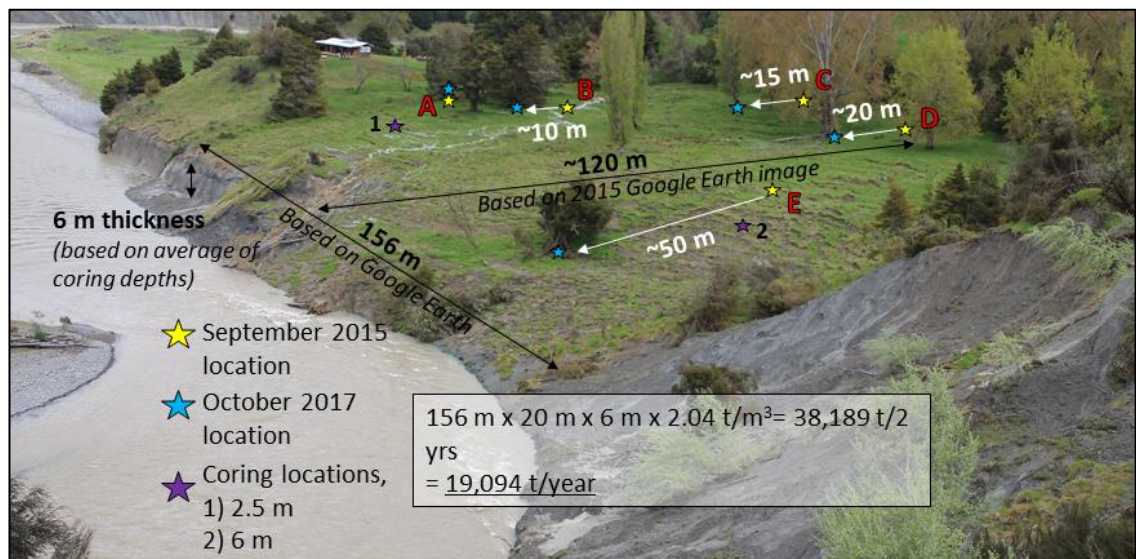
Figure 78. Estimated sediment contribution diagram showing the movement of features on the Rangitikei Slide toe and the estimated sediment contribution equation. A − E are notable features that are visible at the start and end of the study period. The estimated sediment contribution equation uses a conservative average height above the failure surface (from coring the toe, average between site 1 and site 2), the width (from Google Earth), the length (movement of point D), and the sediment unit weight per cubic metre.

5   Discussion

Large, slow-moving landslides have been formerly underestimated in their ability to disrupt the surrounding area and damage infrastructure. As a result, there was a lack of detailed understanding into the influence of movement drivers at a high-temporal resolution in comparison with faster landslide types. Development of higher-temporal resolution methodologies (e.g. time-lapse and photogrammetry) has allowed for detailed studies of slow-moving landslides in recent years (e.g. Massey et al., 2013; Golly et al., 2017).

Sediment contribution from slow-moving landslides is often overlooked even though the capacity for sediment contribution is significant, particularly when feeding into a fluvial system. As many slow-moving, translational landslides are connected to rivers – due to the influence of downcutting on landslide formation – sediment delivery is an important management issue. In this study, the Rangitikei Slide was found to have complex movement patterns and a series of preserved movement phases, highlighting the dynamic nature of movement patterns through time for this landslide. This was unexpected, in both the existence of other movement phases and capturing geomorphic evidence of this, as landslides are classically destructive features that do not generally preserve remnants of older phases within the current active boundary. Rather, the remnants are often remoulded and incorporated into the present movement.

The primary movement drivers for the contemporary movement phase were determined to be erosion by the Rangitikei River and seasonal changes in groundwater within the landslide mass. These drivers fit with initial assumptions, as the landslide lies on the outside of a sharp bend on the river (i.e. susceptible to erosion during high flows) and seasonal movement patterns driven by groundwater fluctuations are a well-known characteristic of many slow-moving, translational landslides (Corsini et al., 2006; Massey et al., 2013).

5.1   Movement patterns of the Rangitikei Slide

5.1.1   Contemporary movement

The results highlighted the complexity of the Rangitikei Slide movement, showing a series of key geomorphic areas within the estimated active landslide boundary. It has been determined through analysis of movement patterns that the Rangitikei Slide is best categorised (using the Hungr, 2014, classification) as a complex slide, composed of a large, slow-moving, translational rockslide in the main body and an earthflow-slide at the toe. This classification aligns with the initial hypothesis on the movement type, as many nearby landslides are classified as slow-moving, translational landslides (i.e. Utiku Slip, Taihape

Landslide, Bird Landslide). This classification for the Rangitikei Slide is supported by the geomorphological mapping, Photogrammetry (DoDs), and RTK-dGPS data, which found that the landslide is almost certainly moving along a low-angle planar clay seam (causing translational movement) and that this is a key driver of instability in the landscape. The earthflow at the toe indicates a more complex movement type than simply translation.

The presence of clay seams within the Taihape area has been well-established in previous works, as well as their role in translational landslide formation (e.g. Brown, 1974; Thompson, 1982; Mountjoy & Pettinga, 2006). It has been found, based on the coring work during installation of piezometers, that the clay seam visible at the toe during low river flows is not the primary failure surface for the Rangitikei Slide, as the material is disturbed (stratigraphically displaced) down to at least 11 m on the north-eastern side of the earthflow. This shows that the earthflow has remoulded sediments lower than the clay seam visible in the earthflow river bank, and the initial assumption about the visible clay seam being the failure surface is incorrect. Coring of the landslide toe also found a difference in the depth to the failure surface between the N-E and S-W side of the earthflow, suggesting that the failure surface is dipping somewhere between the south and the west. The Utiku anticline running roughly NNE-SSW through the landslide is likely responsible (Figure 12) as the stratigraphy in the area will dip as a result of this, but further work is needed to ascertain the dip direction on the Rangitikei Slide.

The geomorphological mapping separated the landslide into eight areas (Figure 29) designated by different movement patterns, determined through surface morphology, and analysis of the hill shade models identified five key geomorphic areas (Figure 35). The hill shade model zones are more simplified than the geomorphological map, merging the head and upper area, and the flanks into the adjacent areas. The RTK-dGPS data separated the landslide into three primary movement zones (upper, middle, and toe area). All the datasets conclude that the Rangitikei Slide is separated into several different landslide blocks. The landslide is therefore not moving as a cohesive unit towards the Rangitikei River, but is comprised of several blocks that move in response to displacement to accommodation space (movement in the blocks below). This is shown by the differing magnitudes in the RTK-dGPS data, with the upper block showing smaller displacement rates than the lower areas. This increase in movement rates downslope suggests that the landslide is experiencing large-scale extension and the landslide is being pulled apart by a trigger at the toe. Extension is also visible in the surface morphology, as there are several grabens and many scarps across the landslide.

The upper area appears to show slow, translational movement southwards, with extension evident by the head scarp graben and the scarps between the head scarp and the central area. There are a series of 'ridges' in the upper area which could indicate some compressional forces. Alternatively, it has been hypothesised that these ridges represent closely-spaced alternating normal faults, which have pushed up blocks and formed these 'ridges' (Figure 79). This hypothesis was not tested during this study, but as the upper area has predominantly experienced extension during the study period it is less likely that the ridges represent recent areas of compression.
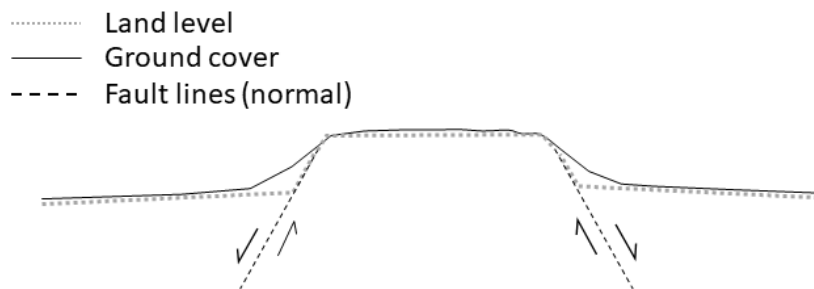
Figure 79. Schematic of the normal fault hypothesis

The ridges could, however, represent compression from an older movement period under a different movement phase. The focus of this study remained on larger-scale movement patterns, and the upper area was generally seen to be experiencing predominantly translational movement during the contemporary phase. This is supported by the RTK-dGPS data, as the southern pegs in the upper area have an elevated movement rate in comparison with the more northern pegs which indicates extension. Therefore, if the ridges were formed from compressive forces, it is likely prior to the present movement phase.

There is a lack of compression at the toe, which indicates rapid removal by the Rangitikei River that prevents debris build-up. A build-up of debris can stabilise a slope by buttressing (supporting) the toe and allowing the landslide to self-stabilise (Golly et al., 2017), as the build-up removes accommodation space and can reduce the effects of extensional forces acting on the landslide. This lack of compression in the Rangitikei Slide is shown by the relatively smooth surface across the toe and no significant increases in elevation between the southern edge of the transition zone and the river (Figure *31*, cross-sections). A slow-moving landslide in the Erlenbach Stream, Switzerland, exhibited a reliance on an alluvial step in the stream channel at its base for stability, and movement rapidly increased when this was eroded during a flood (Golly et al., 2017). It self-stabilised after re-buttressing the toe by accumulating debris at the base and restoring the alluvial step. This shows the importance of debris build-up at the toe, and the effects on the movement rates for some slow-moving

landslides. The lack of buttressing on the Rangitikei Slide prevents stabilisation and thus any subsequent reduction in movement rates.

1.1.1.1 Rangitikei Slide boundary

The estimated landslide boundary was determined by assessing surface morphology and assuming a significant influence by drainage lines. This assumption was supported by surface morphology, with most drainage lines on the 'borders' deeply incised and surface features discontinuing past the drainage lines. The eastern boundary is based on the location of the drainage channel and the western boundary is interpreted between surface deformation features. For many slow-moving landslides, the margins are often obscure unless there are noticeable offsets (Ellen *et al*., 1995), which is certainly the case for the western boundary of the Rangitikei Slide. Because of these obscure borders, the active boundary shown in the geomorphological map may be slightly conservative. While included within the designated boundary, peg 2 and the Camera peg could be outside of the currently active movement area due to their significantly lower total movement rates than the rest of the pegs (<20 cm in >2 years). However, as previously mentioned, the mapping highlighted a strong influence by drainage lines which would contain the camera peg within the active boundary based on the eastern drainage line. If this area is within the boundary, it may be showing lesser movement due to the earthflow movement creating accommodation space within the transition zone. This in turn allows for the land above the transition zone to increase in movement. This seems to 'funnel' the movement towards the head of the earthflow, which is supported by the movement direction of peg 19 and peg 28 (Figure 54). It is difficult to confirm the exact boundary line without further monitoring and analysis of older (1900s) aerial imagery, as the current boundary is determined through interpretation of surface morphology and often lacks definitive features (such as offset linear features) due to time constraints in this study.

The northern extent was determined by the top of the head scarp, but the width of the boundary was estimated based on surface morphology. There is a possible secondary head scarp forming, shown in the geomorphological map (Figure 29) and the October 2017 hill shade model (Figure 80). This could indicate that this area of land is influenced by landslide movement, even while outside of the designated landslide boundary. The same applies to the western side of the northern boundary, as during the study period the farm manager and farm workers repaired the wool shed above the head scarp (outside the designated landslide boundary, Figure 29) due to floor warping which they attributed to the Rangitikei Slide movement. This may indicate a more northern landslide boundary than the geomorphological map landslide boundary (Figure 29) to include the wool shed, which is

further evidence for the secondary head scarp and landslide retrogression. Alternatively, the deformation of the wool shed could be attributed to the Poroa Complex movement, which is assumed to be underlying the Rangitikei Slide movement rates.

The DoDs highlighted some small movement occurring at the toe by the shed, outside of the landslide boundary (Figure 47). This could also show evidence of the Poroa Complex movement or an influence from the landslide boundary particularly due to the proximity to the border. Something to note is the presence of erosion on the bank in front of the shed, which has been assumed to be stable previously. The erosion is much less significant than on the active landslide bank, but the DoD indicates that the land outside of the boundary is still influenced by some erosion (as expected on the bank of a major river) and also a degree of movement, as there is some elevation gain in front of the shed regardless of the landslide boundary. The lesser degree of erosion on the 'stable' land could be from the nature of the sediment, as the landslide material is significantly deformed and broken up, which would be easier to erode than an intact, less deformed bank.
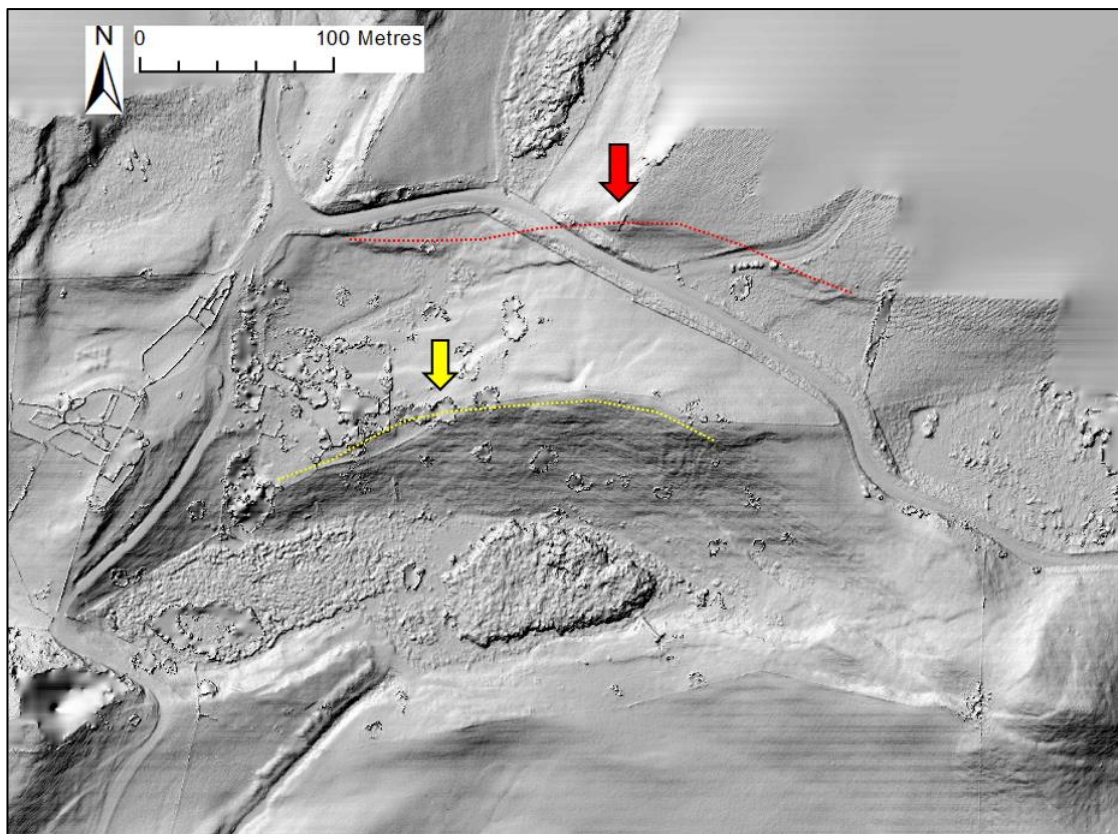
Figure 80. October 2017 hill shade model showing the head scarp (yellow) and the potential secondary head scarp forming behind (red).

It is suspected that the Poroa complex movement has been captured in the RTK-dGPS data (Table 7). Peg 15, which is deemed outside of the active landslide boundary, has a total

horizontal movement of 0.35 ± 0.27 m that appears to represent an alternative mass movement. This movement is much slower than the Rangitikei Slide, and may also be shown in the other survey pegs outside of the landslide boundary below the minimum level of detection (error margin), but this is considered less likely to be real movement. However, the likelihood of capturing the Poroa complex movement rate outside of the active landslide boundary is high, as the Poroa complex (and the ~20 landslides within it) is believed to be moving along a clay planar failure surface (Thompson, 1982) which is likely stratigraphically below the Rangitikei Slide failure surface. This is because the trigger for many slow-moving, translational landslides with planar failure surfaces is river erosion, where rivers cut down into the landscape and allow the failure surfaces to 'daylight' and initiate movement. The Rangitikei Slide was initiated after the Poroa complex (as hypothesised by Thompson, 1982), and it is considered highly likely that the landslide was initiated through post-glacial river incision like many slow-moving landslides around New Zealand (Bilderback, 2012; Bilderback et al., 2014; Cerovski-Darriau et al., 2014).

The age of the Rangitikei Slide is limited to the Poroa complex age, which could be older than 20,000 years due to the presence of Kawakawa Tephra in the landscape (Thompson, 1982). However, Thompson (1982) found that most of the active landslides at present are less than 1,800 years old.

5.1.2   Historical movement phases

Historically, movement phases were not initially considered in this study as it was assumed that the surface morphology was linked to a long-term consistent movement trend. However, the data used to investigate the movement patterns of the Rangitikei Slide captured a series of movement phases with differing movement directions.

The central area contains features that suggest there were movement phases different to the contemporary movement, categorised as historical movement. The most notable features are those shown in Figure 36, offset by what are assumed to be features from a subsequent movement phase. These features (and potentially the upper area ridges) seem to show a movement direction towards the south-east, where a number of distinctive curved parallel ridges are orientated, which indicate a likely rotational influence on the movement. These curved ridges are mirrored on the neighbouring eastern land. The movement is aimed towards the eastern drainage line and differs from the present movement, which is generally S – SSW towards the earthflow at the toe. This is clearly visible in the hill shade models of the Rangitikei Slide, and the smoother surface of zone C may indicate that this movement is no longer active – or at least less active than the present-day movement. This movement

appears to be an older, small mass movement that is possibly related to an earlier alignment of the river.

The historical aerial imagery (Figure 50 - Figure 53) highlights the uneven deformation occurring across the Rangitikei Slide in recent history, with some features remaining seemingly unchanged on the landslide since 2005. This provides further evidence for the theory that there have been a series of movement phases and that the morphological remnants of these historical phases are still visible on the landslide at present. It was previously assumed that the surface features of the Rangitikei Slide were created during the same movement phase, but the aerial imagery contradicts this. For example, the established graben in the transitional zone – a prominent feature in the lower end of the landslide – forms in 2012, while the distinctive ridges on the eastern side remain relatively unchanged between 2005 and 2014. The landslide is only a small section of a very large mass movement complex (Poroa Complex), but it has a diverse movement history within its own boundaries.

There appears to be three main movement phases: towards the eastern drainage line; down the lower central drainage line; and south towards the earthflow. This hypothesis is based on the hill shade models, which clearly identifies the eastern drainage line movement phase, and the historic aerial imagery which shows a much more prominent central drainage line than present. The oldest phase (eastern movement direction) is shown with a smoother surface in the hill shade models (zone c), which may indicate that this movement is no longer active or at least less active than the present-day movement. The arcuate ridges visible in the imagery and hill shade models (zone B) appear to be orientated towards the central drainage line and do not seem to change much in the historic aerial imagery, which could indicate that they were the product of this previous movement phase. The geomorphological map (and site visits) supports the central drainage line movement due to the north-eastern drainage line that borders the earthflow. This watercourse has indications of being a distinctive drainage line in the past (a deep channel with steep banks) but seems to be mostly ephemeral within the study period. This drainage line may have once joined up with the central drainage line and carried the flow to the river, before the transitional zone graben formed and displaced the drainage line connection. However, this drainage line could also have connected to the western drainage line in the past, which could have destabilised the land around the watercourse and triggered the graben formation.

The recent movement phase is considered the current trend, influenced by the drainage line fed from the wetland in the head scarp graben, and movement to the south to south-south-

west feeding into the earthflow. This recent movement is focused on the western side of the lower landslide, as shown in the historical aerial imagery through the formation of the prominent graben within the transitional zone. The deformation and extension within the transition zone developed significantly over several years in the aerial imagery and has continued to develop within the study period, with an RTK-dGPS survey peg (peg 16) in the graben travelling almost 5 m in ~9 months compared to almost 7 m in 22 months by peg 17 (~100 m to the east of peg 16). The DoDs also highlight the small ridges present within the graben showing patterns of elevation change that show a migration southward (elevation loss behind and elevation gain in front).

5.2   Movement drivers

5.2.1   Seasonal movement

Landslide movement can be influenced by many different factors both internal and external, and a landslide can have more than one movement driver affecting movement patterns. Early in the study, the Rangitikei Slide was assumed to be influenced by seasonal fluctuations in groundwater, as the land manager reported more movement in winter and an excess of water across the landslide surface. This was also noticeable during site visits. These assumptions were supported by the data, with a clear seasonal trend shown in the RTK-dGPS, DoDs, and weekly pixel tracking data, with movement rates increasing in the 'winter' periods and slowing in the 'summer'. This is most likely due to high pore-water pressures within the landslide mass as a result of higher rainfall frequency or a long period of lowered evapotranspiration (Massey et al., 2013). It has been established that in many slow-moving landslides, groundwater fluctuations (an increase in pore pressure) are a primary control on landslide movement, and often this is expressed as seasonal cyclic displacements (Picarelli, 2004; Corsini *et al.*, 2006; van Asch, 2007; Schulz et al., 2009; Massey, 2010; Massey et al., 2013). In the Rangitikei Slide, this seasonal trend is distinct, but this study lacks the groundwater regime data required to investigate the influence of groundwater on landslide movement. This means that while groundwater is assumed to have a strong influence based on studies of comparative landslides (e.g. Utiku) and the strong seasonal trend in the datasets, there is no groundwater data at the site or in the nearby area for use within this study. Therefore, more research is needed into the influence of groundwater fluctuations on Rangitikei Slide movement.

The difference between the movement rates in the winter and summer periods are quantified in Table 8 , showing that winter periods have a higher horizontal movement rate than summer periods. This is particularly obvious in the upper block, represented by Peg 9,

where comparison between the two summer periods showed little difference, as did comparison of the winter periods. However, a greater difference was found between both the 2016 and 2017 winter and summer periods, indicating a clear seasonal trend in the movement rates. The DoDs also highlight this seasonality by showing variation in movement patterns between the summer and winter DoD. While the summer DoD (October 2016 – May 2017) showed patterns of elevation loss and gain either side of features to show general southern migration, the winter DoD (May 2017 – October 2017) shows elevation gain behind and loss in front of features, indicating a build-up of material. The RTK-dGPS data shows continued southern movement during winter, so this debris build-up is not occurring as a result of slower movement. The summer DoD shows a more even distribution of elevation loss and gain, which could show a movement rate that is equal to or less than the erosion by the Rangitikei River. In contrast, the winter DoD shows a strong pattern of elevation gain, particularly at the toe, which could indicate that the movement rate is greater than what is removed through river erosion. It is hypothesised that landslide movement is controlled by the rate of erosion by the river, and the movement caused by increased movement pore-water pressures in winter can exceed this fluvial erosion rate.

While this shows a clear seasonal trend in general, upon further investigation of the relationship between individual seasons, the comparison between the RTK-dGPS movement in Summer 2016 and Winter 2016 results in only a small difference in the middle and toe block movement rates (Middle block: -0.25 ± 0.08 m, Toe area: 0 ± 0.08 m). The middle block shows a negative trend, indicating that Summer 2016 experienced more movement than Winter 2016. This does not fit with the movement patterns of comparative slow-moving landslides, where the winter period has a higher movement rate than the summer period. This may be explained by the shortened winter period due to the study period end date (early October 2017), requiring the 2016 winter to be equally shortened. If the full 2016 winter was compared to summer 2016, the difference would be -0.001 m, indicating an almost identical movement rate and an improved relationship compared to the previous -0.25 m pattern. Furthermore, the likelihood of a linear movement rate from March to October – shown in the RTK-dGPS data due to limited July 2016 data points – is very low, which could account for the lack of seasonal trend visible.

According to other studies, continuous GPS monitoring of the Maca landslide by Lacroix et al. (2015) found that movement velocity did not stop rapidly in the dry season as a likely result of the landslide storage capacity and water supply provided by nearby rivers. This effectively blurred the distinction in the timing of the seasonal trend, which could also be

occurring in the Rangitikei Slide, particularly as the Rangitikei River could be supplying water to the landslide. Massey et al. (2013) also found that, while seasonal peaks in pore pressures triggered periods of increased movement, the transition to a slower movement period (i.e. summer) experienced a lag as it was not influenced by lowering pore pressures or a reduction in any other triggering factors. Whether due to water storage or continued water supply from watercourses, there have been numerous studies that have noted the time difference in slow-moving landslide response to increases in movement compared to a reduction following an increased movement period (e.g. Picarelli, 2007; Massey, 2010). This lag in response following pore-pressure-induced movement could be affecting the Rangitikei Slide, and would explain why the designated winter period extends from June – October in the weekly pixel tracking results and July – December in the RTK-dGPS data, when winter in New Zealand is June – August. However, higher resolution data is needed to quantify the timeframe of any lag response, as the RTK-dGPS data is at a 3-monthly resolution and a weekly resolution for the weekly pixel tracking.

There was a difference in the 2016 and 2017 winter periods, and a subsequent difference in the landslide response as captured in the weekly pixel tracking and DoDs. These datasets show an increase in the landslide response to the 2017 winter period. The 2016 winter was visually similar to the 2017 winter (Figure 59), but the 2017 winter was reported as wetter, with rainfall above normal and soil moisture levels from near normal to above normal (NIWA, 2017). A comparison of the weekly pixel tracking movement rates showed that the 2017 winter period experienced almost double the movement of the 2016 winter (Winter 2017: 2.19 pixels/day, Winter 2016: 1.14 pixels/day). It is difficult to determine if this shows a pattern of increasing landslide sensitivity to winter periods, or a response to increased frequency and magnitude of rainfall and flood events (Figure 59), and requires a longer study period containing additional winter periods to ascertain. It is acknowledged that climate change would increase the rainfall and flood events during winter, but there is no conclusive evidence that climate change is influencing the differences between the 2016 and 2017 winters.

The movement rates of the RTK-dGPS data (Table 7), mentioned above, showed that, while there is a seasonal trend between winter and summer periods, there is also a difference between the winter periods and an increase in landslide response through time. However, the cause of this increased response was not determined in this study. While it is assumed that the Rangitikei Slide exhibits the same characteristics of the nearby slow-moving landslides, more data is needed to investigate this seasonal pattern further.

5.2.2 Flood events

At the Rangitikei Slide, it was hypothesised early in the study that the Rangitikei River had an impact on movement, due to the location of the landslide toe on a sharp river bend and the Rangitikei River classified as a large river in the North Island, New Zealand. This hypothesis was tested with hourly pixel tracking of the landslide toe during significant flood events, and found that there was a distinct landslide response to bank erosion.

The floods had varying impacts on the landslide toe and the landslide response itself was spatially-variable, showing patterns of bank erosion and bank fill (Figure 82). These patterns are consistent with our understanding of geomorphic features (based on the geomorphological map, Figure 29), namely the earthflow and bare-rock cliff. The earthflow has a relatively unified movement, where the bank cut by the river moves as a unit when movement is triggered. This highlights the remoulded composition of the earthflow, which is readily moved and easily eroded, unlike the bare-rock cliff which erodes in blocks and experiences small material flows across the surface during flood events (as visible in the time-lapse imagery). This shows that the cliff has more cohesion (and material strength) and is less remoulded than the earthflow material. The earthflow also appears to have a high groundwater level, particularly at the toe front, as the area is consistently saturated year-round and the remoulded mudstone is particularly unstable underfoot. The difference between the earthflow material and the bank outside of the designated active boundary is noticeable in site photos (Figure 81), which shows how unconsolidated the remoulded material (to the right in the photo) is in comparison with a bank of the same material that is not experiencing displacement or being remoulded (to the left in the photo) by an earthflow. In this example, the landslide boundary is very distinct, which differs from the rest of the boundary.

Figure 81. Photograph of the Rangitikei Slide toe front, on the river bank that is not accessible during moderate-high flows. The difference in material behaviour is clear, with the earthflow material to the right and the cohesive bank on the left, and the landslide boundary marked by the stream that flows along the lateral shear (southern-most boundary; shown by the white line and red arrow). The bare-rock cliff is visible to the right.

Less erosion is visible at the front of the earthflow when comparing the bank morphology during and after flood events (Figure 76), which indicates that the erosion has been masked by bank fill. This can be called 'compensating cut and fill', where the earthflow experiences an erosion phase before compensating with a filling phase, shown by the seemingly unchanged boundary line in Figure 82, A. While this could also represent a lack of erosion during the flood events, it is visible in the bank erosion mapping for each event that there were phases of cutting subsequently masked by phases of filling (e.g. Figure 75).

It was also noted that there was movement between flood events based on the difference between the bank position at the end of flood 1 and prior to flood 2 (Figure 77). This indicates two possibilities: the earthflow has a base-level movement rate irrespective of bank erosion from significant flood events and this base-level movement rate is 'managed' by the Rangitikei River through bank erosion; or the bank erosion may initiate increased movement by destabilising the toe and encouraging movement into the newly acquired accommodation space. As established in the previous section, there is a seasonal movement pattern in the Rangitikei Slide likely controlled by groundwater fluctuations. So, in general, there is considered to be a base-level movement rate irrespective of any bank erosion. However, the latter theory is supported by the increased toe movement captured in the hourly pixel tracking data, which is initiated during a significant flood event and particularly after a cutting phase. This means that landslide movement is a combination of the two processes, with a

base-level movement rate exacerbated by flood events and requiring a necessary adjustment period before returning to this lower base-level movement rate. Further work is needed to compare more flood events with a variety of characteristics, as the analysis of three flood events is not enough to gather an in-depth understanding of the thresholds that govern these processes. This conclusion fits with the current understanding of slow-moving landslide mechanics, with a base-level movement influenced by groundwater (highlighted in the seasonal trend visible in the RTK-dGPS data, Figure 56, and the weekly pixel tracking, Figure 58) and an external influence by significant flood events periodically destabilising the toe. The weekly pixel tracking data supports this theory, as the significant flood events (April and May 2017) caused an earlier onset of the increased 2017 winter movement rate (Figure 60) compared to the 2016 winter period, and highlights the influence of flood events on movement. It also shows that an adjustment period longer than a month seems necessary for the landslide to revert to the base-level movement (between the end of the flood events and the beginning of the winter period). Alternatively, it could indicate that the flood events increased pore pressures in the landslide toe, increasing the base-level movement rate. As mentioned previously, increased pore pressures experience a lag following the reduction in the factor that raised the pore pressures and reduce at a slower rate than they rise. This could also be a factor in the early onset of the winter movement rates. However, as stated, more work is needed to identify the drivers of these movement patterns.

The proximity of the three analysed flood events limits the application of any interpretations to the whole study period, as the interaction between fluvial and terrestrial systems are complex. There are a range of influencing factors including sensitivity, connectivity, and recovery (Lisenby et al., 2017), which determine the landslide response to movement drivers. For example, duration between flood events influences landslide sensitivity and recovery, as successive flood events could increase the landslide response to subsequent events of a similar intensity and also extend the recovery time needed to adjust back to pre-flood movement rates. Analysis of the Rangitikei floods allows for a better understanding of the effects of successive flood events in particularly on the toe area, but limits any further understanding of isolated flood events. This area requires further data to better understand the processes affecting the Rangitikei Slide.

As the flood events in this study occurred within a 37-day period, it allows for analysis of the landslide response to successive floods. Flood 1 (April 4th, 2017) caused significant bank fill at the earthflow toe and primarily erosion of the cliff with some areas of bank fill (Figure 66). It is highly likely that the initial stages of the flood caused bank erosion of the toe, but this

was not captured in the time-lapse as this occurred sometime between 5 pm of the 5th April and 8 am on the 6th April. Regarding the following floods, the primary change in flood 2 and 3 is erosion – even after the flood – so it is possible that a rapid filling phase had not yet been initiated. However, bank filling had likely begun in Figure 76 for flood 2 and 3, but either at a slower rate than flood 1, or the cutting phase was more severe and took longer to readjust. Duration between flood events could explain the difference in response by the bank boundaries through time, as Flood 1 occurred 148 days after the last significant flood event, while 10 days passed between flood 1 and 2, and only a month between flood 2 and 3 (Table 10). This could affect the landslide response, as flood 1 followed a long period of limited bank erosion and then substantially cut the toe. As mentioned above, the landslide response to this was conditioned by sensitivity, thresholds, and recovery time (Lisenby et al., 2017), and these factors can change the effectiveness of subsequent flood events. Flood 1 exhibited mostly bank filling at the earthflow toe during the event, while both Flood 2 and 3 showed overall erosion. This could highlight the lack of recovery time between events, increasing the impacts of flood events and reducing the landslide's ability to rapidly adjust to disturbance.

Alternatively, comparison of the bank boundary immediately following each flood event indicates that the landslide continually adjusted to a consistent point regardless of the flood event. This is shown in Figure 82A, which indicates a type of stabilisation by the Rangitikei Slide in response to the flood events. This could show an equilibrium point for the landslide, where a limit may exist for bank erosion. It is difficult to determine if this equilibrium point is dictated by the landslide stability, landslide material, or the Rangitikei River. This was an interesting observation within the hourly pixel tracking data and requires further work to understand the mechanism controlling this.
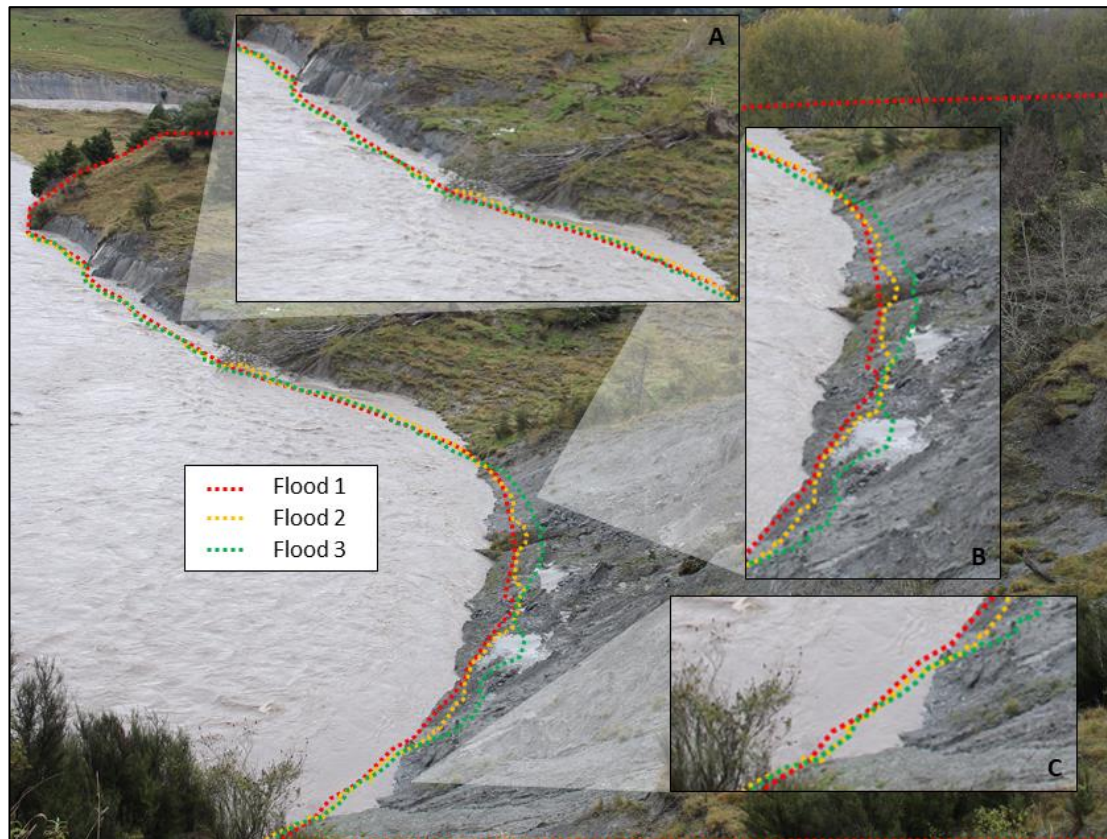
Figure 82. Bank erosion mapping showing the impacts of each significant flood event on the landslide toe. The image is from before the flood peak of the first flood (April 4th, 2017), and the bank boundaries are the resulting bank morphology following each flood event.

Another factor that could explain the difference in response by the landslide toe is the flood duration (above 200 cumecs), which varied for each flood (Table 10). Flood 2 experienced the shortest duration, and while it had the second highest peak discharge, the impact on the landslide toe was less than the longer duration flood events. The bank erosion mapping showed very little change to the bank morphology following the initial cutting phase (Figure 67). This could show that duration is more effective than intensity, which has been reiterated by Massey (2010) in regard to individual rainfall events. A common theme of slow-moving landslides is that longer-term processes are more effective movement drivers than individual high intensity events. Only after a form of long-term cyclic fatigue (and lowering of shear strength) can individual events significantly affect slow-moving landslide movement rates.

River erosion is a well-known trigger for slow-moving landslide movement (Bilderback, 2012; Bilderback et al., 2014; Cerovski-Darriau et al., 2014; Golly et al., 2017; Massey et al., 2013). Zerathe et al. (2016) found that over decadal-scales, some slow-moving landslides were mainly driven by river erosion, specifically lateral movement of the channel. They also found that, for the Maca Landslide in Peru, seasonal patterns of rainfall (precipitation and infiltration) showed a movement trend that was over a shorter time-scale. Based on the

historic movement phases indicated in the movement pattern analysis, the Rangitikei River has had a significant influence on the Rangitikei Slide for decades, possibly longer. So, while it appears that the seasonal trend in the data – producing a base-line movement rate – is the longer-term movement driver, river erosion initiated many slow-moving landslides around New Zealand (and the world) through post-glacial river incision and continues to influence movement rates today.

The use of time-lapse imagery has allowed for the high temporal resolution monitoring of landslide response to movement drivers. This is particularly important for analysing the relationship between significant flood events and movement, as patterns of compensating cut and fill are masked at lower resolution monitoring. Capturing the effects of a flood event at an hourly time-scale has enabled a better understanding of landslide response, and the influence of different factors such as flood peak duration, flood magnitude, and time between flood events.

5.2.3 Anthropogenic activities

Management of landslides can have a significant effect on landslide movement (McCabe, 2013; McSaveney & Massey, 2017), as human-driven morphological change can alter the loading on the landslide, changing movement patterns. On the 23rd August 2017, the Farm manager began lowering the wetland water-level below the head scarp. There may have been historical management of the wetland, including previous water-level lowering, but this is unconfirmed. As the wetland-level lowering occurred at the end of the monitoring period for this study, assessing its impact on movement is beyond the scope of this work. However, it was noted that surface water levels increased following this change, particularly at the toe. The 2017 winter was considered to be wetter than the previous winter, which could also be a factor.

It is important when considering anthropogenic alterations on a slow-moving landslide to identify if the activity is in response to landslide movement (re-active management to repair damage) or active management to reduce future impacts (McColl & McCabe, 2016). In the case of the Rangitikei Slide, the activity was active management, as the Farm manager lowered the wetland level in an attempt to slow the movement and reduce future impacts. Active management is usually superior to re-active management, as active management attempts to understand the cause for movement and address it, while re-active management requires damage by movement to occur first. However, regardless of the management strategy or reason for anthropogenic activity, it is vitally important that the movement drivers for the landslide are identified prior to any substantial activity as landslides are

dynamic features that are influenced by a number of factors, and also have the capacity to self-stabilise (Golly et al., 2017). For example, any earthworks to remove built-up material on a slow-moving landslide could initiate increased movement, as this activity could provide accommodation space for increased movement or remove the buttress that was reducing movement. Therefore, an understanding of the processes driving movement is necessary for successful management of slow-moving landslides (Corsini et al., 2006).

5.3 Sediment delivery to the Rangitikei River

The sediment contribution of slow-moving landslides is not generally quantified in the literature, as the focus has primarily been on catastrophic landslide failures that contribute substantial material in a short time-frame. This has meant that sediment delivery from slow-moving landslides has been previously overlooked. As a result, these features are not prioritised in erosion management plans.

The rough sediment contribution model (Figure 78) provided a conservative estimate of 19,000 tonnes of sediment entering the Rangitikei River from the landslide each year. Dymond et al. (2016) stated the Rangitikei Catchment area as 2739 km^2, and found the measured sediment load was 592,750 t/yr. Using the conservative estimate of Rangitikei Slide sediment contributions, the landslide contributes 3.21% of the total measured sediment load in the Rangitikei River. The contributing earthflow area of the landslide is 0.03 km^2, which is 0.0011% of the Rangitikei Catchment, based on the catchment area in Dymond et al. (2016). Using the conservative estimate of 19,000 t/year, the Rangitikei Slide produces an equivalent of 633,000 t km^{-2} yr^{-2}, which is 2,930 times larger than the catchment average of 216 t km^{-2} yr^{-2}. Therefore, the small area that comprises the Rangitikei Slide in comparison to the Rangitikei Catchment is producing almost 3,000 times more sediment than the non-landsliding areas of the catchment. These estimates are limited to the earthflow sediment contribution and does not account for the bare-rock cliff contributions, which are visible in the time-lapse imagery. However, the bare-rock cliff estimates are difficult to quantify due to the angle of the time-lapse camera and the movement of the sediment. The sediment moves over the surface of the cliff in small flows during flood events and experiences topples throughout the study period, and are more difficult to quantify compared to the earthflow, which has a relatively linear movement across the earthflow front.

5.4 GCD

The GCD output tables show that there is a net elevation gain during the study period (October 2016 – October 2017), which indicates that the sediment budget is not balanced. If the amount of elevation loss and gain were balanced, then the net change would be zero and

it could be categorised as a closed system where the area within the budget is experiencing changes as a result of processes also occurring within the budget area. Within the landslide, there are patterns of compensating elevation changes around landslide features (e.g. ridges) that show a southern migration downslope. However, the Rangitikei Slide shows elevation gain in the lower area of the landslide (the central and toe area) and this is not balanced by compensating elevation loss at the top of the landslide (Figure 46). As the Rangitikei Slide experienced a significant net gain within the study period, it is unlikely to be a closed system and is likely experiencing influences from outside of the designated study area (landslide boundary). This is further evidence that the landslide is either retrogressing or the landslide boundary interpreted in this study is too small.

The net elevation gain in the October 2016 – October 2017 DoD is interesting as the RTK-dGPS data and surface morphology indicates large-scale extension, which should be represented by elevation loss in the DoDs. Elevation gain indicates compression or a build-up of material, which contradicts the rest of the data. This is particularly interesting as the DoD is thresholded and the data is considered to represent real-world geomorphic changes. The concentration of elevation gain in the DoD on the earthflow conflicts with the RTK-dGPS survey network data as the elevation gain indicates material build-up which would cause slower movement of the pegs at the toe when in fact, the pegs are the fastest moving of the survey network. There appears to be no easy explanation for this phenomenon (unless the DoDs are faulty), and represents an area of further work.

5.5   Recommendations

The Rangitikei Slide is considered to be similar to both the Utiku and Taihape landslides, which are representative of many landslides in the area, and also many occurring in different geological environments around the world (Massey, 2010). The findings of this study are applicable on an international-scale, as well as in New Zealand, and improve the understanding of movement patterns for the Rangitikei Slide, the relationship between movement and flood events, and the sediment contribution to the Rangitikei River.

5.5.1   Landslide management

Slow-moving landslides are difficult to classically manage, as hard-engineering methods (building rigid structures) are usually unsuccessful. An example of this is the engineering works on the Utiku Slip, which was found to be highly sensitive to environmental changes over 100 years after the first infrastructure (a main trunk railway line) was built across the landslide (McSaveney & Massey, 2017). Since then, management of the Slip has involved continual re-levelling of the railway in response to displacement, which in turn loads the head

of the landslide while unloading the toe by re-levelling the tracks with gravel extracted from the Hautapu River at the toe.

Slow-moving landslide management has historically involved re-active management strategies that attempt to control movement rather than allow for it. By understanding the movement patterns of a landslide and the drivers causing movement, improved management strategies can be implemented to reduce future impacts and manage any current impacts. This requires a soft-engineering approach which allows for landslide movement while also attempting to reduce it by addressing the drivers of movement. This has been successfully implemented at several of the nearby landslides such as the Utiku Slip, where subsurface drainage was installed to reduce the variability in groundwater levels by rapidly removing water that had infiltrated into the landslide mass (Massey, 2010; McColl & McCabe, 2016). This was done to address groundwater fluctuations and resulting higher pore pressures, identified as a primary movement driver (Massey, 2010). These options are some examples that can be utilised for slow-moving landslides, both in New Zealand and around the world, and further understanding of movement mechanisms will allow for improved management options.

For the Rangitikei Slide, it is recommended that the landslide toe be retired from grazing and subsurface drainage installed to reduce the water content within and entering into the landslide mass. To address the Rangitikei River, an important movement driver, reducing toe cutting would improve the stability of the landslide. However, this process would be costly and likely require some hard-engineering methods to keep the river from reaching the toe. In this regard, based on the scale of the movement, implementing any active management strategies would require addressing ALL movement drivers to improve the probability of success. If a movement driver is not addressed, then movement will continue regardless and the cost of the management strategies would be wasted.

5.6   Further research areas

This work aimed to identify the general movement patterns of the Rangitikei Slide and confirmed the primary drivers influencing this movement. This was the first step in understanding the Rangitikei Slide. Further research should seek to identify movement thresholds. This section provides some areas for further research to better constrain the movement mechanisms of the Rangitikei Slide.

Firstly, it would be worthwhile achieving further in-depth analysis of the relationship between significant flood events and toe movement, comparing the geomorphic

effectiveness of flood events in winter compared to summer, flood events with high local rainfall levels compared to low rainfall levels, and flood events in close succession compared to isolated flood events. The next logical step could be to attain thresholds for effective flood events in regard to discharge and flood peak shape (e.g. rapid increase to flood peak compared to steady increase). Further research is needed to better understand the effects of different flood characteristics on movement rates and the subsequent changes in sensitivity and connectivity. This can be used to ascertain the length of the average adjustment period for the landslide toe (using more flood events), or quantify the base-level movement rate.

To provide more detail in the pixel tracking data, importing and aligning a DEM into the Pointcatcher software to project the points onto a 3-D surface would allow for analysis of real-world high-resolution movement rates. Alternatively, a continuous GPS system could be utilised, as was successfully implemented on the Utiku Slip by Massey (2010).

Lastly, there is a distinct lack of subsurface analysis in this research, which would complement this work by identifying the Rangitikei Slide planar failure surface. Coring of the landslide to determine the clay seams present within the stratigraphy, including the Poroa complex failure surface depth, would improve the understanding of initiation and continued movement. This would provide some context for the observed movement patterns and the primary movement drivers.

6 Conclusions

The findings aimed to improve the understanding of these landslide types in New Zealand in order to propose more effective management strategies both locally and around the world. In the Rangitikei Slide, it was found that the landslide comprised several blocks with differing movement rates, with the movement indicating a strong extensional phase through an increase in rates downslope. Groundwater fluctuations appeared to produce a seasonal movement pattern, while river incision (toe cutting) triggers rapid movement periods. Estimation of sediment contribution to the Rangitikei River found that this southward movement could be contributing more than 19,000 tonnes of sediment per year, which is at least 3 % of the measured annual Rangitikei sediment yield. This highlights an important management issue for catchments that contain slow-moving landslides as this sediment enters the system and is carried and deposited downstream.

Slow-moving landslides are difficult to manage and present a number of hazards, both in regard to movement and sediment contribution. This research provides several recommendations for management and also lists a series of areas for further research.

7 References

Aleotti, P., & Chowdhury, R. (1999). Landslide hazard assessment: summary review and new perspectives. Bulletin of Engineering Geology and the Environment, 58, 21-44.

Alexander, D. (2012). The Rangitikei River, its tributary waterways, and other Taihape waterways: Scoping Report. A report commissioned by Crown Forestry Rental Trust.

Bassett, K. (2014). Book review: The Zealandia drowning debate: did New Zealand sink beneath the waves? New Zealand Journal of Geology and Geophysics, 269.

Bilderback, E. (2012). Hillslope response to climate-modulated river incision and the role of deep-seated landslides in post-glacial sediment flux: Waipaoa Sedimentary System, New Zealand, PhD Thesis. Christchurch: University of Canterbury.

Bilderback, E., Pettinga, J., Litchfield, N., Quigley, M., Marden, M., Roering, J., & Palmer, A. (2014). Hillslope response to climate-modulated river incision in the Waipaoa catchment, East Coast North Island, New Zealand. Geological Society of America Bulletin, 127, 131-148.

Brasington, J., Langham, J., & Rumsby, B. (2003). Methodological sensitivity of morphometric estimates of coarse fluvial sediment transport. Geomorphology, 53, 299-316.

Brasington, J., Rumsby, B., & McVey, R. (2000). Monitoring and modelling morphological change in a braided gravel-bed river using high resolution GPS-based survey. Earth Surface Processes and Landforms, 25, 973-990.

Brown, I. R. (1974). The stability of slopes in tertiary sedimentary rocks of New Zealand. Proceedings of the Symposium on Stability of Slopes in Natural Ground (pp. 7.23-7.33). Nelson: Institute of Professional Engineers New Zealand.

Brunsden, D. (2001). A critical assessment of the sensitivity concept in geomorphology. Catena, 99-123.

Cappa, F., Guglielmi, Y., Viseur, S., & Garambois, S. (2014). Deep fluids can facilitate rupture of slow-moving giant landslides as a result of stress transfer and frictional weakening. Geophysical Research Letters, 41, 61-66.

Cascini, L., Calvello, M., & Grimaldi, G. (2014). Displacement trends of slow-moving landslides: Classification and forecasting. Journal of Mountain Science, 592-606.

Cavalli, M., Trevisani, S., Comiti, F., & Marchi, L. (2013). Geomorphometric assessment of spatial sediment connectivity in small alpine catchments. Geomorphology, 31-41.

Cerovski-Darriau, C., Roering, J., Marden, M., Palmer, A., & Bilderback, E. (2014). Quantifying temporal variations in landslide-driven sediment production by reconstructing paleolandscapes using tephrochronology and lidar: Waipaoa River, New Zealand. Geochemistry, Geophysics, Geosystems, 1-20. doi:10.1002/2014GC005467

Claridge, G. (1960). Clay minerals, accelerated erosion and sedimentation in the Waipoa River catchment. New Zealand Journal of Geology and Geophysics, 3, 184-189.

Corsini, A., Borgatti, L., Caputo, G., De Simone, N., Sartini, G., & Truffelli, G. (2006). Investigation and monitoring in support of the structural mitigation of large slow-moving landslides: an example from Ca'Lita (Northern Apennines, Regio Emilia, Italy). Natural Hazards and Earth System Science, Copernicus Publications on behalf of the European Geosciences Union.

Crawford, J. (1861). Report on a geological tour in the Wairarapa and East Coast country. New Zealand Government Gazette (Province of Wellington), pp. 239-242.

Crozier, M. (1999). Prediction of rainfall-triggered landslides: A test of the antecedent water status model. Earth Surface Processes and Landforms, 25, 65-73.

Crozier, M., Preston, N., & Glade, T. (2016). Antecedent Conditions. In P. Bobrowsky, Encyclopedia of Natural Hazards (pp. 10-13). Springer Netherlands.

Dellow, G., McSaveney, M., Stirling, M., & Berryman, K. (2005). A probabilistic landslide hazard model for New Zealand. In J. Pettinga, & A. Wandres, Geological Society of New Zealand 50th annual conference, 28 November to 1 December 2005, Kaikoura: programme & abstracts (p. 24). Geological Society of New Zealand. Geological Society of New Zealand miscellaneous publication 119A.

Dymond, J., Herzig, A., Basher, L., Betts, H., Marden, M., Phillips, C., . . . Roygard, J. (2016). Development of a New Zealand SedNet model for assessment of catchment-wide soil-conservation works. Geomorphology, 85-93.

Ellen, S., Liu, L., Fleming, R., Reid, M., & Johnsson, M. (1995). Relation of slow-moving landslides to earth materials and other factors in valleys of the Honolulu District of Oahu, Hawaii. Honolulu: U.S. Geological Survey, Open-File Report 95-218.

Falconer, B. (1963). Stability of the hillslide at Tahunanui, Nelson. Unpublished report to the Nelson City Council.

Fleming, R., Varnes, D., & Schuster, R. (1979). Landslide Hazards and their Reduction. Journal of the American Planning Association, 428-439.

Fryirs, K. (2013). (Dis)Connectivity in catchment sediment cascades: a fresh look at the sediment delivery problem. Earth Surface Processes and Landforms, 30-46.

Fryirs, K., Brierley, G., Preston, N., & Kasai, M. (2007). Buffers, barrier and blankets: The (dis)connectivity of catchment-scale sediment cascades. Catena, 49-67.

Fuller, I. C., Large, A., Charlton, M., Heritage, G., & Milan, D. (2003). Reach-scale sediment transfers: an evaluation of two morphological budgeting approaches. Earth Surface Processes and Landforms, 28, 889-903.

Fuller, I., & Marden, M. (2011). Slope-channel coupling in steepland terrain: A field-based conceptual model from the Tarndale gully and fan, Waipaoa catchment, New Zealand. Geomorphology, 105-115.

Fuller, I., Basher, L., Marden, M., & Massey, C. (2011). Using morphological adjustments to appraise sediment flux. Journal of Hydrology, 59-79.

Fuller, I., Riedler, R., Bell, R., Marden, M., & Glade, T. (2016). Landslide-driven erosion and slope-channel coupling in steep, forested terrain, Ruahine Ranges, New Zealand, 1946-2011. Catena, 252-268.

Glade, T., Anderson, M., & Crozier, M. (2005). Landslide hazard and risk. England: J. Wiley.

Godfrey, A., Everitt, B., & Martin Duque, J. (2008). Episodic sediment delivery and landscape connectivity in the Mancos Shale badlands and Fremont River system, Utah, USA. Geomorphology, 242-251.

Golly, A., Turowski, J., Badoux, A., & Hovius, N. (2017). Controls and feedbacks in the coupling of mountain channels and hillslopes. Geology, 45, 307-310.

Gomez, B., & Livingston, D. (2012). The river it goes right on: Post-glacial landscape evolution in the upper Waipaoa River basin, eastern North Island, New Zealand. Geomorphology, 73-83.

Gomez, B., Banbury, K., Marden, M., Trustrum, N., Peacock, D., & Hoskin, P. (2003). Gully erosion and sediment production: Te Weraroa Stream, New Zealand. Water Resources Research.

Haghshenas Haghighi, M., & Motagh, M. (2016). Assessment of ground surface displacement in Taihape landslide, New Zealand, with C- and X-band SAR interferometry. New Zealand Journal of Geology and Geophysics, 136-146.

Harvey. (2001). Coupling between hillslopes and channels in upland fluvial systems: implications for landscape sensitivity, illustrated from the Howgill Fells, northwest England. Catena, 225-250.

Harvey. (2002). Effective timescales of coupling within fluvial systems. Geomorphology, 175-201.

Hennrich, K., & Crozier, M. (2004). A hillslope hydrology approach for catchment-scale slope stability analysis. Earth Surface Processes and Landforms, 29, 599-610.

Hicks, M., Shankar, U., McKerchar, A., Basher, L., Lynn, I., Page, M., & Jessen, M. (2011). Suspended sediment yields from New Zealand rivers. Journal of Hydrology (NZ), 81-142.

Hooke, J. (2003). Coarse sediment connectivity in river channel systems: a conceptual framework and methodology. Geomorphology, 56, 79-94.

Hungr, O., Leroueil, S., & Picarelli, L. (2014). The Varnes classification of landslide types, an update. Landslides, 167-194.

Irfan, T. (1998). Structurally controlled landslides in saprolitic soils in Hong Kong. Getechnical and Geological Engineering, 16, 215-238.

Iverson, R., Reid, M., Iverson, N., LaHusen, R., Logan, M., Mann, J., & Brien, D. (2000). Acute sensitivity of landslide rates to initial soil porosity. Science, 513-516.

James, M., How, P., & Wynn, P. (2016). Pointcatcher software: analysis of glacial time-lapse photography and integration with multitemporal digital elevation models. Journal of Glaciology, 159-169.

Journeaux, T., Kamp, P., & Naish, T. (1996). Middle Pliocene cyclothems, Mangaweka region, Wanganui Basin, New Zealand: a lithostratigraphic framework. New Zealand Journal of Geology and Geophysics, 39, 135-149.

Keefer, D. (2002). Investigaing landslides caused by earthquakes - a historical review. Surveys in Geophysics, 473-510.

Keefer, D. K. (1984). Landslides caused by earthquakes. Geological Society of America Bulletin, 95, 406-421.

Ker, D. (1970). Renewed movement on a slump in Utiku. New Zealand Journal of Geology and Geophysics, 996-1017.

Korup, O., McSaveney, M., & Davies, T. (2004). Sediment generation and delivery from large historic landslides in the Southern Alps, New Zealand. Geomorphology, 61, 189-207.

Kuo, C.-W., & Brierley, G. (2013). The influence of landscape configuration upon patterns of sediment storage in a highly connected river system. Geomorphology, 255-266.

Lacroix, P., Berthier, E., & Maquerhua, E. (2015). Earthquake-driven acceleration of slow-moving landslides in the Colca valley, Peru, detected from Pleiades images. Remote Sensing of Environment, 165, 148-158.

Lee, J., Bland, K., Townsend, D., & Kamp, P. (2011). Geology of the Hawke's Bay Area. Lower Hutt, QMap: Institute of Geological and Nuclear Sciences.

Lei, C. (2012). Earthquake-Triggered Landslides. 1st Civil and Environment Engineering Student Conference (pp. 1-6). London: Imperial College London.

Manga, M., Beresnev, I., Brodsky, E., Elkhoury, J., Elsworth, D., Ingebritsen, S., . . . Wang, C.-Y. (2012). Changes in permeability caused by transient stresses: Field observations, experiments, and mechanisms. Review Geophysics.

Mansour, M., Morgenstern, N., & Martin, D. (2011). Expected damage from displacement of slow-moving slides. Landslides, 117-131.

Massey, C. I. (2010). The dynamics of reactivated landslides: Utiku and Taihape, North Island, New Zealand. Durham: Doctoral thesis, Durham University.

Massey, C., Abbott, E., & McSaveney, M. (2016a). Earthquake-induced displacement is insignificant in the reactivated Utiku landslide, New Zealand. Landslides and Engineering Slopes. Experience, Theory and Practice, 31-52.

Massey, C., Abbott, E., McSaveney, M., Petley, D., & Richards, L. (2016a). Earthquake-induced displacement is insignificant in the reactivated Utiku landslide, New Zealand. Landslides and Engineering Slopes. Experience, Theory and Practice, 31-52.

Massey, C., Petley, D., & McSaveney, M. (2013). Patterns of movement in reactivated landslides. Engineering Geology, 1-19.

Massey, C., Petley, D., McSaveney, M., & Archibald, G. (2016). Basal sliding and plastic deformation of a slow, reactivated landslide in New Zealand. Engineering Geology, 11-28.

McCabe, M. (2013). The geomorphology and dynamics of a deep seated translational landslide: Bird Landslide Taihape North Island New Zealand. Palmerston North: Massey University.

McColl, S. T. (2014). Landslide Causes and Triggers. In T. Davies, Landslide Hazards, Risks, and Disasters (pp. 17-42). Amsterdam: Elsevier.

McColl, S. T., & McCabe, M. (2016). The causes and agricultural impacts of large translational landslides: Case-studies from North Island, New Zealand. Eight International Symposium on Landslides (p. 8). Naples, Italy: A. A. Balkema Publishers.

McSaveney, M., & Massey, C. (2017). Inadvertent Engineered Activation of Utiku Landslide, New Zealand. Advancing Culture of Living with Landslides, 563-568.

Milne, J. (1973). Maps and sections of river terraces in the Rangitikei Basin, North Island, New Zealand. New Zealand Soil Survey Report 4. Wellington: DSIR 1973 Wellington.

Mountjoy, J., & Pettinga, J. (2006). Controls on large deep-seated landslides in soft rock terrain: rock mass defects and seismic triggering. New Zealand Geotechnical Society Symposium: Earthquakes and Urban Development. 31. IPENZ.

Murphy, B. (2014). Coseismic Landslides. In T. Davies, Landslide Hazards, Risks, and Disasters (pp. 91-129). Amsterdam: Elsevier.

Nafarzadegan, A., Talebi, A., Malekinezha, H., & Emami, N. (2013). Antecedent rainfall thresholds for the triggering of deep-seated landslides (Case study: Charmahal & Bakhtiari Province, Iran). Ecopersia, 1, 23-39.

Neverman, A. J., Fuller, I. C., & Procter, J. N. (2016). Application of Geomorphic Change Detection (GCD) to quanitfy morphological budgeting error in a New Zealand gravel-bed river: a case study from the Makaroro River, Hawke's Bay. Journal of Hydrology, 1-19.

New Zealand Geotechnical Society. (2005). Field Description of Soil and Rock: Guidelines for the field classification and description of soil and rock for engineering purposes.

NIWA. (2016, September). Winter 2016. Retrieved from NIWA: https://www.niwa.co.nz/climate/summaries/seasonal/winter-2016

NIWA. (2017, September). Winter 2017. Retrieved from NIWA: https://www.niwa.co.nz/climate/summaries/seasonal/winter-2017

Ohlmacher, G. (2000). The Relationship between geology and landslide hazards of Atchison, Kansas, and vicinity. Kansa Geological Survey.

Park, J. (1886). On the geology of the western part of Wellington Provincial District, and part of Taranaki. New Zealand Geological Survey Reports. Geological Exploration, pp. 24-73.

Peck, R. (1959). Report on causes and remedial measures, Waiomao slide, Honolulu.

Petley, D., & Allison, R. (1997). The mechanics of deep-seated landslides. Earth Surface Processes and Landforms, 22, 747-758.

Picarelli, L. (2007). Considerations about the mechanics of slow active landslides in clay. In K. Sassa, H. Fukuoka, F. Wang, & G. Wang, Progress in landslide science (pp. 27-57).

Pillans, B. (1986). A Late Quaternary uplift map for North Island, New Zealand. Royal Society of New Zealand, Bulletin 24, 409-417.

Pulford, A., & Stern, T. (2004). Pliocene exhumation and landscape evolution of central North Island, New Zealand: the tole of the upper mantle. Journal of Geophysical Research, 109.

Retimana, E., Kealy, A., & Hale, M. (2004). Concepts of position repeatability and position reliability using the Global Positioning System.

Rodriguez, C., Bommer, J., & Chandler, R. (1999). Earthquake-induced landslides: 1980-1997. Soil Dynamics and Earthquake Engineering, 325-346.

Saunders, W., & Glassey, P. (2007). Guidelines for assessing planning, policy and consent requirements for landslide-prone land. GNS Science Miscellaneous Series 7.

Schulz, W., McKenna, J., Kibler, J., & Biavati, G. (2009). Relations between hydrology and velocity of a continuously moving landslide - Evidence of pore-pressure feedback regulating landslide motion? Landslides, 181-190.

Schumm, S. (1979). Geomorphic thresholds: the concept and its application. Transactions of the Institute of British Geographers, 485-515.

Selby, M. (1993). Hillslope Materials and Processes (2nd ed.). Oxford: Oxford University Press.

Stout, M. (1977). Utiku Landslide, North Island, New Zealand. Reviews in Engineering Geology, 3, 169-184.

Thomas, D., & Allison, R. (1993). Landscape Sensitivity. Chichester: John Wiley & Sons Ltd.

Thompson, R. (1982). Relationship of geology to slope failures in soft rocks of the Taihape-Mangaweka area, central North Island, New Zealand. PhD Thesis. Auckland: University of Auckland.

Van Asch, T., Van Beek, L., & Bogaard, T. (2007). Problems in predicting the mobility of slow-moving landslides. Engineering Geology, 46-55.

Varnes, D. J. (1978). Slope movement types and processes. In R. L. Shuster, & R. J. Krizek, Special Report 176, Landslides: Analysis and Control (Vol. 176, pp. 11-33). Washington D. C.: Transportation Research Board.

Wang, G., & Sassa, K. (2003). Pore-pressure generation and movement of rainfall-induced landslides: effects of grain size and fine-particle content. Engineering Geology, 109-125.

Westoby, M., Brasington, J., Glasser, N., Hambrey, M., & Reynolds, J. (2012). 'Structure-from-Motion' photogrammetry: A low-cost, effective tool for geoscience applications. Geomorphology, 300-314.

Yalcin, A. (2007). The effects of clay on landslides: A case study. Applied Clay Science, 38, 77-85.

Zerathe, S., Lacroix, P., Jongmans, D., Marino, J., Taipe, E., Wathelet, M., . . . Tatard, L. (2016). Morphology, structure and kinematics of a rainfall controlled slow-moving Andean landslide, Peru. Earth Surface Processes and Landforms.

7 Appendices

7.1 Appendix 1: RTK-dGPS movement data

Table A11. RTK-dGPS movement data table, showing the movement characteristics between each survey.

	Survey dates	Days	Horizontal movement (m)	Vertical movement (m)	Net Movement (m)	Rate (m/yr)	Trend	Direction	Plunge (-90 and 90)
1	Sept 2015 - Dec 2015	68	0.016 ± 0.3	-0.046	0.049	-0.246	116	South-east	71
	Dec 2015 - March 2016	101	0.041 ± 0.25	0.067	-0.079	0.244	92	East	-59
	March 2016 - July 2016	116	0.026 ± 0.29	-0.073	0.078	-0.231	212	South-west	71
	July 2016 - Oct 2016	104	0.043 ± 0.34	-0.010	0.044	-0.036	226	South-west	13
	Oct 2016 - Dec 2016	52	0.042 ± 0.34	-0.025	0.049	-0.176	217	South-west	31
	Dec 2016 - March 2017	96	0.025 ± 0.34	0.019	-0.031	0.074	137	South-east	-38
	March 2017 - June 2017	101	0.019 ± 0.27	0.035	-0.040	0.126	234	South-west	-61
	June 2017 - Oct 2017	104	0.033± 0.27	-0.065	0.073	-0.228	180	South	63
2	July 2015 - Sept 2015	89	0.013 ± 0.34	0.035	-0.037	0.142	252	West	-70
	Sept 2015 – Dec 2015	68	0.013 ± 0.3	-0.042	0.044	-0.226	211	South-west	73
	Dec 2015 - March 2016	101	0.041 ± 0.25	0.076	-0.087	0.276	67	North-east	-62
	March 2016 - July 2016	116	0.030 ± 0.29	-0.083	0.088	-0.262	211	South-west	70
	July 2016 - Oct 2016	104	0.041 ± 0.34	-0.006	0.042	-0.021	236	South-west	8
	Oct 2016 - Dec 2016	52	0.036 ± 0.34	-0.019	0.041	-0.131	217	South-west	27
	Dec 2016 - March 2017	96	0.026 ± 0.34	0.016	-0.031	0.061	137	South-east	-31
	March 2017 - June 2017	101	0.045 ± 0.27	0.031	-0.055	0.111	234	South-west	-34
	June 2017 - Oct 2017	104	0.038 ± 0.27	-0.046	0.060	-0.162	180	South	50
3	Sept 2015 - Dec 2015	68	0.038 ± 0.3	-0.029	0.048	-0.156	178	South	37
	Dec 2015 - March 2016	101	0.031 ± 0.25	0.054	-0.062	0.196	53	North-east	-61
	March 2016 - July 2016	116	0.032 ± 0.29	-0.066	0.073	-0.208	219	South-west	64
	July 2016 - Oct 2016	104	0.058 ± 0.34	0.027	-0.064	0.093	224	South-west	-25
	Oct 2016 - Dec 2016	52	0.041 ± 0.34	-0.025	0.048	-0.177	151	South-east	32
	Dec 2016 - March 2017	96	0.015 ± 0.34	-0.021	0.026	-0.080	179	South	54
	March 2017 - June 2017	101	0.033 ± 0.27	0.072	-0.079	0.259	274	West	-65
	June 2017 - Oct 2017	104	0.055 ± 0.27	-0.069	0.088	-0.242	180	South	51
4	July 2015 - Sept 2015	89	0.053 ± 0.34	0.049	-0.072	0.199	215	South-west	-42
	Sept 2015 - Dec 2015	68	0.042 ± 0.3	-0.050	0.065	-0.266	135	South-east	50
	December 2015 - March 2016	101	0.016 ± 0.25	0.083	-0.084	0.300	259	West	-79
	March 2016 - July 2016	116	0.008 ± 0.29	-0.087	0.087	-0.272	187	South	85
	July 2016 - October 2016	104	0.071 ± 0.34	0.026	-0.076	0.092	181	South	-20
	October 2016 - December 2016	52	0.044 ± 0.34	-0.008	0.044	-0.060	162	South	11
	December 2016 - March 2017	96	0.004 ± 0.34	-0.011	0.011	-0.040	149	South-east	70
	March 2017 - June 2017	101	0.051 ± 0.27	0.046	-0.068	0.165	249	West	-42
	June 2017 - October 2017	104	0.087 ± 0.27	-0.043	0.097	-0.151	180	South	26
5	July 2015 - September 2015	89	0.055 ± 0.34	0.043	-0.070	0.175	205	South-west	-38
	September 2015 - December 2015	68	0.048 ± 0.3	-0.048	0.068	-0.258	158	South	45
	December 2015 - March 2016	101	0.025 ± 0.25	0.083	-0.087	0.302	96	East	-73
	March 2016 - July 2016	116	0.056 ± 0.29	-0.121	0.133	-0.380	218	South-west	65

	July 2016 - October 2016	104	0.102 ± 0.34	0.004	-0.103	0.015	177	South	-2
	October 2016 - December 2016	52	0.067 ± 0.34	-0.010	0.067	-0.072	197	South	9
	December 2016 - March 2017	96	0.031 ± 0.34	0.013	-0.034	0.051	107	East	-23
	March 2017 - June 2017	101	0.071 ± 0.27	0.029	-0.077	0.106	223	South-west	-22
	June 2017 - October 2017	104	0.088 ± 0.27	-0.056	0.104	-0.198	180	South	33
6	July 2015 - September 2015	89	0.063 ± 0.34	0.022	-0.067	0.092	206	South-west	-20
	September 2015 - December 2015	68	0.031 ± 0.3	-0.031	0.044	-0.167	306	North-west	45
	December 2015 - March 2016	101	0.028 ± 0.25	0.105	-0.109	0.379	137	South-east	-75
	March 2016 - July 2016	116	0.030 ± 0.29	-0.104	0.108	-0.327	181	South	74
	July 2016 - October 2016	104	0.089 ± 0.34	0.002	-0.089	0.006	195	South	-1
	October 2016 - December 2016	52	0.043 ± 0.34	-0.037	0.057	-0.262	211	South-west	41
	December 2016 - March 2017	96	0.612 ± 0.34	-0.604	0.860	-2.298	189	South	45
	March 2017 - June 2017	101	0.567 ± 0.27	0.561	-0.798	2.029	8	North	-45
	June 2017 - October 2017	104	0.055 ± 0.27	0.025	-0.060	0.088	180	South	-24
7	July 2015 - September 2015	89	0.471 ± 0.34	-0.232	0.525	-0.951	115	South-east	26
	September 2015 - December 2015	68	0.463 ± 0.3	0.233	-0.518	1.251	289	West	-27
	December 2015 - March 2016	101	0.031 ± 0.25	0.123	-0.127	0.444	246	South-west	-76
	March 2016 - July 2016	116	0.042 ± 0.29	-0.120	0.127	-0.378	106	East	71
	July 2016 - October 2016	104	0.045 ± 0.34	0.015	-0.047	0.051	209	South-west	-18
	October 2016 - December 2016	52	0.039 ± 0.34	-0.027	0.048	-0.187	194	South	34
	December 2016 - March 2017	96	0.901 ± 0.34	-1.965	2.161	-7.470	196	South	65
	March 2017 - June 2017	101	0.848 ± 0.27	2.019	-2.190	7.296	15	North	-67
	June 2017 - October 2017	104	0.034 ± 0.27	-0.047	0.058	-0.165	180	South	54
8	July 2015 - September 2015	89	0.083 ± 0.34	0.015	-0.084	0.060	195	South	-10
	September 2015 - December 2015	68	0.049 ± 0.3	-0.055	0.074	-0.295	162	South	48
	December 2015 - March 2016	101	0.031 ± 0.25	0.096	-0.101	0.348	192	South	-72
	March 2016 - July 2016	116	0.078 ± 0.29	-0.103	0.130	-0.326	166	South	53
	July 2016 - October 2016	104	0.144 ± 0.34	-0.027	0.146	-0.093	202	South	10
	October 2016 - December 2016	52	0.075 ± 0.34	-0.001	0.075	-0.004	179	South	0
	December 2016 - March 2017	96	0.021 ± 0.34	-0.025	0.032	-0.095	154	South-east	50
	March 2017 - June 2017	101	0.072 ± 0.27	0.052	-0.089	0.188	194	South	-36
	June 2017 - October 2017	104	0.114 ± 0.27	-0.078	0.139	-0.275	180	South	34
9	July 2015 - September 2015	89	0.117 ± 0.34	0.035	-0.122	0.142	201	South	-16
	September 2015 - December 2015	68	0.075 ± 0.3	-0.062	0.097	-0.332	158	South	40
	December 2015 - March 2016	101	0.031 ± 0.25	0.067	-0.073	0.241	148	South-east	-65
	March 2016 - July 2016	116	0.109 ± 0.29	-0.110	0.155	-0.347	197	South	45
	July 2016 - October 2016	104	0.182 ± 0.34	-0.024	0.183	-0.086	181	South	8
	October 2016 - December 2016	52	0.093 ± 0.34	0.007	-0.094	0.047	210	South-west	-4
	December 2016 - March 2017	96	0.042 ± 0.34	-0.027	0.050	-0.103	163	South	33
	March 2017 - June 2017	101	0.102 ± 0.27	0.032	-0.107	0.117	203	South-west	-18
	June 2017 - October 2017	104	0.186 ± 0.27	-0.095	0.208	-0.332	180	South	27
10	July 2015 - September 2015	89	0.027 ± 0.34	0.027	-0.038	0.109	226	South-west	-45

	September 2015 - December 2015	68	0.021 ± 0.3	-0.036	0.042	-0.194	185	South	60
	December 2015 - March 2016	101	0.035 ± 0.25	0.089	-0.095	0.320	92	East	-68
	March 2016 - July 2016	116	0.035 ± 0.29	-0.089	0.095	-0.279	193	South	68
	July 2016 - October 2016	104	0.083 ± 0.34	-0.007	0.083	-0.023	180	South	5
	October 2016 - December 2016	52	0.065 ± 0.34	0.002	-0.065	0.013	199	South	-2
	December 2016 - March 2017	96	0.005 ± 0.34	0.005	-0.007	0.018	145	South-east	-44
	March 2017 - June 2017	101	0.036 ± 0.27	0.042	-0.055	0.151	206	South-west	-49
	June 2017 - October 2017	104	0.045 ± 0.27	-0.059	0.074	-0.207	180	South	53
11	July 2015 - December 2015	157	0.045 ± 0.3	-0.009	0.046	-0.022	176	South	12
	December 2015 - March 2016	101	0.117 ± 0.25	0.124	-0.170	0.447	166	South	-47
	March 2016 - October 2016	220	0.650 ± 0.29	-0.317	0.723	-0.525	174	South	26
	October 2016 - December 2016	52	0.371 ± 0.34	0.164	-0.406	1.152	64	North-east	-24
	December 2016 - March 2017	96	0.534 ± 0.34	-0.427	0.684	-1.624	217	South-west	39
	March 2017 - June 2017	101	0.283 ± 0.27	-0.279	0.397	-1.008	171	South	45
	June 2017 - October 2017	104	0.504 ± 0.27	-0.065	0.509	-0.228	180	South	7
12	July 2015 - September 2015	89	0.185 ± 0.34	-0.036	0.189	-0.148	188	South	11
	September 2015 - December 2015	68	0.109 ± 0.3	-0.096	0.145	-0.518	184	South	42
	December 2015 - March 2016	101	0.104 ± 0.25	0.040	-0.112	0.146	199	South	-21
	March 2016 - July 2016	116	0.136 ± 0.29	-0.076	0.156	-0.240	164	South	29
	July 2016 - October 2016	104	0.377 ± 0.34	-0.159	0.409	-0.558	192	South	23
	October 2016 - December 2016	52	0.098 ± 0.34	-0.025	0.102	-0.179	198	South	15
	December 2016 - March 2017	96	0.084 ± 0.34	0.042	-0.094	0.161	194	South	-27
	March 2017 - June 2017	101	0.270 ± 0.27	-0.137	0.303	-0.496	182	South	27
	June 2017 - October 2017	104	0.360 ± 0.27	-0.216	0.420	-0.759	180	South	31
13	July 2015 - September 2015	89	0.256 ± 0.34	0.046	-0.260	0.189	185	South	-10
	September 2015 - December 2015	68	0.088 ± 0.3	-0.048	0.101	-0.259	185	South	29
	December 2015 - March 2016	101	0.053 ± 0.25	0.073	-0.090	0.265	179	South	-54
	March 2016 - October 2016	220	0.347 ± 0.29	-0.113	0.365	-0.187	187	South	18
	October 2016 - December 2016	52	0.085 ± 0.34	-0.003	0.085	-0.018	196	South	2
	December 2016 - March 2017	96	0.084 ± 0.34	0.054	-0.100	0.205	208	South-west	-33
	March 2017 - June 2017	101	0.139 ± 0.27	-0.033	0.143	-0.121	176	South	14
	June 2017 - October 2017	104	0.222 ± 0.27	-0.077	0.235	-0.269	180	South	19
14	July 2015 - September 2015	89	0.569 ± 0.34	-0.074	0.573	-0.302	168	South	7
	September 2015 - December 2015	68	0.375 ± 0.3	-0.127	0.396	-0.684	167	South	19
	December 2015 - March 2016	101	0.324 ± 0.25	0.038	-0.326	0.138	165	South	-7
	March 2016 - October 2016	220	1.339 ± 0.29	-0.235	1.359	-0.390	168	South	10
	October 2016 - December 2016	52	0.399 ± 0.34	-0.392	0.559	-2.751	169	South	44
	December 2016 - March 2017	96	0.370 ± 0.34	-0.359	0.515	-1.365	166	South	44
	March 2017 - June 2017	101	0.789 ± 0.27	-0.770	1.103	-2.783	167	South	44
	June 2017 - October 2017	104	0.033 ± 0.27	-0.065	0.073	-0.228	180	South	63
15	December 2015 - March 2016	101	0.015 ± 0.25	0.079	-0.080	0.285	146	South-east	-79

	March 2016 - October 2016	220	0.128 ± 0.29	-0.080	0.151	-0.133	177	South	32
	October 2016 - December 2016	52	0.059 ± 0.34	-0.002	0.059	-0.015	185	South	2
	December 2016 - March 2017	96	0.021 ± 0.34	-0.022	0.030	-0.084	85	East	47
	March 2017 - June 2017	101	0.036 ± 0.27	0.061	-0.071	0.220	196	South	-59
	June 2017 - October 2017	104	0.114 ± 0.27	-0.055	0.127	-0.194	180	South	26
16	July 2015 - September 2015	89	4.339 ± 0.34	-4.183	6.027	-17.153	176	South	44
	September 2015 - December 2015	68	1.498 ± 0.3	-1.318	1.995	-7.075	175	South	41
	December 2015 - March 2016	101	4.784 ± 0.25	2.677	-5.482	9.675	304	North-west	-29
17	December 2015 - March 2016	101	0.597 ± 0.25	-0.015	0.597	-0.055	92	East	1
	March 2016 - October 2016	220	2.169 ± 0.29	-0.397	2.205	-0.658	221	South-west	10
	October 2016 - December 2016	52	0.577 ± 0.34	-0.090	0.584	-0.632	217	South-west	9
	December 2016 - March 2017	96	0.657 ± 0.34	-1.851	1.964	-7.036	137	South-east	70
	March 2017 - June 2017	101	2.339 ± 0.27	1.644	-2.859	5.939	234	South-west	-35
	June 2017 - October 2017	104	1.758 ± 0.27	-0.347	1.792	-1.219	180	South	11
18	July 2015 - September 2015	89	0.165 ± 0.34	0.047	-0.172	0.192	200	South	-16
	September 2015 - December 2015	68	0.065 ± 0.3	-0.072	0.097	-0.386	184	South	48
	December 2015 - March 2016	101	0.041 ± 0.25	0.089	-0.099	0.323	186	South	-65
	March 2016 - October 2016	220	0.333 ± 0.29	-0.132	0.358	-0.218	197	South	22
	October 2016 - December 2016	52	0.095 ± 0.34	-0.015	0.096	-0.108	193	South	9
	December 2016 - March 2017	96	0.045 ± 0.34	0.094	-0.104	0.358	222	South-west	-65
	March 2017 - June 2017	101	0.158 ± 0.27	-0.083	0.179	-0.300	194	South	28
	June 2017 - October 2017	104	0.184 ± 0.27	-0.116	0.218	-0.408	180	South	32
19	July 2015 - September 2015	89	0.540 ± 0.34	-0.233	0.588	-0.954	221	South-west	23
	September 2015 - December 2015	68	0.288 ± 0.3	-0.277	0.399	-1.485	221	South-west	44
	December 2015 - March 2016	101	0.249 ± 0.25	-0.010	0.249	-0.035	221	South-west	2
	March 2016 - October 2016	220	0.907 ± 0.29	-0.560	1.066	-0.929	223	South-west	32
	October 2016 - December 2016	52	0.247 ± 0.34	-0.103	0.268	-0.722	217	South-west	23
	December 2016 - March 2017	96	0.198 ± 0.34	-0.096	0.220	-0.366	213	South-west	26
	March 2017 - June 2017	101	0.435 ± 0.27	-0.147	0.459	-0.530	228	South-west	19
	June 2017 - October 2017	104	0.683 ± 0.27	-0.418	0.801	-1.467	180	South	31
20	July 2015 - September 2015	89	0.996 ± 0.34	-0.269	1.032	-1.104	185	South	15
	September 2015 - December 2015	68	0.587 ± 0.3	-0.298	0.659	-1.600	183	South	27
	December 2015 - March 2016	101	0.369 ± 0.25	-0.867	0.942	-3.133	179	South	67
	March 2016 - October 2016	220	1.912 ± 0.29	-0.867	2.099	-1.439	177	South	24
	October 2016 - December 2016	52	0.113 ± 0.34	0.081	-0.139	0.566	190	South	-36
	December 2016 - March 2017	96	0.288 ± 0.34	-0.107	0.307	-0.405	173	South	20
	March 2017 - June 2017	101	0.809 ± 0.27	-0.305	0.865	-1.104	176	South	21
21	July 2015 - September 2015	89	3.278 ± 0.34	-0.574	3.328	-2.352	58	North-east	10
	September 2015 - December 2015	68	1.710 ± 0.3	-0.239	1.726	-1.284	156	South-east	8
	December 2015 - March 2016	101	0.927 ± 0.25	0.120	-0.934	0.434	159	South	-7

Group	Period	n						Direction	
	March 2016 - October 2016	220	4.284 ± 0.29	-0.451	4.307	-0.749	158	South	6
	October 2016 - December 2016	52	1.090 ± 0.34	-0.041	1.091	-0.288	157	South-east	2
	December 2016 - March 2017	96	0.725 ± 0.34	0.010	-0.725	0.037	159	South	-1
	March 2017 - June 2017	101	3.138 ± 0.27	-0.486	3.176	-1.756	156	South-east	9
	June 2017 - October 2017	104	4.766 ± 0.27	-0.871	4.845	-3.055	180	South	10
22	July 2015 - September 2015	89	4.603 ± 0.34	-0.227	4.609	-0.929	126	South-east	3
	September 2015 - December 2015	68	2.979 ± 0.3	-0.172	2.984	-0.921	125	South-east	3
	December 2015 - March 2016	101	1.970 ± 0.25	0.004	-1.970	0.016	124	South-east	0
	March 2016 - October 2016	220	8.756 ± 0.29	-0.895	8.802	-1.485	123	South-east	6
	October 2016 - December 2016	52	2.474 ± 0.34	-0.237	2.485	-1.666	121	South-east	5
	December 2016 - March 2017	96	1.658 ± 0.34	-0.137	1.663	-0.520	121	South-east	5
	March 2017 - June 2017	101	6.561 ± 0.27	-0.808	6.611	-2.921	120	South-east	7
	June 2017 - October 2017	104	9.837 ± 0.27	-0.862	9.874	-3.024	180	South	5
23	July 2015 - September 2015	89	0.020 ± 0.34	0.051	-0.055	0.208	338	North	-69
	September 2015 - December 2015	68	0.041 ± 0.3	-0.060	0.073	-0.323	173	South	56
	December 2015 - March 2016	101	0.004 ± 0.25	0.102	-0.102	0.368	124	South-east	-88
	March 2016 - October 2016	220	0.029 ± 0.29	-0.081	0.086	-0.134	89	East	70
	October 2016 - December 2016	52	0.027 ± 0.34	0.018	-0.032	0.126	284	West	-34
	December 2016 - March 2017	96	0.028 ± 0.34	0.002	-0.028	0.008	155	South-east	-4
	March 2017 - June 2017	101	0.012 ± 0.27	0.031	-0.034	0.114	297	North-west	-69
	June 2017 - October 2017	104	0.023 ± 0.27	-0.043	0.049	-0.152	180	South	62
24	July 2015 - September 2015	89	2.045 ± 0.34	-0.044	2.046	-0.182	172	South	1
	September 2015 - December 2015	68	2.285 ± 0.3	3.286	-4.002	17.637	163	South	-55
	December 2015 - March 2016	101	0.403 ± 0.25	-3.159	3.185	-11.416	240	South-west	83
	March 2016 - October 2016	220	3.625 ± 0.29	-0.050	3.625	-0.082	172	South	1
	October 2016 - December 2016	52	0.946 ± 0.34	-0.141	0.957	-0.988	173	South	8
	December 2016 - March 2017	96	0.831 ± 0.34	0.173	-0.849	0.658	171	South	-12
	March 2017 - June 2017	101	1.937 ± 0.27	-0.012	1.937	-0.045	173	South	0
	June 2017 - October 2017	104	2.700 ± 0.27	-0.080	2.701	-0.279	180	South	2
25	September 2015 - December 2015	68	1.574± 0.3	-0.015	1.574	-0.082	156	South-east	1
	December 2015 - March 2016	101	1.197 ± 0.25	-0.061	1.198	-0.221	160	South	3
	March 2016 - October 2016	220	4.233 ± 0.29	-0.263	4.242	-0.436	157	South-east	4
	October 2016 - December 2016	52	1.131 ± 0.34	-0.074	1.133	-0.523	156	South-east	4
	December 2016 - March 2017	96	0.906 ± 0.34	-0.084	0.910	-0.318	156	South-east	5
	March 2017 - June 2017	101	2.239 ± 0.27	-0.107	2.242	-0.388	157	South-east	3
	June 2017 - October 2017	104	3.208 ± 0.27	-0.277	3.220	-0.971	180	South	5
26	September 2015 - December 2015	68	0.022 ± 0.3	-0.218	0.220	-1.172	23	North-east	84
	December 2015 - March 2016	101	0.045 ± 0.25	0.288	-0.291	1.040	197	South	-81
	March 2016 - October 2016	220	0.023 ± 0.29	-0.065	0.069	-0.107	192	South	70
	October 2016 - December 2016	52	0.024 ± 0.34	0.015	-0.028	0.108	244	South-west	-33

	December 2016 - March 2017	96	0.532 ± 0.34	-0.242	0.584	-0.918	287	West	24
	March 2017 - October 2017	205	0.519 ± 0.27	0.241	-0.572	0.428	110	East	-25
27	July 2015 - September 2015	89	0.051 ± 0.34	0.051	-0.072	0.207	52	North-east	-45
	September 2015 - December 2015	68	0.025 ± 0.3	-0.048	0.054	-0.258	278	West	63
	December 2015 - March 2016	101	0.031 ± 0.25	0.096	-0.101	0.348	203	South-west	-72
	March 2016 - October 2016	220	0.001 ± 0.29	-0.068	0.068	-0.113	181	South	89
	October 2016 - December 2016	52	0.021 ± 0.34	0.010	-0.023	0.070	236	South-west	-25
	December 2016 - March 2017	96	0.029 ± 0.34	-0.010	0.031	-0.040	41	North-east	20
	March 2017 - June 2017	101	0.031 ± 0.27	0.033	-0.045	0.118	197	South	-47
	June 2017 - October 2017	104	0.015 ± 0.27	-0.026	0.030	-0.091	180	South	60
28	July 2015 - September 2015	89	0.874 ± 0.34	0.474	-0.994	1.943	109	East	-28
	September 2015 - December 2016	441	0.776 ± 0.34	-0.638	1.005	-0.530	179	South	39
	December 2016 - March 2017	96	0.097 ± 0.34	0.003	-0.097	0.012	128	South-east	-2
	March 2017 - June 2017	101	0.202 ± 0.27	-0.039	0.206	-0.141	132	South-east	11
	June 2017 - October 2017	104	0.588 ± 0.27	-0.111	0.598	-0.390	180	South	11
29	March 2017 - October 2017	205	4.583 ± 0.34	0.136	-4.585	0.241	179	South	-2
Camera	July 2015 - December 2015	68	0.048 ± 0.3	-0.036	0.060	-0.194	163	South	37
	December 2015 - December 2016	373	0.109 ± 0.3	0.075	-0.132	0.074	175	South	-35
	December 2016 - March 2017	96	0.025 ± 0.34	0.035	-0.043	0.134	246	South-west	-55
	March 2017 - June 2017	101	0.027 ± 0.27	0.028	-0.039	0.102	155	South-east	-46

7.2 Appendix 2: Survey dates and error

Table A2. Survey precision estimated for each survey (by occupation of the same peg at the start and end of each survey).

Survey no.	Survey date	Net survey difference (mm)
Survey 1	3rd July 2015	24
Survey 2	30th September 2015	24
Survey 3	7th December 2015	18
Survey 4	17th March 2016	16
Survey 5	11th July 2016	24
Survey 6	23rd October 2016	24
Survey 7	14th December 2016	24
Survey 8	20th March 2017	19
Survey 9	29th June 2017	12
Survey 10	11th October 2017	24

Table A3. Propagated precision errors measured by calculating the error for the precisions of each survey.

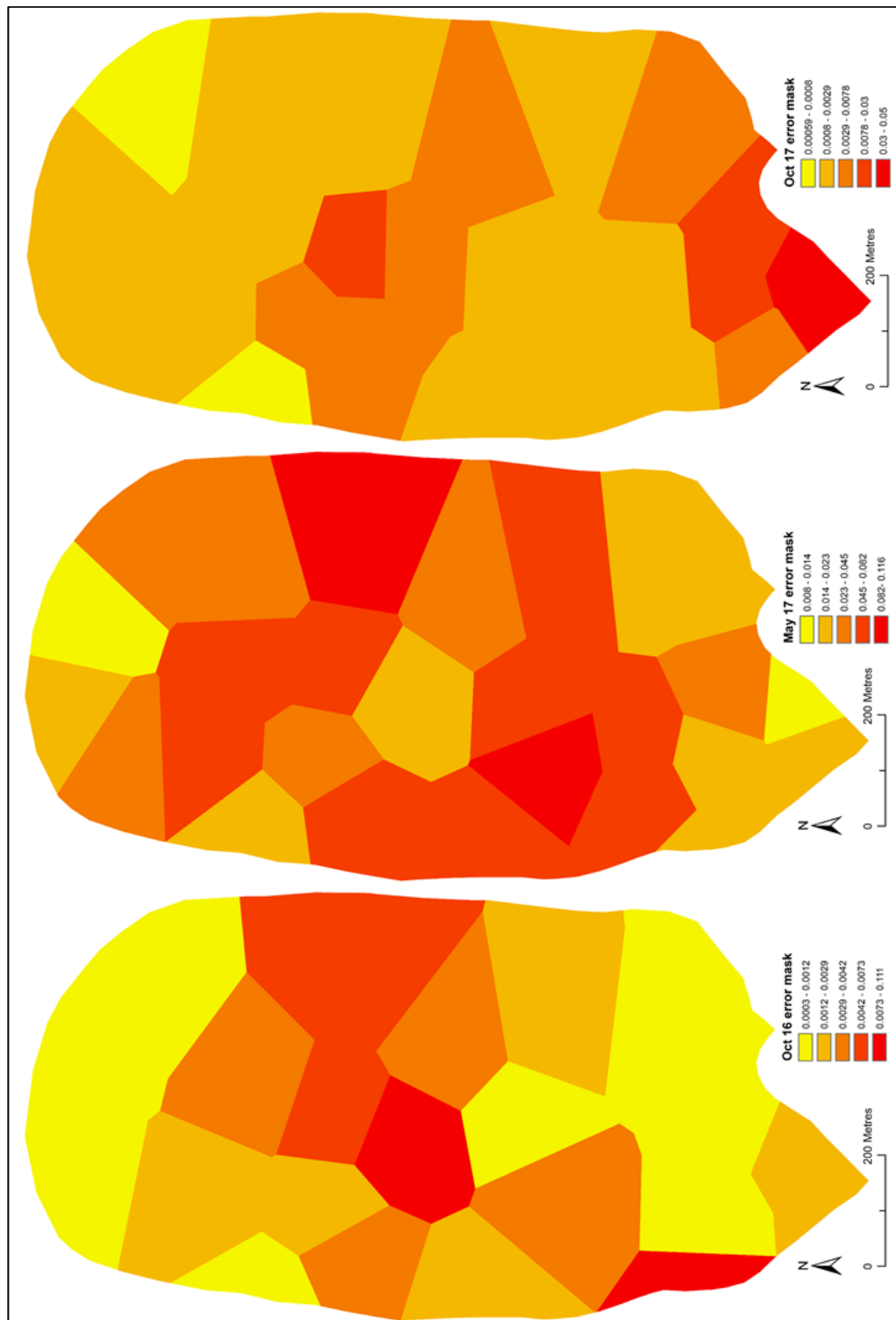| Surveys	Propagated error (mm)
Survey 1 and 2	34
Survey 2 and 3	30
Survey 3 and 4	25
Survey 4 and 5	29
Survey 5 and 6	34
Survey 6 and 7	34
Survey 7 and 8	34
Survey 8 and 9	27
Survey 9 and 10	27

7.3 Appendix 3: DoD error masks

Figure 83. Error masks for the DoD analyses.